Atmospheric River Precipitation Attribution in Reanalysis Data and Comparison with ICESat-2 Altimetry Observations in Antarctica

Sylke van der Kleij

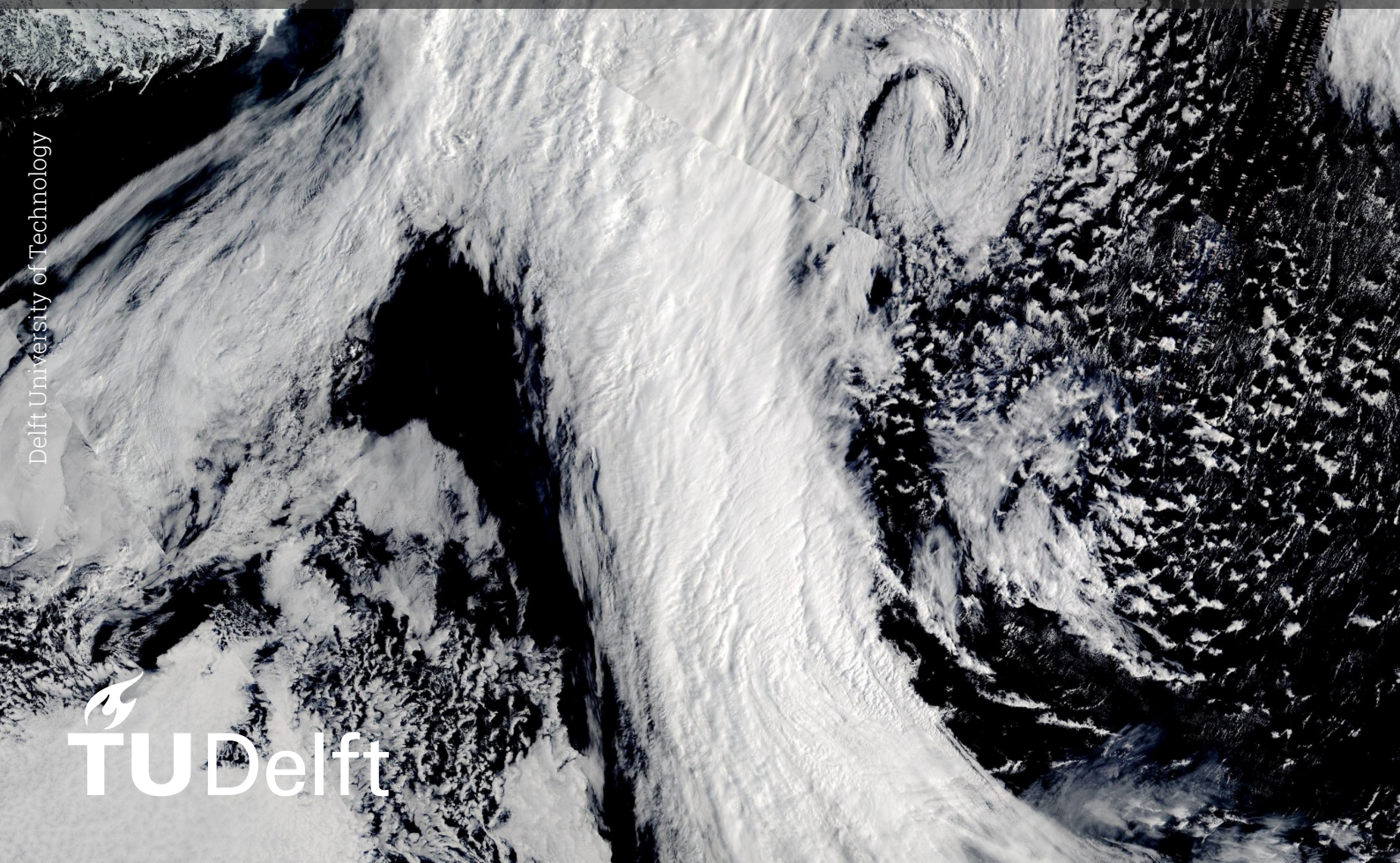

Delft University of Technology

TU Delft

Atmospheric River Precipitation Attribution in Reanalysis Data and Comparison with ICESat-2 Altimetry Observations in Antarctica

by

Sylke van der Kleij

to obtain the degree of Master of Science
at the Delft University of Technology,
to be defended publicly on May 30th, 2023 at 11:45.

Student number:	4465962	
Project duration:	April, 2022 – May, 2023	
Thesis committee:	Dr. Ir. B. (Bert) Wouters,	TU Delft, daily supervisor
	Dr. S.L.M. (Stef) Lhermitte,	TU Delft, daily supervisor
	Dr. M. (Miren) Vizcaino,	TU Delft

Cover: Satellite image of an Atmospheric River spreading clouds above East Antarctica, by J. Wille

TU Delft

Preface

Before you lies my final thesis to obtain my MSc degree in Geoscience and Remote Sensing, and as such this thesis concludes my time as a student at Delft University of Technology. Over the past year I have learned a lot about Antarctica and atmospheric rivers, and I have explained what an atmospheric river is more times than I can count.

I would like to express my gratitude to my supervisors Bert and Stef. I am very thankful for your endless patience and all of the great ideas, and for your guidance in choosing which direction to choose. Also, thank you for your understanding when it all became a little too much, and making me see that it was okay to struggle. I would also like to thank Miren for her valuable feedback and comments as a committee member.

I am also very grateful for the support of my friends and family. Thank you to my parents, who always tried to provide a space where I could forget about Antarctica and atmospheric rivers for a little while, and understood when I could not drop by at home and so they came to Delft instead. Thank you to my friends, for always trying to cheer me up and checking up on me, I promise that I will never miss another night of eating pancakes again. And finally, thank you to Koen, for always cheering me on and for helping me believe in myself.

Sylke van der Kleij
Delft, May 2023

Summary

Atmospheric rivers transport 90% of all atmospheric moisture in the mid-to-high latitudes, while covering only 10% of the Earth's surface at any given time. Atmospheric rivers occur infrequently, and atmospheric river frequency in the polar areas is especially low, but they can have a large impact on the cryosphere when they make landfall. They have been linked to various processes affecting the surface mass balance, such as extreme precipitation events as well as surface melt.

This thesis addresses the importance of atmospheric rivers in the polar regions. The study aims to compare atmospheric river precipitation estimates obtained from reanalysis data with ICESat-2 satellite altimetry observations in Antarctica between 2019 and 2021, to determine whether the two different types of data sets show similar amounts of atmospheric river precipitation.

To achieve this goal, an atmospheric river detection algorithm designed specifically for polar regions was used to identify atmospheric rivers in Antarctica. All precipitation falling within an atmospheric river footprint for the first 24 hours after detection is attributed to the atmospheric river. The detection algorithm and precipitation attribution are performed to MERRA-2 and ERA5 reanalysis data. The resulting atmospheric river precipitation anomalies were then compared to ICESat-2 height change observations using correlation analysis and a metric based on variance reduction. A detailed analysis is presented of specific drainage basins that show promising results based on the comparison of the reanalysis data and ICESat-2 observations, using time series.

The results show a high degree of correlation between the atmospheric river precipitation anomalies from reanalysis data and ICESat-2 height changes in multiple drainage basins. Variance reduction shows that atmospheric river precipitation can explain a significant part of the variance of the ICESat-2 height change observations in these drainage basins. This suggests that in select locations, the atmospheric river precipitation expected based on reanalysis data is indeed observable in ICESat-2 data. A challenge is the coarse temporal resolution of ICESat-2 data. ICESat-2 data has a temporal resolution of 91 days, whereas atmospheric rivers typically last between a few hours up to a few days at most, and occur very infrequently (up to $\sim$2% of the total time over the time period 2019-2021).

Nonetheless, this thesis provides a comprehensive analysis of atmospheric river precipitation in Antarctica using both reanalysis data and satellite observations, contributing to a better understanding of the impact of atmospheric rivers on the surface mass balance of Antarctica. Additionally, it suggests that as long as its limitations are taken into account, ICESat-2 data can be a valuable tool to use in addition to reanalysis data in the study of atmospheric rivers in the polar regions.

Contents

Acronyms

AIS Antarctic Ice Sheet.
AMS American Meteorological Society.
AR Atmospheric River.
ARTMIP Atmospheric River Tracking Method Intercomparison Project.
ATLAS Advanced Topographic Laser Altimeter System.

EAIS East Antarctic Ice Sheet.

FDM Firn Densification Model.

GrIS Greenland Ice Sheet.

ICESat-2 Ice, Cloud and land Elevation Satellite-2.
IVT Integrated water Vapour Transport.
IWV Integrated Water Vapour.

MB Mass Balance.
MERRA-2 Modern-Era Retrospective analysis for Research and Applications, version 2.

NWP numerical weather prediction.

RGT reference ground track.

SMB Surface Mass Balance.
SNR Signal-to-Noise ratio.
SSM/I Special Sensor Microwave Imager/Sounder.

WAIS West Antarctic Ice Sheet.
WCB warm conveyor belt.

1

Introduction

1.1. Motivation

An Atmospheric River (AR) is defined in the American Meteorological Society Glossary of Meteorology as ”a long, narrow, and transient corridor of strong horizontal water vapor transport that is typically associated with a low-level jet stream ahead of the cold front of an extratropical cyclone.” In other words, an atmospheric river is a long narrow band of enhanced moisture fluxes in the atmosphere (J. D. Wille et al., 2022).

The majority of moisture transport in the atmosphere is organised in these ARs (Gorodetskaya et al., 2014). In fact, although ARs cover only around 10% of the Earth's surface at any given time, ARs account for more than 90% of the meridional moisture transport in the mid-to-high latitudes, and are therefore a crucial component of the global hydrological cycle (Zhu and Newell, 1998, Nash et al., 2018). ARs and their effects are not fully understood yet. For example, while ARs have often been linked to extreme precipitation, it is hard to determine the spatial and temporal extent of AR precipitation.

ARs occur most often in the midlatitudes, with a roughly symmetric distribution in both hemispheres. AR frequency is lowest in the polar areas, and they almost never occur over interior Antarctica (Guan & Waliser, 2015).

Despite AR frequency in the polar areas being low, they can have a very big impact on the cryosphere. Recently, there has been increased interest in the effects of ARs on the polar regions as ARs are an important driver of Surface Mass Balance (SMB) over both the Greenland and the Antarctic ice sheets (Skinner et al., 2023).

A key characteristic of why studying ARs in the polar regions is very interesting is that a single AR can cause both strong snowfall and melt (J. D. Wille et al., 2019). Depending on which effect is stronger, the AR has either a negative or a positive contribution to the surface mass balance.

Overall, ARs have a predominantly positive impact on the Antarctic Ice Sheet (AIS) SMB as mass gain from AR related snowfall across the AIS outweigh mass loss from AR-related melting events (Pohl et al., 2021). In fact, due to the positive impact of ARs on the AIS SMB, ARs currently actively mitigate sea level rise driven by dynamic mass loss (J. D. Wille et al., 2021).

While for now the impact of ARs on Antarctic melt is limited, it is suggested that continued warming and an increase in AR activity could lead to an increase in melt frequency in the future (J. D. Wille et al., 2019), with possible SMB loss as a result.

Past research on ARs in the polar regions has helped to improve our understanding of these weather systems and their impacts on the cryosphere. Besides the aforementioned research into the impact of ARs on the SMB, there has also been research into identification and characterisation of ARs (Guan and Waliser, 2015, J. D. Wille et al., 2021). This is relevant because AR detection in a polar climate differs from AR detection in the midlatitudes, since the atmospheric water vapour content in polar regions is significantly lower (Gorodetskaya et al., 2014).

There has also been research into AR contributions to ice sheet hydroclimate at the Last Glacial Maximum (Skinner et al., 2023). ARs may have had an important role in ice sheet growth and melt

during previous glacial periods, and during the Last Glacial Maximum they may have accelerated ice sheet retreat.

Today, climate change and its consequences are a topic of high interest in both the media as well as in research. Recently there has been increased interest in the link between ARs and climate change. Atmospheric river frequency is expected to increase in the future as a result of climate change. While the total number of AR events is projected to decrease, the ARs will be longer and wider (Espinoza et al., 2018). Based on the RCP8.5 scenario, ARs will be 25% longer and 25% wider. This leads to an overall increase in AR conditions of 50% globally. Knowing that the frequency of ARs is expected to increase means that it is even more important to be able to measure how much ARs contribute to snow height increase or to surface melting.

Additionally, it is expected that AR intensity will increase: 25% globally under RCP8.5 (Espinoza et al., 2018). AR intensity has been linked with ice-shelf weakening processes: as the maximum Integrated water Vapour Transport (IVT) of an AR increases, the chances of a temperature extreme, melting extreme, sea ice disintegration or high swell event occurring also increases (J. D. Wille et al., 2021).

A limitation when studying Antarctica is that it is huge and difficult to access, making it hard to collect observational data. Thanks to satellite data, researchers are gaining a better understanding of Antarctica and the many processes that play a role in its climate. However, there are several challenges related to using satellite data. One of the main weaknesses of satellite observations is the trade-off between temporal and spatial resolution. A satellite with a high temporal resolution cannot also have a high spatial resolution. This means that although the time between two subsequent observations at the same place is short, small changes (ie smaller than the spatial resolution) will not be detected. On the other hand, if the satellite has a low temporal resolution but a high spatial resolution, it may capture changes between two subsequent observations at great detail, but it becomes nearly impossible to detect rapid change. Additionally, the satellite record is relatively short.

While ARs can be detected using measurements made from ground-based, airborne, and satellite platforms and regional models (Adusumilli et al., 2021), climate researchers studying ARs in polar regions mostly use atmospheric reanalysis data because of a lack of observations. The benefit of reanalysis data is that it is available at both a high temporal as well as spatial resolution, and there is a long record often dating back several decades.

Past research has found that ARs can drive large amounts of snowfall Gorodetskaya et al., 2014, Maclennan et al., 2022) and snow melt (J. D. Wille et al., 2019) over a period of days, which means that a high temporal resolution is important.

A downside of reanalysis data is that biases can be introduced by non-perfect models, which is particularly relevant in high-latitude regions such as Antarctica (Hassler & Lauer, 2021). Different reanalysis data-sets might model certain parameters differently, which might impact results. It is therefore important to understand the limitations of different reanalysis data-sets, to ensure that the interpretation of results is not influenced by biases in the reanalysis data.

The relationship between ARs and (extreme) precipitation events is of great importance for understanding inter-annual variability and trends of the total Antarctic ice sheet SMB (Gorodetskaya et al., 2014). As reanalysis data is a key input in research into ARs and Antarctic climatology, it is therefore important that ARs are well-represented in reanalysis data.

Ideally, satellite observations and reanalysis data can be used together to study ARs. Currently, multiple satellites are collecting data in and around Antarctica. One of these satellites is Ice, Cloud and land Elevation Satellite-2 (ICESat-2). ICESat-2 collects altimetry data and has been in orbit since October 2018, and is projected to collect data until 2027. Different processes contribute to height changes observed, such as ice dynamics and precipitation. Assuming that the AIS is in long term equilibrium, precipitation anomalies contribute to height change and should thus be observable in ICESat-2 data. Depending on how large the contribution of AR precipitation to the total precipitation is, the AR precipitation signal might also be observable in ICESat-2 data. Then, reanalysis data and ICESat-2 data could be used together to gain additional insights into ARs and their effects in Antarctica. Knowing how much snow is accumulating across the continent can also help in projecting potential sea-level rise from the Antarctic Ice Sheet, and the influence of AR precipitation in mitigating sea-level rise.

This thesis explores whether there is significant correlation between AR precipitation in reanalysis data and the height change observed in satellite altimetry data. If so, this could be an indication that

ARs and their related precipitation is well-represented in reanalysis data. Additionally, it could be an indication that ICESat-2 data is suitable for more detailed research into ARs and their effects on the cryosphere.

1.2. Objective and research questions

The aim of this thesis is to determine how much precipitation is associated with atmospheric rivers detected in/over Antarctica using reanalysis data. The AR precipitation pattern is then compared to satellite altimetry data to determine if there is a noticeable pattern linking AR precipitation to observed height change in Antarctica.

Two reanalysis data-sets are used, to investigate whether the data-sets perform similarly in predicting AR locations and related precipitation, or if choice of reanalysis data-sets significantly changes the results. The reanalysis data-sets used are Modern-Era Retrospective analysis for Research and Applications, version 2 (MERRA-2) and ERA5, the fifth generation ECMWF atmospheric reanalysis of the global climate. MERRA-2 provides hourly data beginning in 1980, while ERA5 provides hourly data beginning in 1959. MERRA-2's spatial resolution is coarser than that of ERA5, 0.625°x0.5° longitude-latitude and 0.25°x0.25° respectively.

Ice, Cloud and land Elevation Satellite-2 (ICESat-2) altimetry data is used to investigate whether the AR precipitation attributed in reanalysis data can be recognised in observational data. ICESat-2 was launched in September 2018 and carries the Advanced Topographic Laser Altimeter System (ATLAS) which provides coverage of the ice sheets up to 88° latitude, repeating its ground tracks every 91 days (Markus et al., 2017).

This leads to the following research objective:
Determine the precipitation pattern of Atmospheric River related precipitation in reanalysis data and investigate whether the same pattern can be recognised in ICESat-2 altimetry observations.

Subquestions to answer this question are as follows:

Q. 1: *In what way do the reanalysis data-sets detect ARs in different locations?*

Although the same AR detection algorithm is used for both reanalysis data-sets, it is possible that the AR detection patterns differ due to a number of reasons. For example, the spatial resolution of the reanalysis data-sets differs, but the data-sets also use different data assimilations, and different underlying atmospheric models, which can impact the detection of ARs. Therefore, a first step is to run the AR detection algorithm for both data-sets and to determine if the AR detection is similar. Ideally, MERRA-2 and ERA5 detect ARs at the same locations and with similar frequency,this would support the validity of the AR detection algorithm and increase confidence in theAR events identified in the study.

Q. 2: *To what extent, spatially and temporally, is the precipitation following an AR detection related to the AR event?*

After having detected AR occurrences, it is important to determine the amount of precipitation associated with said ARs. To do this, several choices have to be made, for example whether to only count precipitation that falls within an AR's footprint or also outside it, and how long after an AR has been detected precipitation is still attributed to the AR. This is done based on a literature study.

Q. 3: *Which processes are responsible for height change observed in ICESat-2 altimetry data?*

ICESat-2 satellite altimetry data provides the estimated height of the Earth's surface every 91 days. From subsequent height measurements, height change is derived. There are multiple processes contributing to this height change, and precipitation is only one of them. In order to attempt to make a link between the modelled (AR) precipitation data and the total height change as observed by the satellite data, it is important to understand which other processes are related to Antarctic height change, and what their magnitudes are.

Q. 4: *To what extent can a precipitation pattern be recognised in ICESat-2 altimetry data?*

In order to determine whether AR precipitation patterns that are present in reanalysis data are captured in ICESat-2 data, it is important that precipitation is a big part of the ICESat-2 observed

height change, and that the precipitation signal can be distinguished from other sources of height variability. The temporal resolution of the measurements is limited, as observations are only available every 91 days. This means that ICESat-2 data likely misses some of the temporal variability of precipitation, possibly affecting the possibility of recognising a precipitation signal.

Q. 5: *What is the correlation between reanalysis data and ICESat-2 satellite altimetry data?*

The aim of this thesis is to investigate whether there is a relationship between AR precipitation patterns detected in the reanalysis data and the height changes observed in the ICESat-2 altimetry data. A strong correlation would suggest that the precipitation patterns detected in the reanalysis data are indeed present in the ICESat-2 data, which would mean that ICESat-2 data is a good option for research into ARs.

1.3. Report outline

This introduction chapter introduces the topic of this thesis and forms the basis of the following chapters.

Chapter 2 aims to provide background information that is needed to answer the research questions and develop a methodology to answer them. This chapter includes information about the Antarctic Ice Sheet and its (surface) mass balance, as well as information about atmospheric rivers, their effects, and how to detect them. Additionally, the ICESat-2 mission is highlighted.

Chapter 3 discusses the methodology used, including the AR detection and AR precipitation contribution, and the comparison between reanalysis data and satellite altimetry data.

Chapter 4 presents the results following the methods described in chapter 3.

In chapter 5 the results are discussed, including the limitations.

Finally, chapter 6 concludes this thesis, and answers the research questions. Additionally, a number of recommendations for further research are given based on the results of this study.

2

Background

2.1. The Antarctic Ice Sheet

In the last decade, there has been raised attention toward the increased mass loss from the polar ice sheets, both the Greenland Ice Sheet and the Antarctic Ice Sheet (AIS) (Gorodetskaya et al., 2013, King et al., 2012). This thesis focuses on the AIS, and therefore the processes causing mass loss in Greenland will not be discussed further.

The AIS can be roughly divided in two parts: the West Antarctic Ice Sheet (WAIS) and the East Antarctic Ice Sheet (EAIS). Figure 2.1 shows a map of Antarctica, including the division between West and East Antarctica. Additionally, it shows the locations of a number of regions. Ice shelves are shaded in gray.

Figure 2.1: Map of Antarctica, the ice shelves are shaded grey (via Abrahamsen, 2012)

2.1.1. Surface Mass Balance and Mass Balance

It is important to distinguish between the Mass Balance (MB) and the Surface Mass Balance (SMB).

Ice sheet mass loss/gain is expressed as the ice sheet Mass Balance (MB), and is determined by surface mass fluxes (the SMB), and the flux of ice across the grounding line (the discharge D) (Lenaerts et al., 2019). The mass balance can thus also be expressed as $MB = SMB - D$.

The SMB is the difference between accumulation and ablation at the surface of a glacier or ice sheet, so the ice in contact with the atmosphere only (Mottram et al., 2021). In Antarctica, accumulation is

primarily due to snowfall, while surface ablation is mainly a result of erosion and sublimation due to high winds and a dry atmosphere (Agosta et al., 2019). The SMB does not include dynamic mass loss and basal melting, but is still an important component of the mass balance as a negative SMB may result in a negative mass balance, meaning the ice sheet loses mass (Lenaerts et al., 2019). The SMB also plays an important role in controlling the stability and evolution of the ice sheet (Mottram et al., 2021).

2.2. Atmospheric Rivers

2.2.1. A brief history on AR research

Research on atmospheric rivers is relatively young, as ARs were only ”discovered” in the late 20th century. They were first termed ”tropospheric rivers” by Newell et al., 1992. This study analysed the transportation of atmospheric carbon dioxide, but then also observed narrow plumes of intense vertically Integrated water Vapour Transport (IVT) meandering through the atmosphere. Zhu and Newell, 1998 then first called these plumes atmospheric rivers. They researched water vapor fluxes in the atmosphere, and discovered that the strongest fluxes have a filamentary form where the length is several times larger than their width.

Something that has greatly helped AR research was the increasing number of Special Sensor Microwave Imager/Sounder (SSM/I) satellites, allowing for Integrated Water Vapour (IWV) observations in near real time. Researchers realised that the IWV signature of ARs in SSM/I satellite data was very distinct, and could be used to objectively detect and track ARs (Ralph et al., 2004, Wick et al., 2013). Figure 2.2 shows ARs detected using IWV as observed by SSM/I satellites (Ralph et al., 2011).

Recently, IVT has become the preferred metric for AR identification, mostly thanks to the more recently available high-quality atmospheric reanalysis products. The added benefit of IVT over IWV is that IVT also accounts for wind, which is necessary to produce the moisture transport associated with ARs (Sodemann et al., 2020). Additionally, using IVT was shown as more robust because IWV sometimes never dropped below the standard 2-cm threshold at lower latitudes, while at higher latitudes, some ARs were well defined by IVT while IWV remained below the 2-cm threshold due to the cooler air (Ralph, Dettinger, et al., 2020). ARs identified using SSM/I IWV are typically consistent with IVT based on using reanalysis data (Sodemann et al., 2020).

With the development of AR detection and tracking methods, research into the effects of ARs also emerged, linking ARs to heavy coastal precipitation and flooding events (Sodemann et al., 2020). As extreme precipitation/flooding events can have a big impact on urban areas, a lot of AR research is focused on urban areas such as the west coasts of the USA, and Europe.

Research on ARs in polar regions is very recent, with the first papers identifying polar ARs only published in 2014 (e.g. Gorodetskaya et al., 2014).

Additionally, there is a lot of interest in how ARs will change as the global climate changes (Sodemann et al., 2020).

2.2.2. What is an AR?

There has been a lot of debate over the precise definition of atmospheric rivers. There have been varying perspectives on the term, as some considered it a duplicate of pre-existing concepts such as the warm conveyor belt (WCB), and some thought that the analogy to terrestrial rivers is inappropriate (Ralph et al., 2018).

Only in 2018 an agreement was reached and a consistent AR definition emerged and was published in the American Meteorological Society (AMS) Glossary of Meteorology:

”a long, narrow, and transient corridor of strong horizontal water vapor transport that is typically associated with a low-level jet stream ahead of the cold front of an extratropical cyclone. The water vapor in atmospheric rivers is supplied by tropical and/or extratropical moisture sources. Atmospheric rivers frequently lead to heavy precipitation where they are forced upward—for example, by mountains or by ascent in the warm conveyor belt. Horizontal water vapor transport in the midlatitudes occurs primarily in atmospheric rivers and is focused in the lower troposphere.”

The majority of moisture transport in the atmosphere is organised in these ARs (Gorodetskaya et al., 2014). In fact, although ARs cover only around 10% of the Earth’s surface at any given time, ARs account for more than 90% of the meridional moisture transport in the mid-to-high latitudes (Zhu and Newell, 1998, Nash et al., 2018).

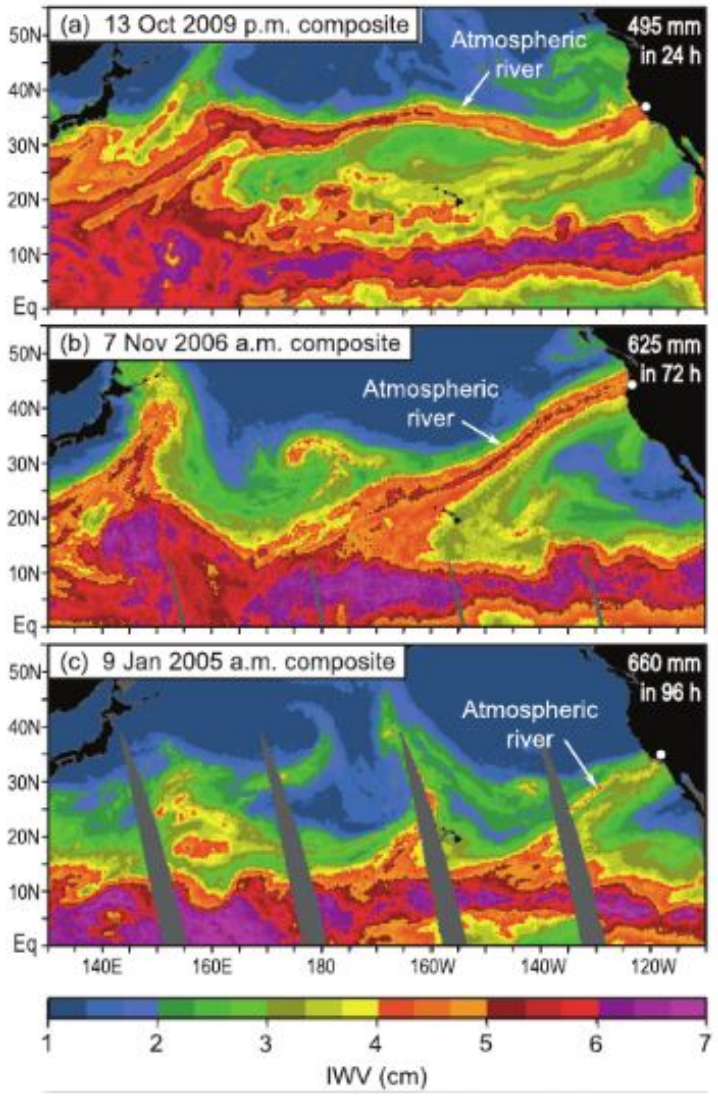

Figure 2.2: Examples of ARs that caused extreme precipitation along the US west coast, and exhibited spatial continuity with the tropical water vapour reservoir as seen in SSM/I satellite observations of IWV. Composite SSM/I satellite images of IWV (cm) of an AR emanating from the tropical (a) western Pacific on the afternoon of 13 Oct 2009, (b) central Pacific on the morning of 7 Nov 2006, and (c) eastern Pacific on the morning of 9 Jan 2005 (via Ralph et al., 2011)

The defining characteristic of ARs is the moisture contained and transported within ARs. Atmospheric Rivers typically form due to moisture convergence along the cold front in warm sectors of an extratropical cyclone, as the cold front that sweeps up water vapour in the warm sector catches up with the warm front (Dacre et al., 2015). ARs are more frequent over ocean areas, as there is abundant moisture there, allowing cyclones to intensify substantially (Ralph, Dettinger, et al., 2020).

Based on SSM/I satellite imagery of ARs (figure 2.2) it looks like an AR is directly transporting moisture from the (sub)tropics to higher latitudes, and thus suggests that the tropics is the source of the water vapour in the AR (J. D. Wille et al., 2019). This is not actually the case, as ARs do not need to contain moisture of tropical origin, and most of them do not have a tropical origin (Ralph, Dettinger, et al., 2020, Dacre et al., 2015). This perception that ARs directly transport water vapour from the tropics to the higher latitudes may be because often, research on ARs is focused on the ”mature” stage of an AR, without focusing on the early formation of an AR (Ralph, Dettinger, et al., 2020). In reality, the AR loses moisture in the form of precipitation as air masses inside the AR ascend when they move poleward, and is replenished from horizontal moisture convergence along the cold front of the AR in the extratropics (Dacre et al., 2015, Bao et al., 2006). So then moisture source regions differ as an AR

evolves, with lower-latitude source regions being initially most important, and then later higher-latitude sources becoming more important as the AR moves poleward (Ralph, Dettinger, et al., 2020).

Vertically integrated humidity values are generally larger in the warm season, which is beneficial for the formation of ARs. Using seasonally uniform AR thresholds then leads to a clear maximum in AR frequency during summer. For this reason, it is currently still unclear whether many summer ARs identified using a fixed threshold are meaningful (Ralph, Dettinger, et al., 2020). Some AR detection algorithms use a combination of relative and absolute thresholds for IVT and/or IWV to counteract this seasonal variability (Guan & Waliser, 2015). Then, the threshold during winter is lower than during summer. Additionally, in polar regions atmospheric water vapour content is lower than in lower latitudes (Gorodetskaya et al., 2014, Guan and Waliser, 2015), which has to be accounted for in AR detection algorithms used for these regions. Section 2.3 provides more information about (polar) AR detection algorithms.

Zhu and Newell, 1998 found that there are typically three to five ARs in each hemisphere at any given time. More recently, Guan and Waliser, 2015 developed a technique for AR detection on the global domain and found that on average, there are 11 ARs globally at any given time, of which 24% make landfall. Upon making landfall, ARs can cause several effects, which the next section focuses on.

2.2.3. Effects of polar ARs

ARs can have a range of effects, both hazardous as well as beneficial. ARs become very important to snowfall and melt processes in the cryosphere when they reach the poles (J. D. Wille et al., 2021). In fact, ARs are critical in understanding cryosphere changes, due to their link to warming/melt, as well as anomalous precipitation events in the polar regions (Rutz et al., 2020). This section aims to give an overview of the different effects an AR can have in specifically the polar regions.

Precipitation

ARs reaching either the Greenland or Antarctic ice sheet are subject to orographic uplift due to the relatively steep slopes of the ice sheets' escarpment regions. These ARs are expected to strongly influence polar precipitation as they make landfall (Ralph, White, et al., 2020). Previous research has found that ARs are linked to precipitation events on the ice sheets (Gorodetskaya et al., 2014, J. D. Wille et al., 2021, Adusumilli et al., 2021). Despite the rare occurrence of ARs across Antarctica, ARs are responsible for a majority of extreme precipitation events and 10%-20% of the total accumulated snowfall across East Antarctica (J. D. Wille et al., 2021). Anomalous snow accumulation in East Antarctica in the 2009-2012 period can be attributed to a few extreme precipitation events, all of which were associated with ARs. As such accounting for ARs is crucial for understanding the East Antarctic SMB (Gorodetskaya et al., 2014). In West Antarctica, Adusumilli et al., 2021 found that 41% of increases in height during winter were caused by snow accumulation via extreme precipitation events, of which 63% were associated with ARs that only occurred a small fraction of the time.

Most AR-related precipitation occurs around the Antarctic coastline, although sometimes marine air intrusions linked with ARs can reach further inland (Turner et al., 2019, J. D. Wille et al., 2021).

J. D. Wille et al., 2021 found that while ARs appear to control long-term snowfall trends only in certain areas of Antarctica, they control interannual variability of snowfall across most of the ice sheet. Maclennan et al., 2022 found that while total AIS precipitation has decreased over the time period spanning from 1980 to 2020 (albeit at a non-significant rate), AR precipitation shows a clear and statistically significant upward trend.

Melt

In addition to transporting moisture, Atmospheric River (AR)s also have the ability to transport heat, which becomes consequential for the cryosphere. A single AR can cause strong snowfall as well as melt (J. D. Wille et al., 2019). Depending on which effect is stronger, the AR contributes either positively or negatively to the surface mass balance.

In the Arctic, Mattingly et al., 2020 analysed the surface energy balance, cloud properties, and synoptic- to local-scale atmospheric conditions during AR events, and found that in the immediate vicinity of an AR making landfall, the atmospheric conditions over the Greenland Ice Sheet (GrIS) were cloudy, moist, warm, and windy. This resulted in enhanced downward longwave radiation and warm air advection causing ice mass on the GrIS to decrease. Similar results were found by J. D. Wille et al.,

2019 for West Antarctica. When ARs make landfall over the WAIS, they trigger melting through various physical mechanisms such as turbulent heat fluxes and the development of mixed-phase clouds resulting in enhanced downward longwave radiation. The impact of ARs on the melt is currently limited in Antarctica, but it is suggested that continued warming and an increase in AR activity could lead to an increased melt frequency (J. D. Wille et al., 2019).

Winds

Atmospheric River (AR)s are inevitably linked with winds, as they are defined by Integrated water Vapour Transport (IVT) and wind is a necessary part in IVT calculations (Dettinger et al., 2020). Waliser and Guan, 2017 found a close association between ARs and global wind extremes. They found that in mid-latitude regions about 30% to 60% of all wind extremes coincided with ARs, and that the association of ARs with wind extremes extended all the way onto northern Antarctica, where extreme winds typically do not occur in the absence of AR conditions. Similar relationships occur between AR occurrence and peak precipitation events (Waliser & Guan, 2017).

Foehn events

ARs can also trigger foehn events due to warm and moist air advection associated with the AR. The foehn event then causes high temperatures and subsequent melting events, for example the record high temperatures in the Antarctic Peninsula in 2015 (Bozkurt et al., 2018). Combined with the potential of ARs to produce high-impact coastal winds and extreme events (Waliser & Guan, 2017), it can be argued that ARs play a crucial role in the occurence of foehn events, as well as in determining the extremity of these events (Bozkurt et al., 2018). As for the Arctic, Mattingly et al., 2018 also found that a foehn effect caused enhanced melt energy in the northeast GrIS ablation zone during strong AR events affecting north-west Greenland.

Antarctic shelf instability

An increase in melt can lead to enhanced surface runoff, ponding and hydrofracturing (J. D. Wille et al., 2019). These effects, as well as foehn winds, can in turn be linked to ice-shelf collapse. As ice shelves collapse, the loss of the buttressing effect from these ice shelves leads to further continental ice loss and subsequent sea-level rise. Overall, 60% of calving events from 2000–2020 were triggered by atmospheric rivers (J. D. Wille et al., 2022).

2.2.4. Expectations for the future

Knowing the effects ARs can have on polar regions and the SMB of the ice sheets, it is important to consider future changes in AR frequency and intensity as a response to climate change.

The thermodynamic response of ARs to climate change means that ARs will contain more moisture in the future. Precipitation related to ARs is expected to increase due to the moistening of the atmosphere and the thermodynamic response of IVT to warming (Payne et al., 2020). The response of atmospheric circulation to warming is much less certain, but ARs have been shown to shift towards the poles in recent years, which is consistent with the poleward shift of the westerly jet (Espinoza et al., 2018, Ma et al., 2020).

Future projections under the Representative Concentration Pathway (RCP) 4.5 and RCP8.5 warming scenarios indicate that there will be fewer ARs in the future, but also that ARs will be longer, wider, and have stronger IVT. Due to these changes, the frequency of AR conditions increases significantly ($\sim$50% globally), and the mean magnitude increases by 25% globally (Espinoza et al., 2018).

2.3. Detecting Atmospheric Rivers

Having discussed the basics of what an atmospheric river is and what its effects are, it is time to focus on how an AR can be detected.

Since the term atmospheric river was first used by Newell et al., 1992, a lot of different authors have developed numerous different methods to identify ARs (Ralph, White, et al., 2020).

AR identification methods used in literature differ in a variety of ways, but generally follow the following steps:

- First, a characteristic variable is chosen to perform thresholding, typically either Integrated Water Vapour (IWV) or Integrated water Vapour Transport (IVT).

- Then, a decision is made whether the threshold is held constant, or if it is relative. If a relative threshold is chosen, a decision also has to be made whether the threshold changes as a function of location, season, and/or climatology.
- Next, the actual thresholding value is chosen. In the case of an absolute threshold a certain value is chosen (e.g. IVT $\geq$ 250 $kg\ m^{-1}\ s^{-1}$), while for a relative threshold a percentile is used (e.g. IVT $\geq$ 85th percentile).
- Then, geometric criteria for AR identification are defined. Length, width, and aspect ratio are the most common criteria.
- Optionally, some methods also identify the centroid and directional orientation of the AR.
- Next, a decision is made on how to track the ARs, either Eulerian (looking at single time slices of spatial fields) or Lagrangian (following the AR).
- Optionally, a temporal criterion may be included, which means that the AR must be consistently identified over a number of subsequent time-steps.
- Optionally, some detection algorithms end in filters that filter out non-AR phenomena that may have similar features to ARs, such as tropical cyclones.

ARs are either identified subjectively by analysis, or objectively using an algorithm. Alternatively, machine learning may be used to identify ARs without requiring a specific threshold or geometric criteria (Muszynski et al., 2019).

Figure 2.3 summarises the differences between AR algorithms. The parameters used in the Antarctic AR detection algorithm developed by J. Wille, 2021 are highlighted in green. This is the detection algorithm used in this thesis and is further touched upon in chapter 3.

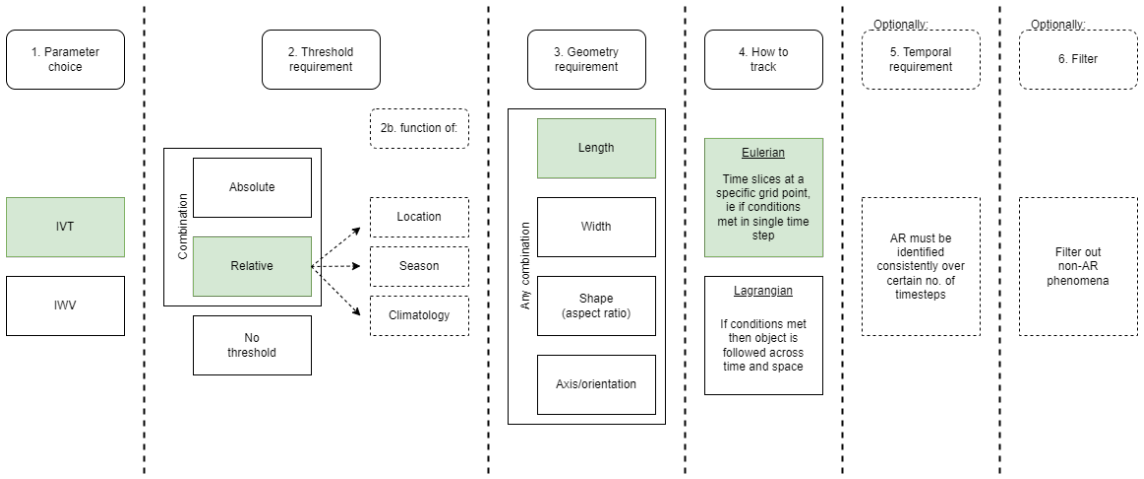

Figure 2.3: Visualisation of how an AR detection algorithm is built, showing the different steps and the different options per step. Boxes that have a dotted outline are optional choices that may be skipped. The green shaded boxes are the choices made for the AR detection algorithm as described by J. D. Wille et al., 2021, which is used in this thesis.

2.3.1. ARTMIP

Looking at the different choices that can be made in building an AR detection algorithm, it is not surprising that there are a lot of different AR algorithms being used by researchers. Recently, efforts have been made toward greater agreement on the definition of ARs as well as on the methods best suited to identify them. An important part of this is the Atmospheric River Tracking Method Intercomparison Project (ARTMIP) (Ralph, White, et al., 2020).

ARTMIP aims to understand and quantify the uncertainties in AR science based on different detection algorithms alone. Additionally, it strives to provide the scientific community with information on different methodologies and help scientist decide on the most appropriate algorithm for a specific question or region of interest (Shields et al., 2018).

Previous studies used different atmospheric data-sets, over different time periods and often also over a certain region of interest rather than the entire globe, making it difficult to compare the performance of different detection algorithms. In ARTMIP, analyses are performed using the same atmospheric data set over the same period, namely Modern-Era Retrospective analysis for Research and

Applications, version 2 (MERRA-2) reanalysis data from January 1980 to June 2017. The analysis is performed over the entire globe, allowing for a clean comparison of AR-related metrics across all methods (Rutz et al., 2019).

The metrics proposed include AR frequency, duration, intensity, and precipitation attributable to an AR (Shields et al., 2018).

2.3.2. Polar detection algorithm

Detecting ARs in the polar regions varies slightly from detecting ARs around other latitudes. This is mainly because the polar troposphere has a decreased saturation capacity, and therefore low atmospheric water vapour content compared to the entire globe (Gorodetskaya et al., 2014, Guan and Waliser, 2015).

Generally, relative thresholds perform better over polar regions than methods using a single absolute threshold (Rutz et al., 2019).

Optionally, an absolute threshold may be added in addition to the relative threshold, as polar areas have low moisture content, and therefore IVT values corresponding to a percentile can be very small.

The detection algorithm developed by J. D. Wille et al., 2021 that is used in this thesis does not use an additional absolute threshold, instead a higher percentile IVT (98th percentile) is used to account for the reduced atmospheric water vapour content in polar regions. The 98th percentile was found to avoid detecting shapes that lack a clear filament of narrow but intense moisture transport extending from the subtropics and midlatitudes (that therefore do not qualify AR criteria).

A notable difference in polar detection algorithms using IVT compared to global algorithms is that only the meridional component of IVT is used, while studies outside polar areas also use the zonal component of IVT (Payne et al., 2020, Zhu and Newell, 1998).

Whether a detection algorithm based on IWV or IVT is more suitable depends on the atmospheric effects studied. IWV is a slightly more appropriate choice when studying surface melting caused by ARs, because ARs detected using IWV last slightly longer after landfall when melting is still ongoing. Meanwhile, vIVT is more appropriate for studying snowfall patterns, as adding the meridional wind reflects the dynamical processes that lead to precipitation (J. D. Wille et al., 2021). Both IWV as well as IVT detection algorithms were found to lead to similar AR frequencies in polar regions (J. D. Wille et al., 2019).

2.4. ICESat-2

The Ice, Cloud and land Elevation Satellite-2 (ICESat-2) is part of NASA's Earth Observing System and was launched in September 2018. The satellite carries a single instrument, the Advanced Topographic Laser Altimeter System (ATLAS), and provides coverage of the ice sheets up to 88° latitude, repeating its ground tracks every 91 days (NASA, 2018). Its main purpose is to measure the height of our planet's ice in unprecedented detail, but besides this it also provides information on land and vegetation heights on a global scale.

2.4.1. Concept

ATLAS measures height by timing how long it takes individual photons to travel from the satellite to Earth and back (NASA, 2018).

ATLAS uses green laser light with a wavelength of 532 nm, releasing 10,000 laser pulses per second. As a pulse is fired, ATLAS splits the single laser beam into six laser beams, so more ground is covered. The six beams are arranged in three pairs, allowing scientists to gauge the slope of the terrain in one pass.

The six beams have unequal energy, with three strong beams and three weak beams (Neumann et al., 2019). The beams contain approximately 80% of the total laser pulse energy, with each strong beam containing 21% of the transmitted energy, and the weak beams each containing 5.2%, thus the strong beams are roughly 4 times stronger. The strong/weak beam configuration was designed to provide the necessary dynamic range to capture enough return photons for both bright (e.g. ice) as well as dark surfaces (e.g. the ocean or vegetation). Both the strong and weak beams provide sufficient signal-to-noise ratios for altimetry measurements over bright surfaces such as ice.

Each photon hitting a detector is recorded individually, this technique is known as photon counting. ATLAS provides the arrival time of individual photons, which can be assigned latitudes, longitudes and

heights relative to a reference ellipsoid when combined with the pointing angle of individual beams and the position of ICESat-2 in space (B. Smith et al., 2019). For bright surfaces, only about a dozen of photons from each laser pulse are detected upon returning to the satellite, while approximately 10^{14} photons leave the ATLAS sensor with each pulse (Neumann et al., 2021).

Figure 2.4 shows a schematic of the ATLAS six beam setup. Beam pair separation is 3.3 km, while the beam pair width is 90 m. Each laser pulse has a 17 m diameter footprint and an along-track sampling interval of 0.7 m.

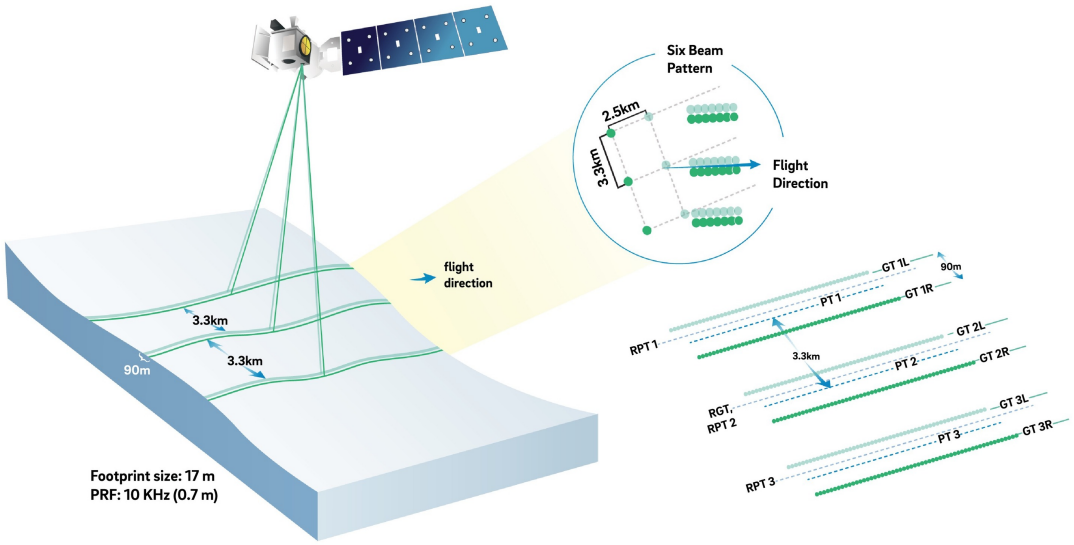

Figure 2.4: Schematic of the ATLAS six beam setup. The central Reference Pair Tracks (RPT) follows the Reference Ground Track (RGT). GTNX where N is the beam pair number and X is L (left) or R (right) are the ground tracks generated by successive ATLAS spots (green circles). Here ATLAS is shown in the forward direction, which means that the weak beams are on the left side of the beam pair. In this figure the separation of ground tracks within each pair is greatly exaggerated compared to the separation between RPTs (via B. Smith et al., 2019)

ICESat-2 has different modes depending on where in its orbit it is. Over the polar regions, the satellite is in repeat-track mode enabling seasonal repeat measurements (Markus et al., 2017).

In the mid-latitudes the goal of ICESat-2 is to fill in the gaps between reference ground track (RGT)s. To do this, ICESat-2 points off-nadir above land to create a dense mapping of canopy and ground heights (Neumann et al., 2019).

Over the ocean ICESat-2 generates ocean elevation maps, but it also performs regular calibration maneuvers. Altimetry data collected during ocean scan maneuvres is used for the generation of ocean elevation maps as well as to calibrate pointing and separate these errors from ranging errors.

2.4.2. ICESat2 vs ICESat

ICESat-2 has multiple improvements over its predecessor, the ICESat mission. ICESat's Geoscience Laser Altimeter System (GLAS) only had a single beam with a broad footprint (B. Smith et al., 2019). This reduced the accuracy of single shot heights due to waveform broadening, and also introduced uncertainties in height-change estimates from repeat-track analysis due to non-exact repeat tracks. This lead to limited performance when measuring sloping surfaces, making it difficult for researchers to tell whether ice had melted between passes, or if the laser beam was simply pointed a bit off the path and down a hill (NASA, 2018).

ICESat-2 can determine the slope across the laser's path on a single pass thanks to the pairs of beams used (NASA, 2018). With the beam pairs, one beam is to the left and one beam is to the right of the RGT every time the satellite passes over, making it possible to calculate local cross-track slope and interpolate the elevation to the RGT. Thanks to this concept, elevation change can be determined between subsequent passes for ICESat-2. In contrast, for ICESat several years of data were required before surface slope and elevation change could be determined, and even then under the assumption that the slope did not change over that time period.

2.4.3. Precision and performance

How precise the elevation measurements are depends on the number of data points collected over a given area. Over large areas with bright surfaces such as the Antarctic ice sheet, ICESat-2 gathers enough data points to estimate the annual elevation change within 4 millimeters (NASA, 2018).

Over relatively flat reflective surfaces, such as the interior of the Antarctic ice sheet, 1.6–12.0 return photons per pulse are expected for the strong beams and 0.4–3.0 photons for the weak beams (Markus et al., 2017). Little pulse spreading or geolocation error due to slopes is expected as the interior is relatively flat and smooth, leading to a standard deviations of the signal photons averaged over 100 shots of 1.5 cm and 2.8 cm for the strong and weak beams respectively (Neumann et al., 2019).

Over low reflectivity surfaces, such as ocean water, signal photon rates and background photon rates are significantly lower: 0.2-1 return photons per pulse are expected for the strong beams and 0.05-0.2 photons for the weak beams (Markus et al., 2017). The standard deviation of the returned photons for 100 shots is 3 cm for the strong beam and 5 cm for the weak beam (Neumann et al., 2019).

If there is a significant surface slope within a laser footprint, the return pulse broadens, which increases the standard deviation of the signal photon distribution (Neumann et al., 2019). Over outlet glaciers, the standard deviation is predicted to be 10 cm and 20 cm for the strong and weak beams respectively.

2.4.4. Data levels

The National Snow and Ice Data Center in Boulder, Colorado, distributes various ICESat-2 data products, at multiple data processing levels. Firstly, there are two Level-1 products: ATL01, which computes photon times of flight, and ATL02, which removes biases in timing and pointing measurements and corrects for the effects of temperature and voltage variations on ATLAS electronics. Next, there are two Level-2 scientific data products: ATL03, which reports latitude, longitude, and elevation for each photon, and ATL04 with atmospheric profiles of normalised relative backscatter. The Level-3 products comprise surface-specific data products for land ice, sea ice, the atmosphere, vegetation and land, and oceans and inland water. The ATL03, ATL06, ATL11 and ATL15 products will be elaborated on in the following paragraphs. ATL15 is the (level 3B) gridded data product used in this thesis, and the other data levels are the basis of ATL15.

ATL03

The ATL03 data product is used by higher level surface-specific data products to determine glacier and ice sheet height, sea ice freeboard, vegetation canopy height, ocean surface topography, and inland water body height.

ATL03 is a level-2 product. ATL03 combines the photon times of flight provided by ATL02 with the position of ICESat-2 in orbit to determine the latitude, longitude, and height of individual received photons with respect to the WGS-84 ellipsoid (Neumann et al., 2019).

The return photons captured by ICESat-2 contain both signal and background photon events. ATL03 processing uses an algorithm to determine whether a photon is likely to be a signal or noise by generating along-track histograms and finding regions where the photon event rate is significantly larger than the background photon event rate (Neumann et al., 2021). Photons are classified depending on the Signal-to-Noise ratio (SNR): high-confidence signal (SNR ≥ 100), medium-confidence signal (100 > SNR ≥ 40), low confidence signal (40 > SNR ≥ 3), or likely background (SNR < 3) (Neumann et al., 2019).

Geolocating every received photon would be computationally very expensive. Instead, a single photon in every 20 m along-track segment on the surface is selected, referred to as a reference photon. The reference photon is chosen from high-confidence signal photons if present, or medium- or low-confidence photons if no high-confidence photons are found. If there are also no medium- or low-confidence photons, a likely background photon is used as the reference photon.

A number of geophysical corrections are required to account for deformations (Neumann et al., 2021). ATL03 photon height (H_{GC}) is then computed using equation 2.1.

$$H_{GC} = H_P - H_{OPT} - H_{OL} - H_{SEPT} - H_{SET} - H_{TCA} \tag{2.1}$$

where H_P is the photon height about the WGS-84 ellipsoid, H_{OPT} is ocean pole tides, H_{OL} is the height of the ocean load tide, H_{SEPT} is the height of the solid earth pole tide, H_{SET} is the height of the solid earth tide, and H_{TCA} is the height of the total column atmospheric delay correction.

ATL06
ATL06 is a level 3A product containing Land Ice Along-Track Height, derived from the ATL03 product. Besides altimetry data (latitude, longitude, height, uncertainty, and timing of segments), the ATL06 product contains additional parameters that allow users to distinguish high-quality segments from segments that potentially have large errors (B. Smith et al., 2019).

ATL11
ATL11 is a level 3B product providing time series of land-ice surface heights, derived from the ATL06 product (S. Smith et al., 2022). Height changes are computed along individual ICESat-2 ground tracks in polar regions for repeat observations every 91 days. It is intended primarily as an input for higher level gridded products, but can also be used on its own.

ATL15
ATL15 is a level 3B product containing Antarctic/Greenland Gridded Ice Sheet Height Change (B. Smith et al., 2022). The data set contains land ice height changes for the Antarctic ice sheet and regions around the Arctic at 3-month intervals. The data is derived from the ATL11 product. Four spatial resolutions are available: 1 km, 10 km, 20 km, and 40 km. This coarser resolution allows for visualisation of height-change patterns and the calculation of integrated regional volume change.

The ATL15 algorithm works through a couple of steps to fit height-change maps to the ATL11 repeat-track-corrected height estimates:

- Define subdomains: to reduce computational costs the ice sheet is divided into square tiles of 61x61 km. Independent calculations are performed on tiles centered on a 40 km grid to minimise edge effects.
- Select high-quality data: Reliable along-track and crossover ATL11 data is selected based on a combination of geographic and parameter based factors.
- Compute two-component solution: the solution is a combination of the model comprising the interpolating funtions between the model parameters and ATL11 height measurements and a set of estimated height biases, and a regularised least-squares solution which identifies the simplest model that fits the height data, while statistically outlying measurements are rejected. This is iterated to remove outliers.
- Calculate model errors: a big error source in ATL11 is the effect of geolocation errors over sloping surfaces.
- Combine solutions: Error estimates are calculated, each tile solution is recomputed by applying linear constraint at the edges, and the solutions are combined using a weighting scheme to form the final ATL15 product. Each data point is assigned an error estimate based on the ATL11 data and bias-parameter constraints.

The resolution of ATL15 is limited by the spatial resolution of the ICESat-2 tracks, the temporal sampling of the tracks, and the resolution of the grids chosen for these data products.

3
Methods

The methods can be roughly divided into two parts. The first part focuses on AR detection and precipitation attribution using reanalysis data. The second part compares ICESat-2 observations with the results of the first part.

3.1. Area of interest and data used

Firstly, the area of interest is briefly introduced, as well as the data used. A combination of reanalysis data and satellite altimetry data is used.

3.1.1. Area of interest

AR detection and precipitation contribution are performed for the whole of Antarctica and its surroundings, including the ice shelves and the Southern Ocean. The reanalysis data spans from 37.5° S to 85° S latitude and -180 to 180° longitude, covering the entirety of Antarctica except the interior at latitudes greater than 85 degrees South. This also incluses the ice shelves. This latitude range is identical to the latitude range as used by Maclennan et al., 2022, a study on contribution of atmospheric rivers to Antarctic precipitation. By using the same latitude range, the results from Maclennan et al. can be compared to the AR precipitation computed using the algorithm used in this thesis.

The ICESat-2 data spans from 60° S to 88° S latitude and -180 to 180° longitude. As latitudes up to 85° S are considered in the reanalysis data, the ICESat-2 data is cropped to 60° S to 85° S. Although the region from 37.5° S to 60° S is not covered by the ICESat-2 data, this is not a problem. The ATL15 product only covers land ice height changes, and all of Antarctica's land ice is located south of 60° S.

All ocean pixels are masked out using a land/ocean mask. For Antarctica, a distinction can be made between only land(/land-ice) or whether ice shelves should be included. Figure 3.1 illustrates the differences between including and excluding floating ice. The mask was provided by Morlighem, 2020 and contains 5 classes: [0 = ocean, 1 = ice-free land, 2 = grounded ice, 3 = floating ice, 4 = Lake Vostok], with a spatial resolution of 500m x 500m. The mask was regridded to the correct resolutions for ERA5/MERRA-2/ATL15 data using nearest neighbour interpolation, so as to keep the integer values. After regridding, the mask is modified so that ice-free land, grounded ice, floating ice, and Lake Vostok are all set to 1, masking out only ocean pixels.

3.1.2. Reanalysis data

Reanalyses are gridded global meteorological data sets that are available over long time periods. These data sets are produced by assimilating different kinds of available observations. Data assimilation is a process in which available information is used to estimate the state of a system as accurately as possible. Information used in atmospheric data assimilation typically includes observations and forecasts from numerical weather prediction (NWP) models, where the NWP forecast serves as a first guess of the atmospheric state that is then updated using observations. To create reanalysis data, data assimilation is performed for past periods, using a current NWP model and observational data that is available for those periods (Parker, 2016).

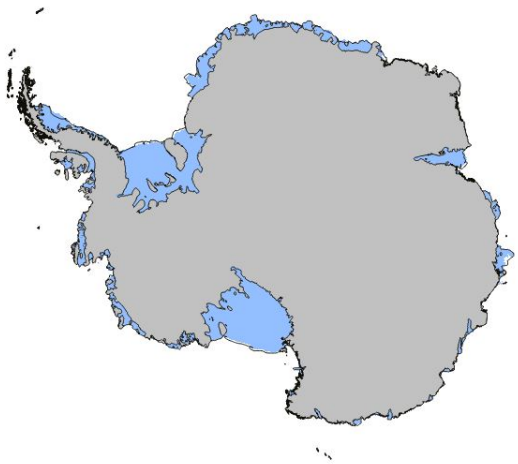

Figure 3.1: Map of land/sea mask Antarctica and ice shelves. Grey is ice-free land and grounded ice, light blue is floating ice (dataset provided by Morlighem, 2020)

Reanalysis products provide comprehensive, gridded estimates of atmospheric conditions at regular intervals over long time periods, which makes them very convenient for many climate and atmosphere related studies (Parker, 2016). Reanalysis data is also very useful in areas where there are little observations, such as the polar regions.

Reanalysis data is sometimes referred to and used in a similar way as “observations”, but some researchers warn that reanalysis data should not be equated with ”real” observations and measurements. The most important difference between reanalysis data and real observations is that errors and uncertainties associated with reanalysis results are often less well understood than those associated with observations (Parker, 2016).

Reanalysis products are often used for studying ARs, especially in polar regions, as there are limited observations available (Ralph, White, et al., 2020). The benefit of reanalysis data is that it is available at both a high temporal as well as spatial resolution, and there is a long record often dating back several decades. The resolution and length of the record available differs per reanalysis data set. A downside of reanalysis data is that biases can be introduced by non-perfect models, which is particularly relevant in high-latitude regions such as Antarctica (Hassler & Lauer, 2021). This is because the fields are largely driven by the model physics and parameterisations, as there are very few observations available.

For this study, based on literature, Modern-Era Retrospective analysis for Research and Applications, version 2 (MERRA-2) and ERA5, the fifth generation ECMWF atmospheric reanalysis of the global climate, are used. Both data-sets have been shown to perform well in polar regions.

MERRA-2

MERRA-2 is the baseline data set for the ARTMIP (Shields et al., 2018), therefore it is used in a lot of AR studies. MERRA-2’s resolution of $\sim$50 km is sufficient to resolve weather features, such as atmospheric rivers, along with their associated precipitation (Shields et al., 2022). However, the modest horizontal resolution (0.5° × 0.625° longitude-latitude) may lead to an underestimation of the highest precipitation rates, such as those associated with ARs, which also means an underestimation of the total precipitation assigned to ARs (Maclennan et al., 2022). MERRA-2 is also used by Maclennan et al., 2022’s study on the contribution of ARs to Antarctic precipitation.

Two different data sets are used. For this thesis a 3-hourly interval is used, but data is also available at hourly resolution.

Firstly, the vIVT is a parameter already provided in the dataset tavg1_2d_int_Nx (M2T1NXINT): Vertically Integrated Diagnostics specifically. Only the meridional component is required, VFLXQV.

Secondly, precipitation is computed from the tavg1_2d_lfo_Nx (M2T1NXLFO): Land Surface Forcings dataset, by summing PRECCUCORR (liquid water convective precipitation, bias corrected), PRE-

CLSCORR (liquid water large scale precipitation, bias corrected), and PRECSNOCORR (snowfall, bias corrected). The precipitation is entirely model-generated, and not observation-corrected.

ERA5
ERA5 is the fifth generation ECMWF atmospheric reanalysis of the global climate, and is an improvement over its predecessor ERA-Interim.

ERA5 has a higher resolution than MERRA-2, namely 0.25 x 0.25°. Previous analysis has shown that there is very little difference in AR detection frequency when comparing ERA5 and MERRA-2 ARs detected using the same algorithm (J. D. Wille et al., 2021). Combining these two facts makes it an interesting second data set to see whether the higher resolution leads to a better representation of AR precipitation.

Two different ERA5 datasets are used. Firstly, the "ERA5 hourly data on pressure levels from 1959 to present" data-set is used to detect the ARs at a 3-hourly time interval, specifically 00:00hr, 03:00hr, 06:00hr, 09:00hr, 12:00hr, 15:00hr, 18:00hr, 21:00hr every day.

There is no vIVT parameter provided in the dataset, therefore the vIVT is calculated using the specific humidity q $[kg\ kg^{-1}]$ and the meridional wind component V-wind $[m\ s^{-1}]$ at different pressure levels. Pressure levels used range from 300 hPa to 1000 hPA.

So, the vIVT has to be calculated based on two variables over multiple pressure levels, which means that data-sets can get very big. To be able to handle the large amount of data, it is first opened and preprocessed in a separate script before being used in the AR detection/precipitation algorithm.

Secondly, the "ERA5 hourly data on single levels from 1959 to present" data-set provides the total precipitation in meters at a 3-hourly time interval.

3.1.3. Satellite altimetry data

ICE-Sat2 was already introduced in chapter 2. ATL15 data is used, a level 3B product containing Antarctic Gridded Ice Sheet Height Change. ATL15 provides height-change maps at 3-month intervals at coarser resolution, allowing visualisation of height-change patterns. Based on the resolution of the reanalysis data-sets used in this thesis, the resolution of ATL15 should be good enough to be able to compare ICESat-2 derived height changes with AR precipitation found in reanalysis data. In this case the 10 km resolution data product is used.

Cycles 1 and 2 (all data collected before April 2020) were collected with larger off-nadir angles than is typical for other cycles, and as a result these data have larger errors than other cycles (B. Smith, 2022). Therefore, these cycles should be treated with caution. Cycle 3 provides the first high-quality reference track data.

3.2. AR detection and precipitation attribution

3.2.1. AR detection

The detection algorithm used in this thesis is the detection algorithm described bt J. D. Wille et al., 2021. This detection algorithm was already mentioned in chapter 2, and was developed especially for use in polar regions. This detection algorithm was also used by a number of other studies on ARs (Maclennan et al., 2022, Pohl et al., 2021); Adusumilli et al., 2021 used a previous version of the same detection algorithm (described in J. D. Wille et al., 2019).

The algorithm uses the meridional (v) component of Integrated water Vapour Transport (IVT), vIVT. The meridional component is used because it reflects the dynamical processes associated with ARs (Maclennan et al., 2022).

The 98th percentile is computed over all monthly vIVT values. The data record used to compute the vIVT threshold value should be long, as a single extreme event in a short time period (ie only a couple of years) could lead to a threshold that is too high and thus an underestimation of ARs. For this thesis, the 98th percentile threshold vIVT is computed over the time period 1980-2021.

Additionally, the object has to extend at least 20° in the meridional direction.

Then, consecutive grid points above the relative threshold that also extend at least 20° in the meridional direction are classified as ARs.

MERRA-2 contains vIVT as a variable, but ERA5 does not. Therefore vIVT is first calculated using equation 3.1.

$$vIVT = \frac{1}{g} \int_{1000\ hPa}^{300\ hPa} qV\, dp \tag{3.1}$$

Where g is the Earth's gravitational acceleration, q is the specific humidity in $[kg\ kg^{-1}]$, and V is the meridional wind component in $[m\ s^{-1}]$. $vIVT$ is in $[kg\ m^{-1}\ s^{-1}]$.

The detection algorithm is run for ERA5 and MERRA-2 separately, at 3-hourly resolution. In this stage ocean pixels are not yet masked out, to allow for comparison with a previous study by Maclennan et al., 2022.

3.2.2. AR-related precipitation

AR precipitation and AR contribution to total precipitation are computed using the method detailed in Maclennan et al., 2022.

AR associated precipitation is defined as precipitation that falls directly within each AR footprint, as well as in the 24 hours after an AR was detected. The period of 24 hours after AR detection was previously used by multiple studies (Maclennan et al., 2022, Adusumilli et al., 2021, J. D. Wille et al., 2021), and is likely to be more on the conservative side.

This 24 hour time period was selected after careful analysis of precipitation rates in MERRA-2 during and after ARs (Maclennan et al., 2022). Precipitation rates decrease by half in the first $\sim$10 hours after an AR has made passage, and after that the precipitation rates decrease very slowly.

An additional benefit of using a 24 hour window is that is available in the 3-hourly temporal resolution that was used in AR detection. So, precipitation at the time of AR detection as well as the 8 following time steps is attributed to the AR.

It is likely that the same AR is detected in the same location in subsequent time steps as it evolves. In that case precipitation during the AR is attributed to the AR, as well as the precipitation that falls within the 24 hours following the last time the AR was detected in a specific location.

In some cases a new AR is detected before the 24 hour window is over. For example, if an AR is detected at $t = 0$, the algorithm assigns the precipitation in the same location of the following 8 time-steps to that AR, so until $t = 8$. However, if a new AR is detected at $t = 6$ (ie 18 hours after AR detection), the precipitation should not be attributed to both ARs and thus counted twice. In these cases, the 24 hour window restarts when the new AR is detected, so the precipitation is only assigned to the newly detected AR.

Computing total precipitation weight

The AR precipitation as well as the total precipitation are computed for ice-free land, grounded ice, and floating ice.

The precipitation in reanalysis data is given as the mean amount in $m\ (w.e.)$ over the entire grid cell. Not every grid cell has the same area since the Earth is a sphere, this is especially important to take into account near the poles. In order to compute the weight of the precipitation over Antarctica, it is necessary to compensate for the differences in grid cell size.

Using MERRA-2 resolution and the grid-area file, the area of Antarctica (including ice shelves) is estimated to be 12,739,157 km^2, which corresponds with values found in literature. This is also done for ERA5 resolution, finding an estimated area of 12,803,831 km^2. The difference may be due to the resolution of the data.

The precipitation in MERRA-2 reanalysis data is given as the mean amount in $[kg\ m^{-2}\ s^{-1}]$ over the entire grid cell. The precipitation value is multiplied by 3600 to go from seconds to hours (see equation 3.2). As the data is 3-hourly, the resulting hourly value is multiplied by 3 to remove time from the units. Knowing the total area of Antarctica and compensating for grid cell size, the weight of precipitation is computed by multiplying the precipitation grids with the grid-area file to correct for the different grid sizes, and then dividing by the total area of Antarctica.

$$Precipitation\ [kg\ m^{-2}\ s^{-1}]\ *3600s\ =\ Precipitation\ [kg\ m^{-2}] \tag{3.2}$$

$$Precipitation\ [kg\ m^{-2}]\ *\ Area\ [m^2]\ =\ Weight\ of\ precipitation\ [kg] \tag{3.3}$$

$$Weight\ of\ precipitation\ [kg]\ /\ 10^{12}\ =\ Weight\ of\ precipitation\ [Gt] \tag{3.4}$$

In ERA5 reanalysis data, precipitation is given as the mean amount in $[m\ (w.e.)]$ over the entire grid cell. Precipitation is an accumulated parameter, which means that values represent the accumulation up to 'time'+'step', from the previous 'step', and at 'step' 0 all data is zero. Therefore, to get the precipitation in the 24 hours following AR detection, the precipitation in hours 1 up until 25 has to be summed.

To convert this to the weight of precipitation in Gt, the following relationship is used:

$$1\ m\ w.e.\ =\ 1000\ kg\ m^{-2} \tag{3.5}$$

$$1000\ mm\ w.e.\ =\ 1\ m\ w.e. \tag{3.6}$$

$$1\ mm\ w.e.\ =\ 1\ kg\ m^{-2} \tag{3.7}$$

Then using the land/ocean mask the precipitation in ocean pixels is masked out, keeping only the precipitation over land and ice shelves.

3.3. Comparison of reanalysis data and ICESat2 observations

The amount of AR precipitation found using reanalysis data is not an observation, but rather an expectation of the AR precipitation. The next step is therefore to compare the attributed AR precipitation to ICESat-2 observations. Height change estimates from ICESat-2 can be unambiguously linked to surface and dynamic processes, as there is negligible penetration of the laser into the snowpack (Adusumilli et al., 2021). However, it does not capture the different processes responsible for observed height change separately.

It is assumed that height change is mainly driven by dynamic changes and precipitation anomalies. The ice sheet gains mass through precipitation, and assuming that the ice sheet is in a long-term equilibrium, it loses a similar amount through discharge. Then, the precipitation anomaly is the height change that would be expected due to precipitation, which can be observed in the ICESat-2 data. In regions where the ice velocity is low, the ICESat-2 observed height changes should then be roughly equal to the precipitation anomaly. From here on, all analyses are therefore performed using the anomalies rather than the absolute values. In regions where the ice velocity is high, a large part of the observed height changes are likely linked to ice dynamics rather than precipitation or other atmospheric processes. This may be solved by masking out regions of high velocity, however, this may also remove regions of high AR precipitation contribution.

The analysis is done per drainage basin. The AR precipitation analysis already showed that there were significant differences between different regions. Dividing Antarctica into these drainage basins ensures that signals are not averaged out and lost. The drainage basin definition produced by Zwally et al., (2012) are used (see figure 3.2a). The map was created using surface elevation data derived from ICESat, with the drainage basins delineated based on ice source.

3.3.1. Velocity-based data masking

Figure 3.2b shows the InSAR-Based Antarctica Velocity Map available from NSIDC. The map shows that ice velocities are generally largest on the ice shelves. This does not affect the results as the ice shelves are not included in the drainage basin mask, and are therefore already masked out.

Ice velocities on the Antarctic plateau are very small, less than 5 m/year. Besides the ice shelves, ice velocities are largest near the coast. Ice dynamics are assumed to be the major source of height changes observed by ICESat-2 besides precipitation. In regions where there is a lot of ice dynamics, precipitation will thus have a smaller contribution to observed height change than in regions where there is little to no ice dynamics. Therefore, known regions with a lot of ice dynamics are masked out.

The ice velocity is provided in a component in the x-direction (VX) and the y-direction (VY). To convert the VX and VY velocity components into magnitude (speed), equation 3.8 is used. To identify height difference measurements that are likely not strongly affected by ice dynamics, a mask is created that masks out areas where the ice speed exceeds 100 meters per year (see appendix A).

$$Speed = \sqrt{VX^2\ +\ VY^2} \tag{3.8}$$

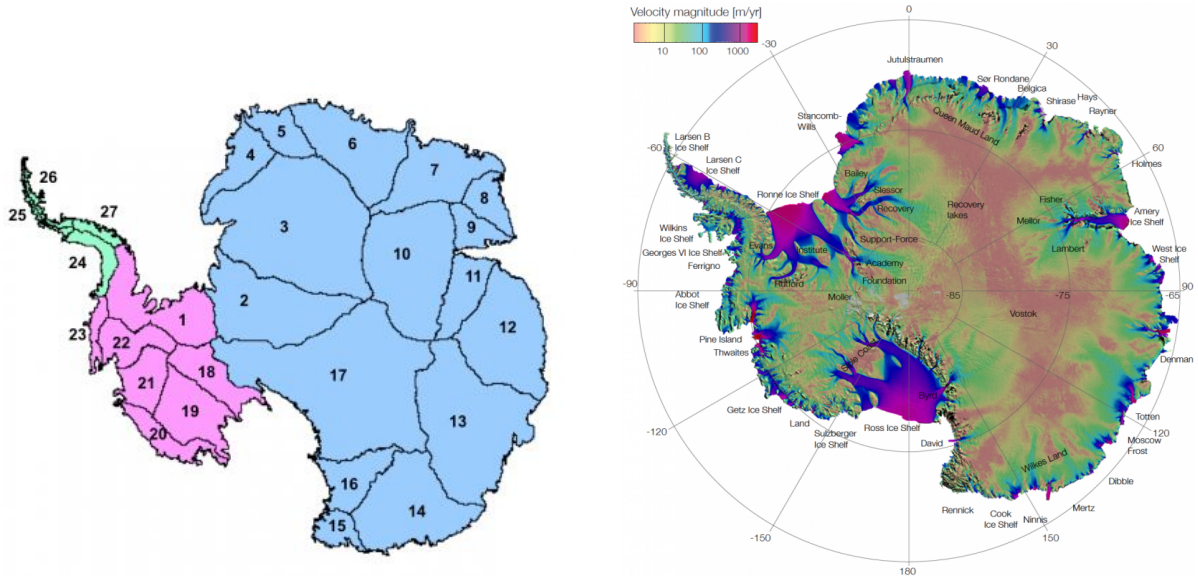

Figure 3.2: a) Antarctica drainage basin and ice sheet definitions, produced by Zwally et al., (2012) and used by IMBIE 2016. Basins in East Antarctica are shaded blue, basins in West Antarctica are shaded pink, and basins in the Antarctic Peninsula are shaded green. b) MEaSUREs InSAR-Based Antarctica Ice Velocity Map (nsidc-0484) available from the NSIDC DAAC. Velocity is in meters per year. Highest velocities appear in magenta and red, intermediate velocities appear in blue and green, and lowest velocities appear in yellow and peach. Credit: AIV

3.3.2. Snow density

The units of the reanalysis data are in $[mm\ w.e.]$. Snow has a significantly lower density than water, and therefore the actual height changes caused by precipitation are larger than the precipitation values found in the previous AR precipitation analysis. It is assumed that all precipitation falls in the form of snow. In reality a small fraction of the precipitation falls as rain, but rain is generally limited to the ice shelves (Maclennan et al., 2022), which are outside the drainage basins and thus not under consideration here.

To convert precipitation from $[mm\ w.e.]$ to snow depth $[m]$ equation 3.9 is used.

$$snow\ depth = \frac{SWE}{\rho_{snow}} \tag{3.9}$$

where SWE is the snow water equivalent, or the amount of water that would result from a snow pack melting instantaneously. In this case the precipitation WE is the same as the SWE, as it is assumed that all precipitation falls as snow.

The density of snow in Antarctica can vary widely, which means that using a constant density for snow in Antarctica can lead to inaccuracies in predicting snow depth. The density of snow is therefore derived from a Firn Densification Model (FDM) provided by IMAU. The IMAU-FDM determines the fresh snow density for each grid point using a parameterisation based on average annual accumulation, 10 m wind speed and surface temperature.

Figure 3.3 shows the mean surface snow density for 2021 as provided by IMAU. The mean surface snow densities for 2019 and 2020 are very similar, except for some small regional differences (see appendix A). Surface snow densities are generally larger near the coast, which is also where AR contribution is higher (see figure 4.4).

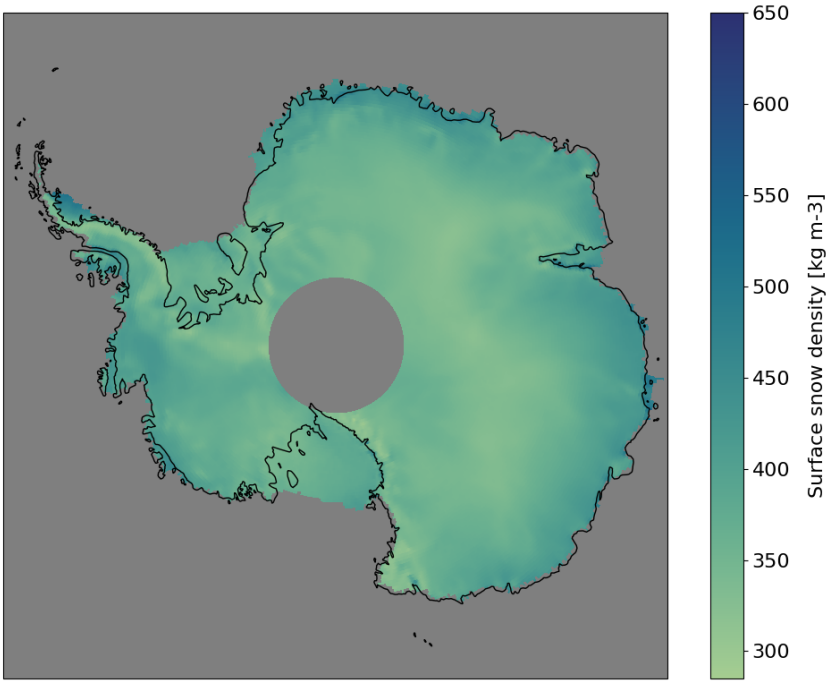

Figure 3.3: Mean surface snow density in 2021 in $[kg\ m^{-3}]$, as provided by IMAU. Grey indicates no data, which is in this case over the ocean, and over the interior of Antarctica where the latitude >85° (as the study area in this thesis is also up to a latitude of 85°). Mean surface snow densities for 2019 and 2020 are shown in appendix A.

3.3.3. Correlation

To get a first idea of the relationship between the reanalysis datasets and ICESat-2, a correlation map is used. A Pearson correlation coefficient between 0 and 1 indicates a positive relation, whereas a correlation coefficient between 0 and -1 indicates a negative relation. The Pearson correlation coefficient is calculated using equation 3.10.

$$\rho_{X,Y} = \frac{cov(X,Y)}{\sigma_X \sigma_Y} \tag{3.10}$$

where cov is the covariance, σ_X is the standard deviation of X and σ_Y is the standard deviation of Y. The correlation is calculated separately for each pixel, using the time series at that pixel as input.

In order to compute the correlation between the two rasters, both rasters have to have the same spatial and temporal resolution. The ICESat-2 data has a higher spatial resolution, and is resized to match the resolution of the reanalysis data. The resolution of the correlation map between ICESat-2 and MERRA-2 therefore has a lower spatial resolution than the correlation map between ICESat-2 and ERA5. Interpolation is done using bi-linear interpolation.

Additionally, the reanalysis data has a higher temporal resolution. In order to match the ICESat-2 resolution, all time steps between the ICESat-2 data points are summed, so as to create an array with the same temporal resolution as ICESat-2.

There are both advantages as well as disadvantages of using correlation to determine whether ICESat-2 shows AR precipitation patterns.

An advantage is that correlation is easy to implement and provides a quick quantitative measure of the relationship between the two variables. This makes it possible to compare the strength of the relationship as well as whether it is negative or positive. Correlation also allows for easy spatial visualisation, which can help in identifying spatial patterns.

A disadvantage is that correlation only says something about whether or not there is a relationship between two variables (and whether it is positive or negative). It does not explain why there is a relationship, nor does it differentiate between cause and effect. Additionally, it only works if there is a linear relationship between the variables of interest.

Correlation can therefore provide insights as to whether there is a relationship between reanalysis data and ICESat-2 data, but it is important to interpret the results with caution and to use additional statistical methods to gain a full picture of the relationship between ERA5/MERRA-2 AR precipitation anomalies and ICESat-2 height changes.

3.3.4. Variance reduction

To evaluate how much of the ICESat-2 height change is explained by AR precipitation and total precipitation, a metric based on variance reduction is used:

$$1 \; - \; \frac{var(\Delta h \; - \; \Delta h_{signal \; of \; interest})}{var(\Delta h)} \tag{3.11}$$

where Δh is the ICESat-2 observed height change and $\Delta h_{signal \; of \; interest}$ is the signal of which we want to determine the related variability in ICESat-2 observations. This method is similar to the method used by Adusumilli et al., 2021, where the same equation was used but the signal of interest was firn layer thickness change.

As equation 3.11 shows, the resulting value can never be greater than 1. If $\Delta h_{signal \; of \; interest}$ is equal to Δh, the resulting value of equation 3.11 will be exactly 1, as the $var(\Delta h \; - \; \Delta h_{signal \; of \; interest})$ term is 0. This then means that the signal of interest explains all the variance in Δh.

If at least part of the variance is explained by the signal of interest the resulting value of equation 3.11 will be between 0 and 1. The variance is always bigger than 0, but the variance of $\Delta h \; - \; \Delta h_{signal \; of \; interest}$ may exceed the variance of Δh. This can happen because the height differences observed by ICESat-2, and thus the values in Δh, can be both positive as well as negative. In that case, the value of 3.11 will be smaller than 0.

By using this method, the variance in the observed height change related to a specific signal can be estimated, and thus the influence of said signal on the observed height change. The variance reduction represents the proportion of the variance in the total height changes that can be attributed to the signal of interest. A higher variance reduction indicates a stronger association between the signal and the observed height changes. A value of 1 indicates that all of the variance in the observations is explained by the signal of interest, and there are no other processes causing height change. A lower value indicates a weaker association. A negative value indicates that the signal of interest does not explain the observed variance, but is in fact causing the variance to increase.

The variance reduction metric values are calculated in a similar way to the correlation values: for each pixel separately, using the time series at that pixel. The result is a map showing a pattern of variance reduction metric values visualising in which regions the AR precipitation signal from reanalysis data can explain larger parts of the total variance in the ICESat-2 observations. As the variance reduction metric values are calculated per pixel, the grids have to have the same dimensions. Since the grids were already resized for the correlation analysis, this does not have to be repeated.

The analysis is done with AR precipitation anomaly as the signal of interest, but it is also done with the total precipitation anomaly as the signal of interest. This allows us to determine whether precipitation is indeed the main process contributing to the ICESat-2 observed height change or if there are other processes responsible for significant height change. In places where precipitation is indeed the main process contributing to height change, the variance reduction value using AR precipitation anomaly as the signal of interest are more meaningful. This is because there is apparently no other process causing significant height change.

3.3.5. Signal-to-noise ratio

The Signal-to-Noise ratio (SNR) measures the strength of the signal relative to the background noise. In this thesis, it is used to investigate how strong the AR precipitation signal is compared to background noise. The SNR is computed using equation 3.12. The SNR is determined per season, as noise due to seasonal variability leads to a very low SNR otherwise.

$$SNR = \frac{var(signal)}{var(noise)} \tag{3.12}$$

If the SNR is smaller than 1, there is considered to be too much noise to distinguish the signal from noise.

To estimate the SNR, the AR precipitation anomaly as estimated from reanalysis data is considered as the signal. The difference between the ICESat-2 observed height change and the non-AR precipitation anomaly from reanalysis data is considered to be noise.

By taking the difference between the ICESat-2 observed height change and the non-AR precipitation anomaly from reanalysis data as the noise, the SNR gives an idea of how well the expected AR precipitation signal (based on reanalysis data) is captured in the ICESat-2 data. The non-AR precipitation anomaly is used rather than the total precipitation anomaly or the AR precipitation anomaly because the non-AR precipitation anomaly is considered to be a proxy for the background noise in the ICESat-2 height change data that is not related to AR precipitation. This is based on the assumption that the ICESat-2 height change is mostly due to the total precipitation anomaly, because then the non-AR precipitation anomaly represents the background noise that is not related to the AR precipitation signal. By subtracting the non-AR precipitation anomaly from the ICESat-2 height change, the background noise is essentially removed and the AR precipitation signal is isolated.

Then by comparing the SNR values across different basins, the locations where the AR precipitation signal is the strongest and most likely to be reliably captured by ICESat-2 can be identified. This information helps to narrow down in which regions the quarterly maps of ICESat-2 height change and AR precipitation anomaly, and the basin time series, should be further investigated to determine if the AR precipitation signal is indeed visible in the ICESat-2 data.

3.3.6. Time series analysis

Based on the correlation and variance reduction analyses, in combination with the AR contribution and the SNR, specific areas might stand out. These areas are investigated more closely using time series analysis.

In the time series, the ICESat-2 observed height change is plotted together with the reanalysis data AR precipitation anomaly and the total precipitation anomaly. Additionally, AR detections are also highlighted.

The added benefit of time series analysis compared to correlation and variance reduction is that it shows the evolution of the variables over time. Then the time series would show where and when to look for an AR precipitation signal in the ICESat-2 data. Whether the AR precipitation signal is indeed visible in the ICESat-2 data is then investigated by plotting the AR precipitation anomalies and the ICESat-2 observed height changes per time-step, so every 3 months.

All time series are plotted with their 2σ around it.

4

Results

This chapter presents the results of the previously explained methods.

Firstly, the results of the AR detection and precipitation attribution are presented.

Secondly, the results of the comparison between AR precipitation and ICESat-2 observations are presented. The comparison between reanalysis and ICESat-2 data exists of a number of different parts, namely a correlation analysis, variance reduction, and Signal-to-Noise ratio (SNR).

Finally, a case study is presented for a number of basins that stood out based on the AR attribution results and the correlation and variance reduction maps.

4.1. AR detection and precipitation attribution

Firstly, the results of the AR detection algorithm are presented.

Secondly, the precipitation attributed to the detected ARs is presented, which includes the long-term AR precipitation between 1980 and 2021, as well as the contribution of AR precipitation to the total precipitation over the same period. In addition to this, a time series of the total AR precipitation and contribution per year shows the yearly amount of AR precipitation over the entire continent.

4.1.1. AR detection

Figure 4.1 shows the detected ARs for MERRA-2 and ERA5 over the time period between 2019-2021.

The mean AR count per pixel over the entire area and over the entire time period is $\sim$59 (0.67%) for both MERRA-2 and ERA5. At least 1 AR was detected $\sim$37% of the time in MERRA-2 and $\sim$41% of the time in ERA5.

When the ocean areas are masked out, the situation changes slightly. Over the entire time period the mean AR count per pixel is $\sim$57 (0.65%) for MERRA-2 and $\sim$51 (0.58%) for ERA5. The mean AR count per pixel is thus very similar whether both land and sea pixels are included in the analysis or whether only land pixels are included. Looking at moments at which at least one AR was detected, this reduces significantly compared to when ocean pixels were also included: at least 1 AR was detected $\sim$16% of the time in MERRA-2 and $\sim$17% of the time in ERA5. This is because only a few ARs make landfall.

Figure 4.2 shows the differences in AR detection frequency between MERRA-2 and ERA5 spatially. Red indicates that more ARs were detected in MERRA-2, while blue indicates that more ARs were detected in ERA5. Over most of the continent, MERRA-2 detects more ARs than ERA5, with the exception of some regions in Dronning Maud Land and in Queen Elizabeth Land. In Queen Elizabeth Land AR detection frequency was low to start with, but in Dronning Maud Laud the highest AR detection frequencies in both data-sets are found.

4.1.2. AR-related precipitation

Figure 4.3 shows the average precipitation attributed to ARs over the 1980-2021 time period.

The precipitation attributed to ARs is very similar for MERRA-2 and ERA5. It should be noted that these images show the average over a long time period, which means that large differences on shorter time scales do not stand out.

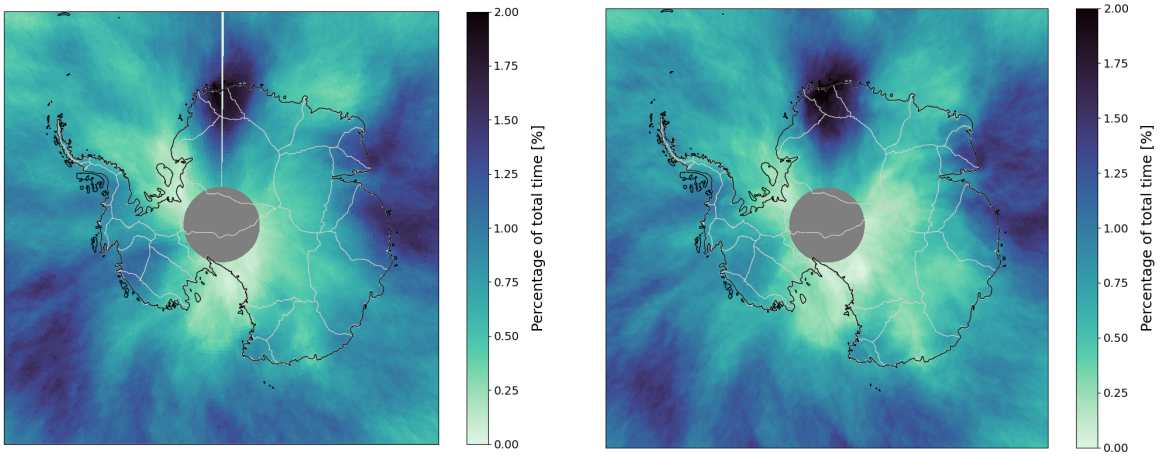

(a) MERRA-2 **(b)** ERA5

Figure 4.1: Percentage of time that an AR was detected between 2019 and 2021 in every pixel for a) MERRA-2 and b) ERA5. Darker blue shaded areas indicate a higher AR detection frequency, while light green indicates a low AR detection frequency. The grey circle in the middle are pixels where the latitude >85°, meaning they fall outside the study area. The drainage basin divides are shown in light grey contour lines.

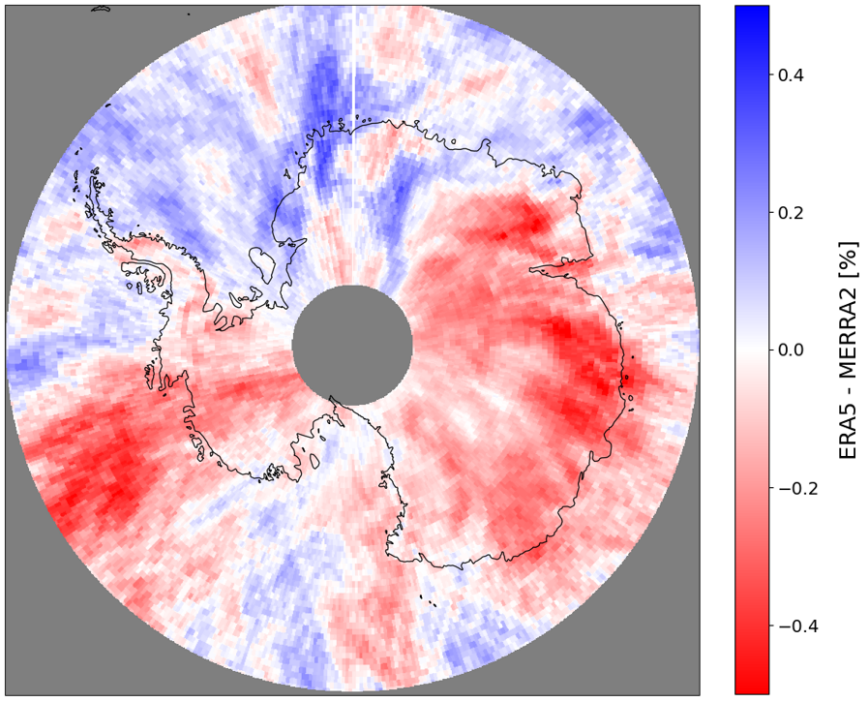

Figure 4.2: Map of difference between MERRA-2 and ERA5 AR detections in 2019-2021. Red indicates that more ARs were detected in MERRA-2, while blue indicates that more ARs were detected in ERA5. The grey circle in the middle are pixels where the latitude <60 ° or >85°, meaning they fall outside the study area.

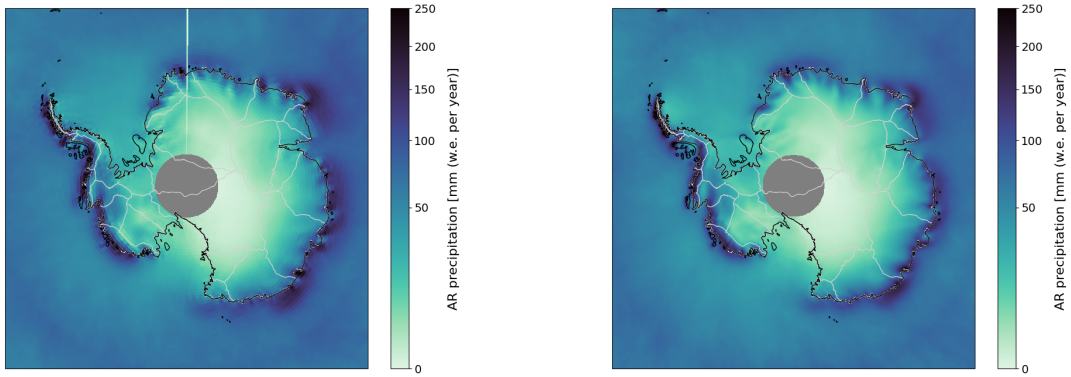

(a) MERRA-2 **(b)** ERA5

Figure 4.3: 1980–2021 average precipitation attributed to atmospheric rivers [mm w.e. per year]. The grey circle in the middle are pixels where the latitude >85°, meaning they fall outside the study area. The drainage basin divides are shown in light grey contour lines.

Both figures show that precipitation that can be attributed to ARs is very low on the Antarctic plateau (less than 1 mm w.e. per year), while it gradually increases towards the coast (>100 mm w.e. per year).

Figure 4.4 shows the contribution of ARs to total precipitation. Similarly to the AR precipitation, the percentage is lowest on the Antarctic plateau and increases towards the coast. The contribution of ARs to total precipitation is higher in East Antarctica, where contribution is larger than 20% of total precipitation in large areas. This is a significant percentage compared to how often ARs are detected over Antarctica, which was $\sim$2% in the locations where ARs were detected most frequently. The contribution of ARs to total precipitation is thus an order of magnitude higher than the AR frequency.

Figure 4.5 shows the AR precipitation for every year as well as the relative contribution of AR precipitation to total precipitation between 1980 and 2021. Overall, the time series are very similar.

The integrated AR precipitation equals 371 $\pm$ 86.4 Gt yr^{-1} for MERRA-2. This is equivalent to 13.6 $\pm$ 2.9% of total precipitation, which is equal to 2713 $\pm$ 135 Gt yr^{-1}. The standard deviation is relatively large for AR precipitation compared to total precipitation, namely 23.3% compared to 5.0%. Non-AR precipitation equals 2342 $\pm$ 116 Gt yr^{-1}, so the standard deviation is 5.0%.

For ERA5, the integrated AR precipitation equals 375 $\pm$ 76.7 Gt yr^{-1}. This is equivalent to 14.4 $\pm$ 2.6% of total precipitation, which is equal to 2593 $\pm$ 121 Gt yr^{-1}. Again, the standard deviation is relatively large for AR precipitation compared to total precipitation, namely 20.5% compared to 4.7%. Non-AR precipitation equals 2218 $\pm$ 92.6 Gt yr^{-1}, so the standard deviation is 4.2%.

This shows that inter-annual variations in AR precipitation are large compared to variations in total precipitation. This suggests that ARs can also explain a part of inter-annual variability in total precipitation. The variability in non-AR precipitation is slightly lower than in total precipitation, particularly in ERA5.

Figure 4.5a and 4.5b both show an increasing trend in AR precipitation, namely $\sim$2.6 Gt yr^{-2} and $\sim$1.0 Gt yr^{-2} for MERRA-2 and ERA5 respectively when fitting a linear line through the time series.

The time period of 2019-2021 is especially of interest due to the availability of ICESat-2 data. In 2019 and 2020 ARs contributed roughly the same percentage to total precipitation ($\sim$13%), but AR precipitation in 2019 was clearly higher in 2020 ($\sim$345 Gt in 2019 as opposed to $\sim$385 Gt in 2020)). Then, 2019 was overall a drier year than 2020. 2021 had both high AR contribution and AR precipitation.

4.2. Height change in ICESat2 observations

Figure 4.6 shows the observed height changes in ICESat-2 data. The data was provided in the ATL15 data product. Figures A.4 and A.5 in appendix A show only the positive and negative height changes respectively.

Blue signifies a positive height change, and thus an increase in height over the period mentioned

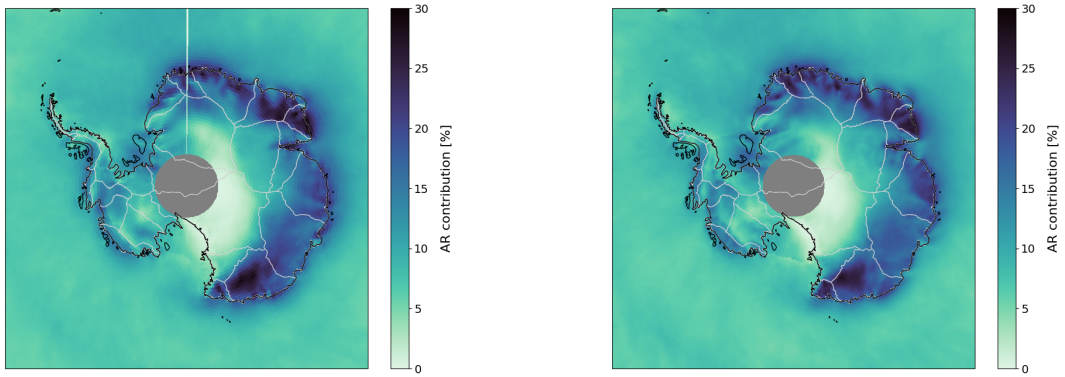

(a) MERRA-2 **(b)** ERA5

Figure 4.4: 1980–2021 average relative contribution of AR precipitation, so the percentage of total precipitation that is linked to ARs. The grey circle in the middle are pixels where the latitude >85°, meaning they fall outside the study area. The drainage basin divides are shown in light grey contour lines.

above the sub figures, and red a negative height change. Areas where the ice speed exceeded 100 m/year are masked out. Comparing the ICESat-2 heights before and after masking out regions of high ice speed shows that the regions where ICESat-2 observed the biggest height changes are also regions of high ice speed. This reaffirms the assumption that precipitation has a smaller contribution to observed height change in regions where there is active ice dynamics. Please refer to figure A.3 in appendix A for the same figure without the ice speed mask applied.

Figures A.6 and A.7 in appendix A show the total precipitation anomaly in MERRA-2 and ERA5 respectively. Both figures show a precipitation pattern very similar to the ICESat-2 height change, although the magnitudes are slightly smaller than in ICESat-2.

The ICESat-2 height change maps are compared with the AR contribution maps (figure 4.4), to determine whether there is overlap between regions of high AR contribution and positive height change. This is done separately for West Antarctica and East Antarctica.

In West Antarctica the total precipitation anomalies are relatively large. Generally there is a mix of positive and negative height change between January and September, but no clear pattern. Negative height change is more common along the coast.

In contrast, there was a relatively large positive height change in April-June 2020 and 2021, and in July-September 2019. There was a relatively large negative height change in January-March 2021. Between October and December there is a clear negative height change in all years, and thus either not a lot of precipitation or a lot of runoff.

AR precipitation contribution in West Antarctica is relatively low. Looking at the time series, there are a lot of AR detections from July 2019 to September 2019, coinciding with a positive total precipitation anomaly. In this same period a large positive height change was observed in ICESat-2. From April to June 2020 another large positive height change was observed in ICESat-2, but not a lot of ARs were detected, and the AR detections did not coincide with large positive total precipitation anomalies. There are barely any AR detections after October 2020 in basins 18-21, and in the remaining West Antarctic basins AR detections were also less frequent compared to the period before October 2020. This matches with the observation that there was not a lot of positive height change. Combining the low average AR contribution with the fact that there were very few AR detections for a large part of the period of interest, it is not expected to find a clear AR precipitation signal in ICESat-2 data, although the positive height change in July to September is likely related to AR precipitation.

In East Antarctica, there are three regions that are slightly different, and therefore interesting to highlight separately, roughly split per 60 degrees longitude: 0-60° E, 60-120 ° E, and 120-180 ° E.

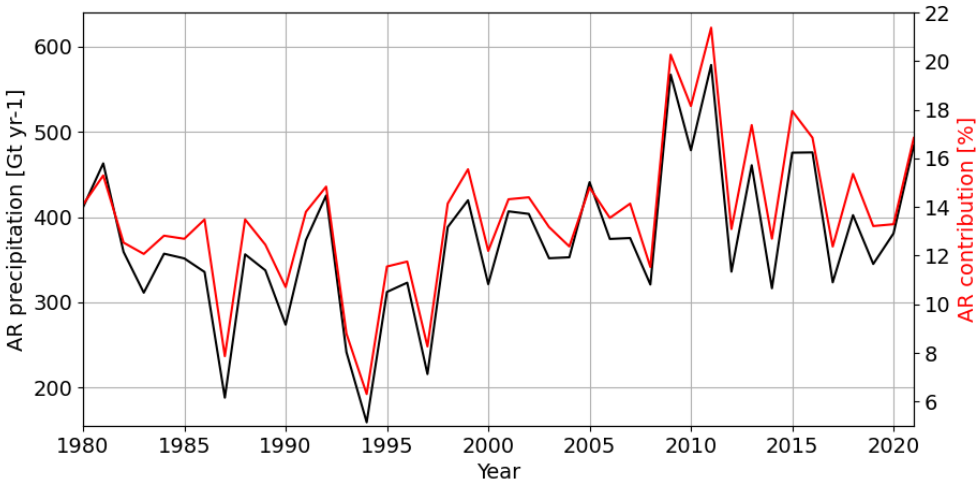

(a) MERRA-2

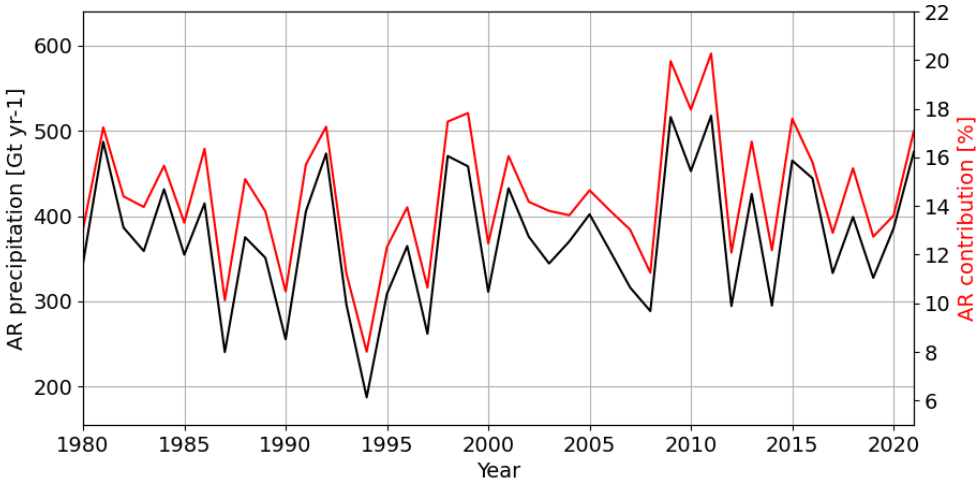

(b) ERA5

Figure 4.5: Time series 1980-2021 of AR precipitation (black, $[Gt\ yr^{-1}]$) and relative contribution of AR precipitation to total precipitation (red, $[\%]$) over the total Antarctic ice sheet, grounded ice sheet and ice shelves.

The first region is from 0-60° E. The basins near the coast, so basins 4-9, are particularly interesting. In this region, both AR frequency as well as AR contribution are high. ICESat-2 height change is generally slightly positive from April-September, although there are a few areas with negative height change. Height change is generally negative in October to December, with the exception of 2021, when there was a large height increase along the coast. Looking at the time series in basins 4-9, ARs are most frequent in October to December 2020 and 2021, but not in 2019. Especially in 2021 a lot of large positive precipitation anomalies coincided with AR detections.

The second region is from 60-120 ° E. Again, the basins along the coast are most interesting, 12 and 13. In this region, AR frequency is high, and AR contribution is also high, but slightly lower than in the previously described region. Height change derived from ICESat-2 shows the clearest pattern in this region. Height change is generally slightly positive in April-June, then clearly positive throughout July-September. Height change is mostly negative from October-March, with the exception of October-December 2021, where there was a clear positive height increase, and January-March 2020, when there was a mix between positive and negative height changes, but height changes were relatively small compared to other moments. Based on the time series, ARs are detected mostly evenly throughout the year. Most ARs coincide with increases in total precipitation anomaly, and although they are not very large increases, there are also very few large increases in total precipitation anomaly that do not coincide with an AR. There are also a lot of AR detections in October-December 2021, which is the time period showing a positive height change in ICESat-2. All things considered, there is a good chance that an AR precipitation pattern can be recognised in these basins.

The third region is from 120-180 ° E. Basins 14-16 are most interesting, again located along the Eastern coast. In this region AR detection is not very high compared to other regions in Antarctica, but AR contribution is the highest. This suggests that the AR events making landfall in this region carry a lot of precipitation. However, the ICESat-2 height changes show that there are no clear positive height changes. This may be because the ARs also cause melting conditions besides carrying a lot of precipitation. The chance that AR precipitation patterns can be recognised in these basins is small since ICESat-2 height changes shows no clear positive height changes, but it might still be interesting to further investigate this region due to the high AR contribution.

4.3. Comparison of reanalysis data and ICESat2 observations

The next step is to compare the results of the AR precipitation for MERRA-2 and ERA5 using ICESat-2 observations and various statistical tools as described in chapter 3.

4.3.1. Correlation

Figure 4.7 shows the correlation maps for MERRA-2 and ERA5. Correlation is computed between the ICESat-2 height change and AR precipitation anomaly, both for ERA5 and MERRA-2. Two masks have been applied. Firstly, all pixels where the ice speed exceeds 100 m per year have been masked out. Secondly, all pixels where the variance reduction with total precipitation as the signal of interest was negative have also been removed.

Correlation between MERRA-2 and ERA5 are very similar. Correlation is mostly positive along the coast. There are a few regions where correlation is higher, these are also regions where AR contribution is relatively high. Correlation in the interior is mostly negative, these are mostly areas where AR contribution is low.

These correlation maps do not yet give a clear picture of how well AR precipitation is captured in specific regions, but they do give a first indication as to which basins should be investigated further.

Additionally, appendix A shows correlation maps for the correlation between ICESat-2 data and total precipitation anomalies from reanalysis data.

4.3.2. Variance reduction

Variance reduction was performed twice. Firstly with total precipitation as the signal of interest, and secondly with AR precipitation as the signal of interest.

Figure 4.8 shows the variance reduction metric values where the signal of interest is total precipitation anomaly. The maps for MERRA-2 (figure 4.8a) and ERA5 (figure 4.8b) are very similar. Both maps are predominantly blue, indicating positive values and therefore also indicating that a (large) part of the

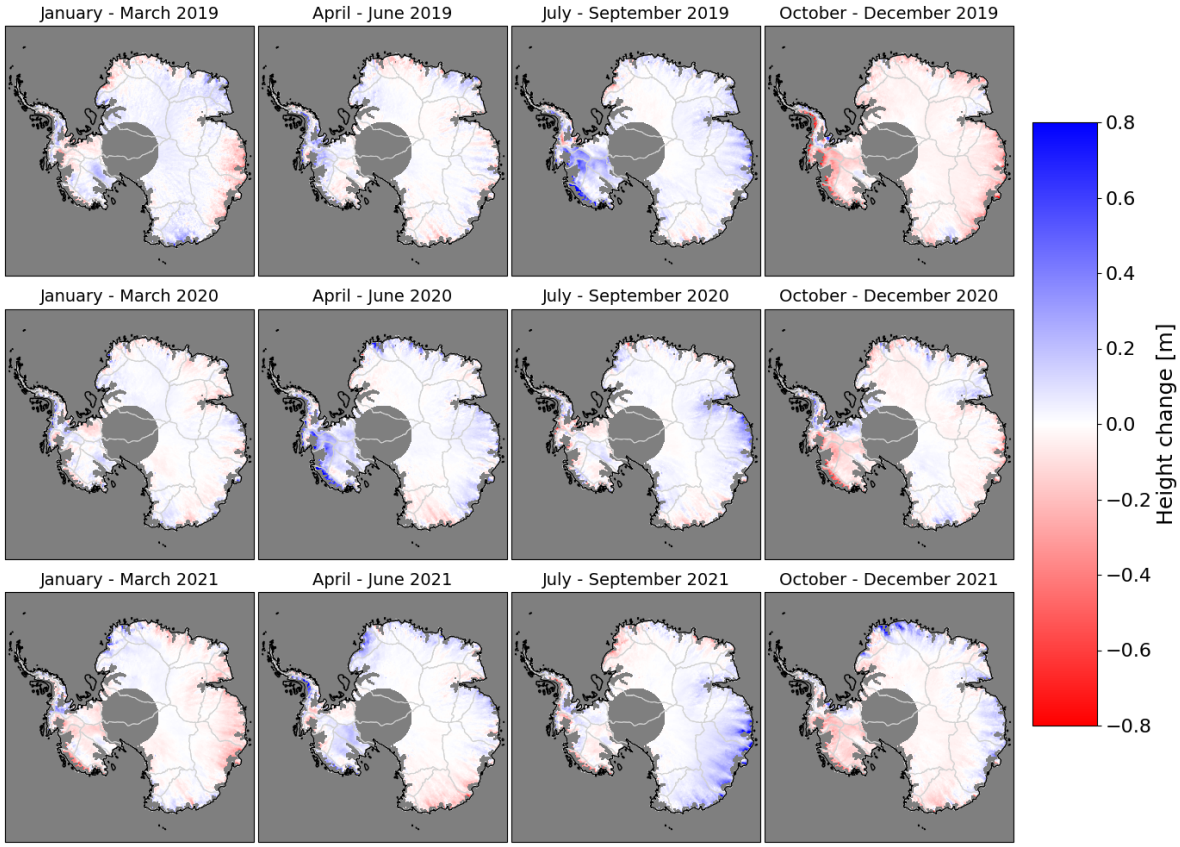

Figure 4.6: ICESat2 satellite altimetry derived height changes. This figure shows the recorded height at the end of the period minus the recorded height at the beginning of the period, so the height change recorded over said period. Each period lasts 91 days, and starts at the beginning of the first month and lasts until the end of the last month indicated above each subfigure. The ice shelves are excluded, as well as pixels where the ice speed exceeds 100 m per year. The grey circle in the middle are pixels where the latitude >85°, meaning they fall outside the study area. Positive height changes are shown in blue and negative height changes in red. The drainage basin divides are shown in light grey contour lines.

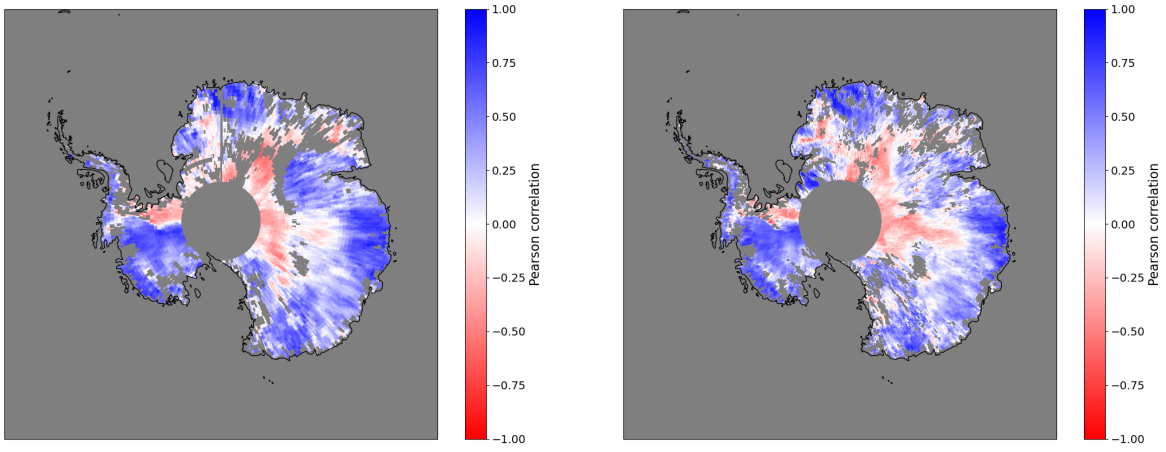

(a) MERRA-2 **(b)** ERA5

Figure 4.7: Correlation between height differences observed by ICESat-2 and AR precipitation derived from a) MERRA-2 and b) ERA5. Grey pixels over Antarctica where the latitude <85 ° are pixels that have been masked out, either because the ice speed exceeds 100 meters per year, or because the total precipitation variance reduction is negative. The grey circle in the middle are pixels where the latitude >85°, meaning they fall outside the study area.

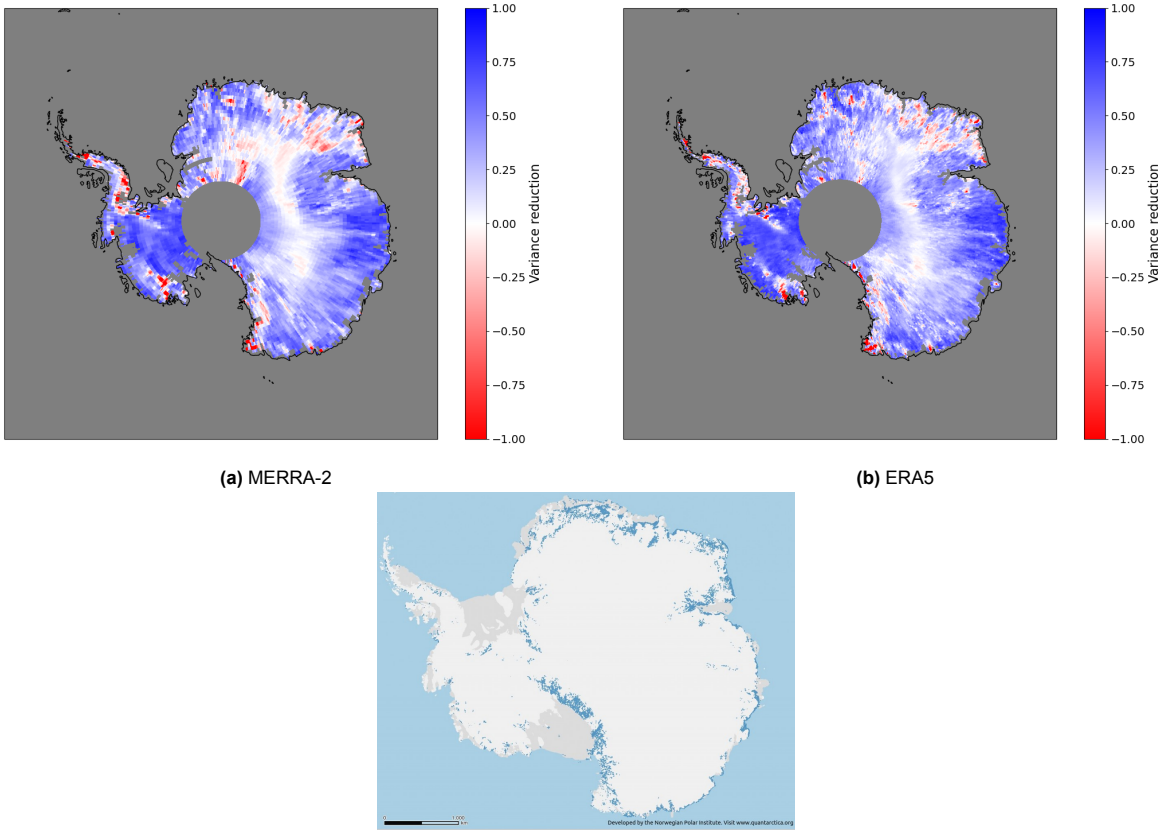

(a) MERRA-2

(b) ERA5

(c)

Figure 4.8: Variance reduction metric values where Δh is the height difference observed by ICESat-2 and $\Delta h_{signal\ of\ interest}$ is total precipitation anomaly derived from a) MERRA-2 and b) ERA5). The grey circle in the middle are pixels where the latitude >85°, meaning they fall outside the study area. c) shows the locations of blue ice in Antarctica in blue (via Quantarctica Database, Norwegian Polar Institute)

variance in ICESat-2 is explained by precipitation. As areas with a high ice velocity (>100 m per year) have already been masked out, it would be expected that most of the height change in the left-over pixels to be due to precipitation anomalies, which is indeed the case for large parts of Antarctica.

Looking back at AR precipitation contribution (figure 4.4), it appears that in areas where AR precipitation contribution is high, the total precipitation anomalies explain a large part of the variance. This indicates that the variance reduction metric can be suitable for AR precipitation as well, because most of the ICESat-2 observed height change in places with a lot of AR precipitation is linked to precipitation rather than other processes.

Further away from the coast, in the Antarctic interior, the variance reduction metric values are smaller. This is also an area where the snow density is on the lower side (see figure 3.3), and the same goes for the ice velocity (see figure 3.2b). It is not clear then why exactly less variance is explained by precipitation here. However, this is also an area where overall precipitation and AR precipitation contribution are low (see figure 4.4), so it should not have a significant impact on the further analysis.

Finally, there are also some red specks where the precipitation does not explain the variance in the ICESat-2 observations. They are mainly noticeable in Dronning Maud Land, as well as in Victoria Land and the Transantarctic Mountains, but also in Marie Byrd Land and the Antarctic Peninsula. These pixels are masked out in further analysis. Possible explanations for these negative variance reduction values are further discussed in chapter 5.

Figure 4.9 shows the variance reduction map with AR precipitation anomaly as the signal of interest. Similar to the correlation maps, two masks have been applied: the ice speed >100 m per year, and the variance reduction with total precipitation <0.

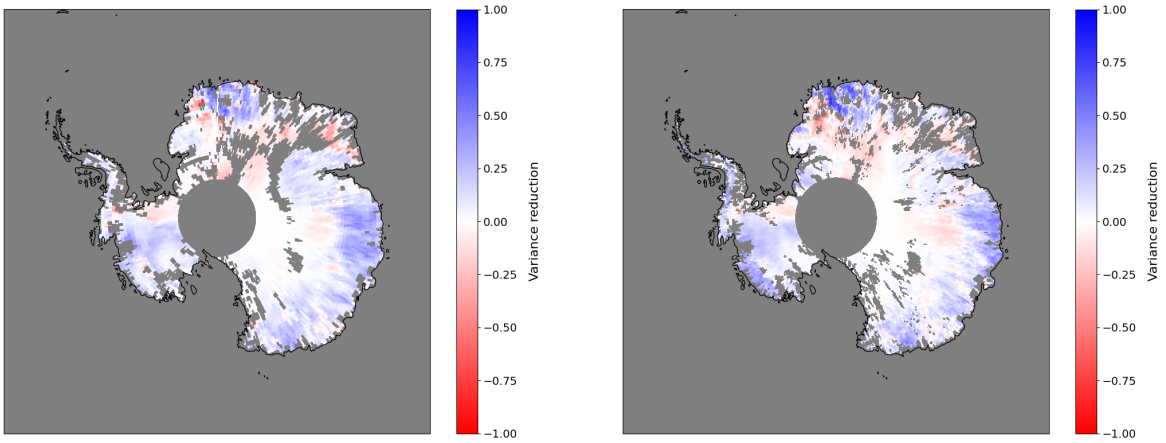

(a) MERRA-2 **(b)** ERA5

Figure 4.9: Variance reduction metric values where Δh is the height difference observed by ICESat-2 and $\Delta h_{signal\ of\ interest}$ is AR precipitation anomaly derived from a) MERRA-2 and b) ERA5). Grey pixels over Antarctica are pixels that have been masked out, either because the ice speed exceeds 100 meters per year, or because the total precipitation variance reduction is negative. The grey circle in the middle are pixels where the latitude >85°, meaning they fall outside the study area.

Mostly the same areas as in the correlation maps show positive variance reduction. This indicates that AR precipitation explains a part of the variance in the ICESat-2 observations, and thus that the height changes observed by ICESat-2 are influenced by the presence of AR precipitation and the AR precipitation signal might be recognisable in the observations.

4.3.3. Weighting per basin

Previously, the correlation and variance reduction were computed using only the AR precipitation anomaly and the ICESat-2 height change observations. However, as figure 4.4 already showed, ARs do not contribute equally to total precipitation everywhere. The proportion of total precipitation that can be attributed to ARs varies significantly across Antarctica, which means that some drainage basins are more susceptible to the influence of ARs than others. It would be expected that it is more likely to be able to observe an AR precipitation signal in areas where AR contribution is high. If ARs are responsible for 30% of total precipitation in a specific location, then it is more likely that the AR precipitation is distinguishable from other precipitation or height change than in regions where ARs are only responsible for 2% of total precipitation. Still, the AR contribution is a mean over a longer time period, so it is possible that over shorter time periods there is an observable signal.

Figure 4.10 shows the contribution of AR precipitation anomaly to total precipitation anomaly between the 1st of January 2019 and the 31st of December 2021 for ERA5, which is used to weight the ERA5 correlation and variance reduction results. The contribution for this time period is very similar to the contribution between 1980 and 2021 (figure 4.4). Similarly, the contribution of AR precipitation anomaly to total precipitation anomaly between the 1st of January 2019 and the 31st of December 2021 for MERRA-2 is used to weight the MERRA-2 correlation and variance reduction results.

The weighted correlation and variance reduction maps thus take into account the contribution of AR precipitation to the total precipitation. As such, they provide a more accurate representation of the spatial AR precipitation signal strength relative to the total precipitation signal, and can be used to identify regions where the AR precipitation signal is more dominant. The weighted correlation and variance reduction maps can be used to further narrow down in which specific drainage basins the AR precipitation signal is most likely to be visible in ICESat-2 observations. Then, only the basins that are likely to have a significant AR influence on precipitation, and thus also likely on height change, are analysed more closely.

Figure 4.11 shows the mean per basin of the correlation weighted by the AR precipitation per pixel, while figure 4.12 shows the mean per basin of the AR precipitation variance reduction weighted by the AR precipitation per pixel. Both the weighted correlation as well as the variance reduction show

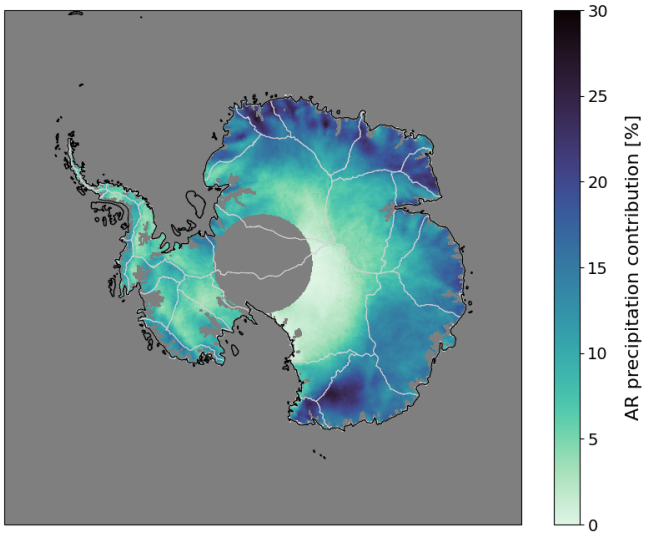

Figure 4.10: Mean contribution of AR precipitation anomaly to total precipitation anomaly between the 1st of January and the 31st of December 2021 for ERA5, where the AR precipitation and total precipitation anomaly is calculated based on the difference from the long-term mean between 1980 and 2021. Grey pixels over Antarctica are pixels that have been masked out because the ice speed exceeds 100 meters per year. The grey circle in the middle are pixels where the latitude >85°, meaning they fall outside the study area. The drainage basin divides are shown in light grey contour lines.

generally higher values in East Antarctic basins located in Queen Maud Land, Wilkes Land and Victoria Land. In Marie Byrd Land values are also relatively high, especially in basin 20, which covers a large part of the coast.

From these figures, a couple of basins show more promise in how well the AR precipitation signal could be captured in ICESat-2 data. These are basin 5, 12, 14, and 20. Basins 5, 12, and 14 are located in East Antarctica, basin 20 in West Antarctica. The time series of these basins are further investigated to determine if the AR precipitation signal is indeed visible in the ICESat-2 data.

When looking at the entire continent, the mean contribution weighted correlation (between AR precipitation from reanalysis data and ICESat-2 height change) for MERRA-2 is 0.272 and 0.248 for ERA5. The mean variance reduction (signal of interest is AR precipitation) with AR precipitation as the signal of interest is 0.0680 for MERRA-2 and 0.0669 for ERA5.

In contrast, the mean non-weighted correlation over the entire continent is 0.196 for MERRA-2 and 0.170 for ERA5, and the mean variance reduction with AR precipitation as the signal of interest is 0.0454 for MERRA-2 and 0.0409 for ERA5.

4.3.4. Signal-to-noise ratio

Signal-to-Noise ratio (SNR) maps are computed to identify areas where the AR precipitation signal is expected to be more easily detectable. Ideally, areas of high SNR match the areas that stood out based on the correlation and variance reduction analyses.

Figure 4.13 shows the SNR maps per season, where the signal is the AR precipitation anomaly from reanalysis data and the noise is the difference between the ICESat-2 observed height change and the non-AR precipitation anomaly from reanalysis data. The map only shows areas where the AR precipitation signal is stronger than the noise of the difference between the ICESat-2 observed height change and the non-AR precipitation anomaly from reanalysis data. The figures for MERRA-2 are shown on the left side, and the figures for ERA5 on the right side. The SNR is generally low across Antarctica.

Table 4.1 shows the percentage of pixels (land only) in which the SNR > 1 and the signal is thus

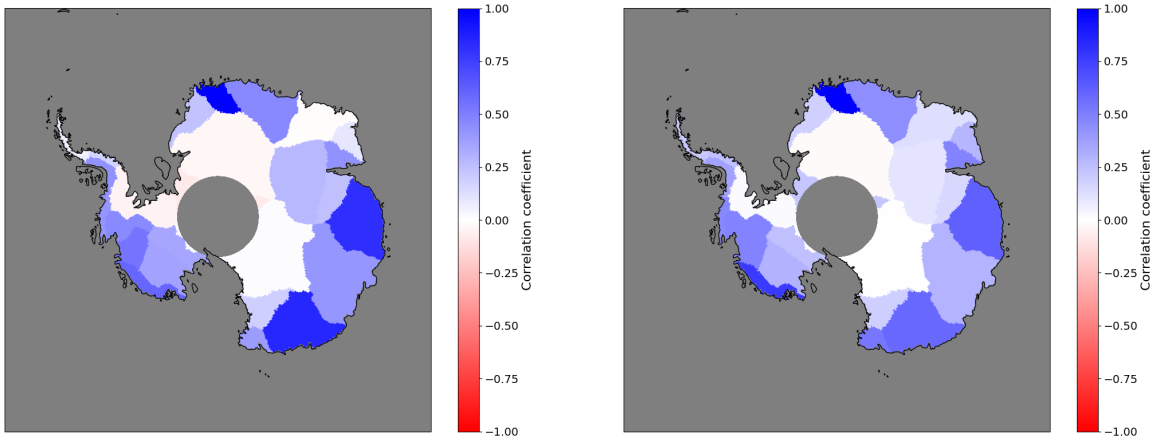

(a) MERRA-2 **(b)** ERA5

Figure 4.11: Correlation between height differences observed by ICESat-2 and AR precipitation from reanalysis data, weighted by AR contribution per pixel. The mean per basin is shown, so for all weighted pixels (this excludes the pixels where the ice speed exceeds 100 meters per year, or the total precipitation variance reduction is negative). The grey circle in the middle are pixels where the latitude >85°, meaning they fall outside the study area. Derived from a) MERRA-2 and b) ERA5.

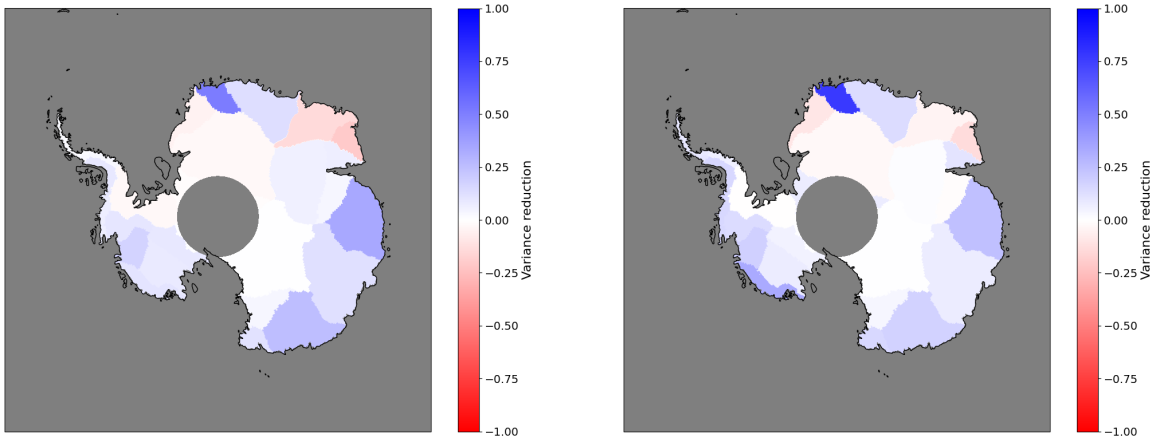

(a) MERRA-2 **(b)** ERA5

Figure 4.12: Variance reduction metric values where Δ_h is the height difference observed by ICESat-2 and $\Delta_{signal\ of\ interest}$ is AR precipitation anomaly, weighted by AR contribution per pixel. The mean per basin is shown, so for all weighted pixels (this excludes the pixels where the ice speed exceeds 100 meters per year, or the total precipitation variance reduction is negative). The grey circle in the middle are pixels where the latitude >85°, meaning they fall outside the study area. Derived from a) MERRA-2 and b) ERA5.

stronger than the noise. MERRA-2 has a higher percentage in Q2 and Q3, so during the austral winter, while ERA5 has a higher percentage in Q4 and Q1, so during the austral summer. The percentage is between 4.3 and 11.1% of all land pixels in Antarctica. These small values can be explained by the fact that the AR precipitation contribution to total precipitation only makes up more than 20% of total precipitation in very few places. If the signal is weak compared to the noise to start with (so AR precipitation compared to total precipitation), it makes sense that the SNR will also be low in these places.

The SNR suggests that MERRA-2 may be better at capturing the Atmospheric River (AR) precipitation signal in the ICESat-2 height change data in winter, and ERA5 in summer. However, the correlation and variance reduction values are slightly lower in MERRA-2, suggesting that ERA5 performs slightly better overall.

Of the basins that stood out based on the correlation and variance reduction analyses, basins 5 and 12 show somewhat larger regions with a SNR larger than 1 in specific seasons. Basin 5 is mainly interesting in Q4 and Q1, and basin 12 in Q4, and to a lesser extent in Q2 and Q3. Basin 14 shows small regions with a SNR larger than 1 in Q1. Basin 20 does not show a lot of promise based on the SNR, but is still further investigated based on the correlation and variance reduction analyses and considering the fact that it is the only West Antarctic basin out of the four.

Table 4.1: Percentage of land pixels with SNR > 1, AR precipitation anomaly as signal, and difference between the ICESat-2 observed height change and the non-AR precipitation anomaly from reanalysis data as noise.

	MERRA-2	ERA5
Q1	4.8%	5.3%
Q2	4.8%	4.3%
Q3	5.7%	5.5%
Q4	9.0%	11.1%

4.4. Case studies for specific basins

This section further analyses a number of basins where the previous analyses over the entire continent showed promising results. Whereas previous analyses mainly focused on the mean values over the entire 3-year study period, these basins are also analysed in more detail over shorter time scales. The quarterly AR precipitation anomaly maps are compared to the quarterly ICESat-2 height change observations. Furthermore, the time series are analysed, where the AR and total precipitation anomalies are plotted at 3-hourly resolution, together with the 3-hourly AR detections, and the 3-monthly ICESat-2 height change. The time series of the basins not highlighted in this section can be found in appendix B.

Figures 4.14 and 4.15 show the AR precipitation anomalies per quarter for MERRA-2 and ERA5 respectively. The AR precipitation has already been converted to snow heights using the snow density map. Overall, the AR precipitation anomalies are similar for the two reanalysis data sets. Both show that generally the AR precipitation anomaly is only positive in select areas and moments, which matches the notion that ARs are uncommon. Neither MERRA-2 nor ERA5 consistently predicts larger areas of positive AR anomalies. In July-September 2020 and July-December 2021 both data-sets predict a relative large area with a positive AR precipitation anomaly, covering large parts of East Antarctica.

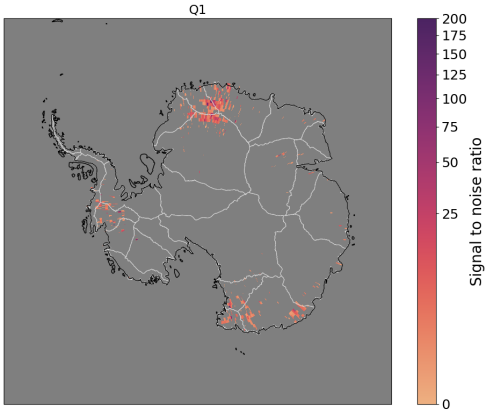

(a) Q1, start of January to end of March, MERRA-2

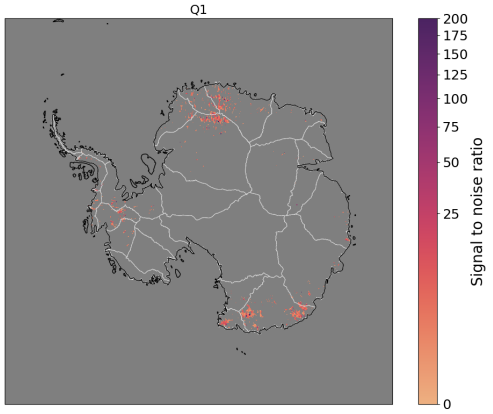

(b) Q1, start of January to end of March, ERA5

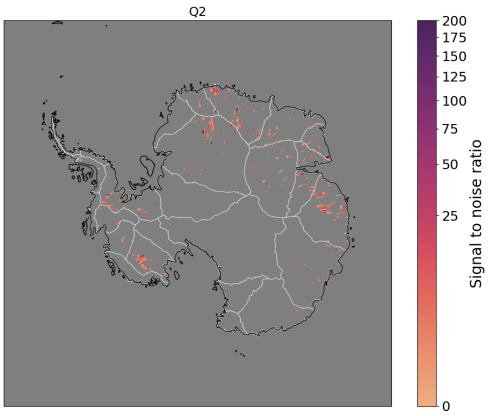

(c) Q2, start of April to end of June, MERRA-2

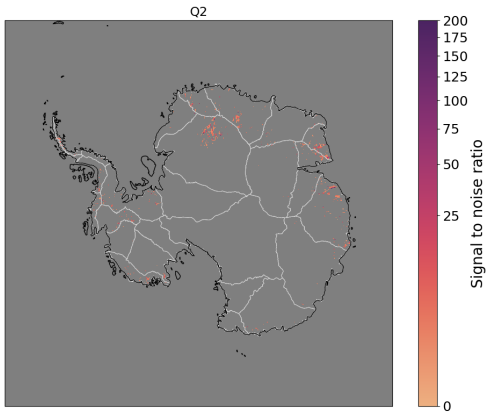

(d) Q2, start of April to end of June, ERA5

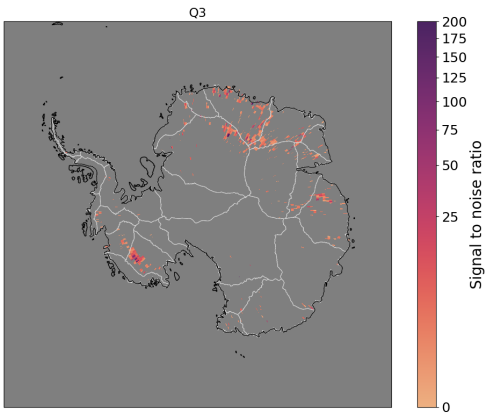

(e) Q3, start of July to end of September, MERRA-2

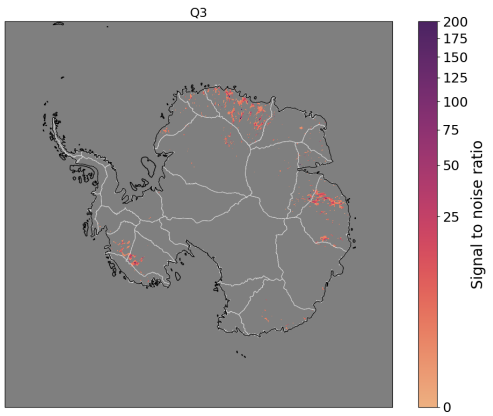

(f) Q3, start of April to end of June, ERA5

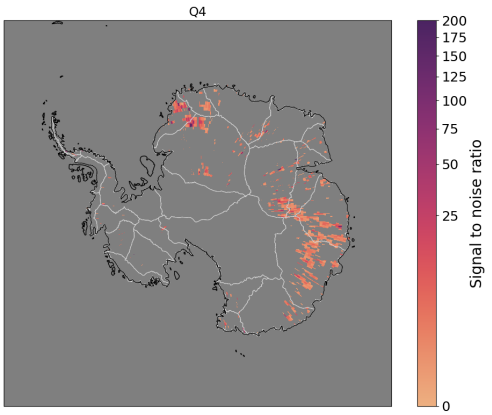

(g) Q4, start of October to end of December, MERRA-2

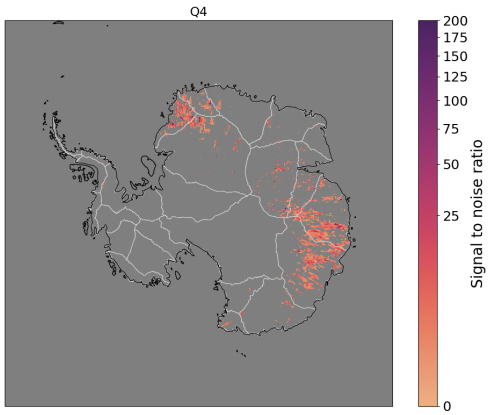

(h) Q4, start of April to end of June, ERA5

Figure 4.13: SNR with reanalysis AR precipitation anomaly as the signal, and ICESat-2 observed height change - reanalysis non-AR precipitation anomaly as the noise. Pixels with a SNR<1 have been masked out. The drainage basin divides are shown in light grey contour lines.

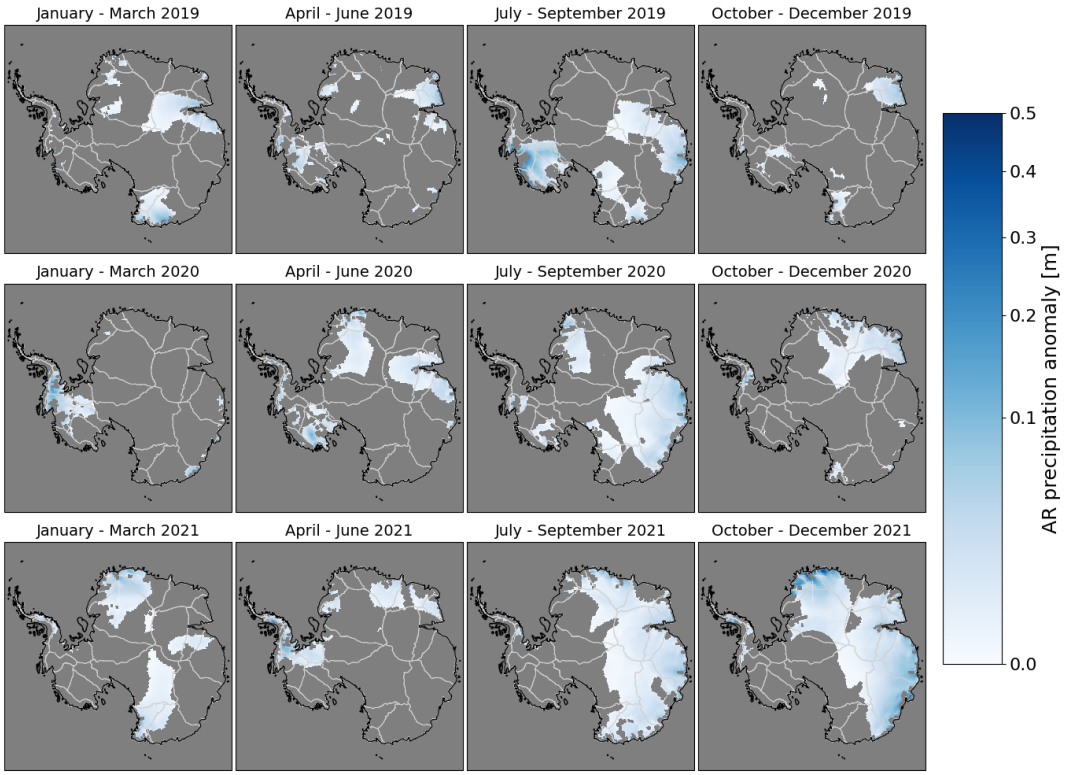

Figure 4.14: Mean contribution of AR precipitation anomaly per quarter in MERRA-2, only positive AR precipitation anomalies. Each quarter starts at the beginning of the first month and lasts until the end of the last month indicated above each subfigure. The drainage basin divides are shown in light grey contour lines.

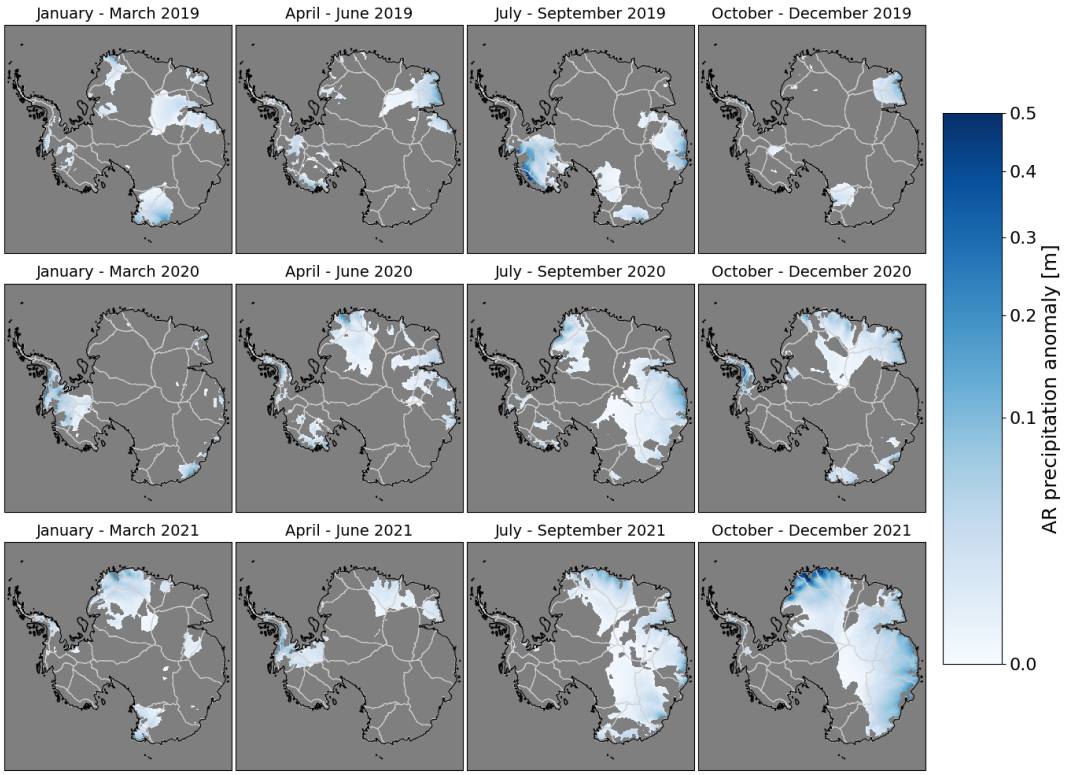

Figure 4.15: Mean contribution of AR precipitation anomaly per quarter in ERA5, only positive AR precipitation anomalies. Each quarter starts at the beginning of the first month and lasts until the end of the last month indicated above each subfigure. The drainage basin divides are shown in light grey contour lines.

Basin 5

Section 4.2 already established that basin 5 has both high AR frequency as well as AR contribution. Based on the SNR analysis, it would be expected to find AR precipitation signals mainly from October to March.

The time series (figures 4.16a and 4.17a) show that AR detections are most frequent between October and December (though only in 2020 and 2021). There are also relatively many AR detections between January and March 2021. Most AR detections coincide with a significant increase in total precipitation anomaly. The expectation of finding AR precipitation signals mainly from October to March thus appears to be true.

Looking at figures 4.14 and 4.15 there is a clear positive AR precipitation anomaly between October and December in 2020 and 2021, and between January and March 2021. The time series also show one AR causing a large total precipitation anomaly between April and June 2020, which is also visible in the AR precipitation anomaly maps. All other moments do not show a lot of AR precipitation in both reanalysis data-sets, although figure 4.15 shows that in ERA5 there is also a positive AR precipitation anomaly in a large part of the basin in January-March 2019, October-December 2020, and July-September 2021.

When comparing the AR precipitation anomalies (figures 4.14 and 4.15) with the ICESat-2 height change (figure 4.6), several things stand out. Especially between October and December 2021 there was a clear positive AR precipitation anomaly, which is also present in the ICESat-2 data. In combination with the time series showing a lot of AR detections coinciding with large total precipitation anomalies, it is very likely that a significant part of the observed height change can be attributed to ARs. The positive height change as observed by ICESat-2 from April-June 2020 also appears to match the AR precipitation anomaly closely in spatial location, and from January-March 2021 there was also a positive height change observed. In July-September 2021 and January-March 2019 there is no clear positive height change, but in these time periods only ERA5 showed a a clear positive anomaly over a significant part of the basin, and based on the time series there were no AR events causing large amounts of precipitation in these time windows. Over the entire time period, there are no large-scale

positive height changes in this basin that can not be explained by AR precipitation anomalies.

All in all, the expectation of finding AR precipitation mainly between October and December, and to a lesser extent from January to March, is true. This is mainly thanks to a lot of ARs from October to December in 2020 and 2021. However, a significant AR event also occurred outside these months in April-June 2020, which is evident based on the time series as well as AR precipitation anomaly maps and the ICESat-2 height change map. AR events outside these months do still contribute to the high correlation and variance reduction, as those are based on the time series.

Basin 12

Section 4.2 already established that basin 12 has both high AR frequency as well as AR contribution, although the AR contribution is slightly lower than in basin 5. Based on the SNR analysis, it would be expected to find AR precipitation signals mainly from July to December, and to a lesser extent also from April to June.

The time series (figures 4.16b and 4.17b) show that AR detections are very frequent from July to September in 2020 and 2021. Although AR detections were not very frequent from July to September in 2019, the three AR events that were detected did carry a lot of precipitation based on the increase in total precipitation anomaly. Most of the large total precipitation anomalies between July and September coincided with ARs. ARs were also frequently detected between April and June in 2020. There are also a lot of AR detections between October and December 2021, but figures 4.14 and 4.15 already showed that there was a lot of AR precipitation in these months over most of East Antarctica. Other than that, there are a couple of isolated ARs detected from October to July, but those do not coincide with large total precipitation anomalies, and therefore probably either did not carry a lot of precipitation or did not cover a large part of the basin.

Looking at figures 4.14 and 4.15 there is indeed a positive AR precipitation anomaly between July and September in all years. In 2019 a smaller part of the basin shows a positive AR precipitation anomaly, likely due to the fact that there were relatively fewer AR events compared to 2020 and 2021, and they did not cover the entire basin.

The map for April to June 2020 shows a positive AR precipitation anomaly for only a part of basin 12. The ARs then probably do not cover the entire basin. Based on the SNR it was not expected to find a clear AR precipitation signal in this time window.

Finally, there was also a significant amount of AR precipitation between October and December 2021, which was not expected based on the SNR analysis.

Comparing the AR precipitation anomalies (figures 4.14 and 4.15) with the ICESat-2 height change (figure 4.6) confirms this. In all cases where there is a positive AR precipitation anomaly in most of the basin, there is also a clear height increase in ICESat-2. However, there are also large-scale positive height changes that do not fully match the positive AR anomalies, or at least not in both reanalysis data-sets, most noticeably between April-June in 2020 and 2021. In 2021 there were simply hardly any AR occurrences. In 2020 there were a number of AR occurrences based on the time series that also generally matched positive height change. However, one AR causing a noticeable total precipitation anomaly lasted for a longer time period in the MERRA-2 time series than in the ERA5 time series. The area of positive height change was noticeably larger than the area covered by positive AR precipitation anomalies in ERA5, but not in MERRA-2. This is thus likely caused by a difference in AR detection.

Then, the expectations of finding AR precipitation mainly between July and September is true. However, there were a lot of ARs between October and December 2021 too, that are not expected based on the SNR. This could be because there was no AR precipitation in 2019 and 2020, and thus the SNR was low. There were also a lot of AR detections between October and December 2021 in basin 5, that were associated with large amounts of precipitation. A longer data record might lead to a clearer picture as to whether there was abnormally high AR frequency for this season in 2021, or abnormally low AR frequency for this season in 2019 and 2020.

Basin 14

Section 4.2 already established that basin 14 has very high AR contribution, but lower AR frequency compared to basins 5 and 12. However, despite the high AR contribution the ICESat-2 data did not show clear height increases.

Based on the SNR analysis, AR precipitation signals might be observable from January to March.

The time series (figures 4.16c and 4.17c) show that AR detections are frequent from January to April in 2020 and 2021. However, AR detections were also frequent from April to June in 2019 and

2020, and the AR events contributing the most to total precipitation anomaly occured during Q3, so from July to September. This is not expected based on the SNR. Most of the ARs inside the January to June window did not last very long. Additionally, compared to basins 5 and 12 there are also many clear increases in total precipitation anomaly that did not coincide with an AR. Overall, the time series does not show a very clear picture in this basin.

Looking at figures 4.14 and 4.15, there was only one moment in time that a large part of the basin shows a positive AR precipitation anomaly (July-September 2021). This does coincide with a clear increase in total precipitation anomaly in the time series, but is outside the January-June window in which it would be expected to find the AR precipitation signal in ICESat-2 data based on the SNR analysis. Looking at figure 4.6, there was a clear height increase from July-September 2021 over nearly the entire basin. Combined with the positive AR precipitation anomaly over the same time period, it is plausible that a significant part of the height change is related to AR precipitation.

In a lot of other time steps some AR precipitation is detected in the basin, but the larger part of the basin does not show a positive AR precipitation anomaly. The same is true for the observed height change: there are some smaller areas showing an increase in height, but not a significant part of the basin. An exception is January-March 2019, in which a somewhat larger part of the basin shows a relatively large height increase, and a positive AR precipitation anomaly is observed in the same area in both ERA5 as well as MERRA-2.

Still overall, basin 14 does not show a clear AR precipitation signal in ICESat-2 data. This could be due to multiple reasons. One possible reason is that the amount of total precipitation is low. Then even if the contribution from AR precipitation is large, and thus a large part of the total precipitation is linked to ARs, there is still not a clear height change signal because there is not a lot of (AR) precipitation. Another reason is that the ARs are relatively short, judging by the intensity of the red lines in the time series, or less intense. They are then likely to carry less precipitation.

Basin 20

Section 4.2 already established that basin 20 has relatively low AR contribution, and very few AR detections after September 2020. Based on the low AR contribution and long period without frequent AR detections, it is not expected that a clear AR precipitation signal is visible in ICESat-2 data. Still, basin 20 shows the most promise of West Antarctic basins based on correlation and variance reduction analyses.

It is also not expected to find AR precipitation signals at any moment based on the SNR analysis.

Figures 4.14 and 4.15 show that there is a significant positive AR precipitation anomaly only from July to September 2019. The time series (figures 4.16d and 4.17d) show that ARs were indeed frequent between July and September 2019, and contributed to the total precipitation anomaly.

Looking at the height changes in this basin in figure 4.6, there is a clear increase in height in the same period, and in the same part of the basin, so this could very well be due to AR precipitation. Other than that there is also a relatively large increase in height in part of the basin from April to June 2020, and a smaller height increase from April to June 2021. This is also evident from the time series, but this is not related to AR precipitation based on both the time series and the AR precipitation anomaly maps. There were also a few AR detections from April to September 2020, and also a number of large precipitation anomaly increases, but they did not coincide most of the time. As a whole, the total precipitation anomalies in this basin are large in magnitude compared to the previously discussed basins, both positive as well as negative.

The AR precipitation signal can not readily be recognised in ICESat-2 data, which makes sense considering the fact that there is almost never a positive AR precipitation anomaly in reanalysis data.

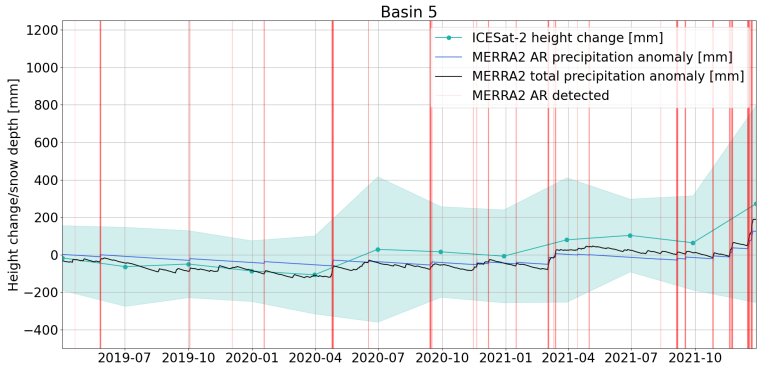

(a) Basin 5, MERRA-2

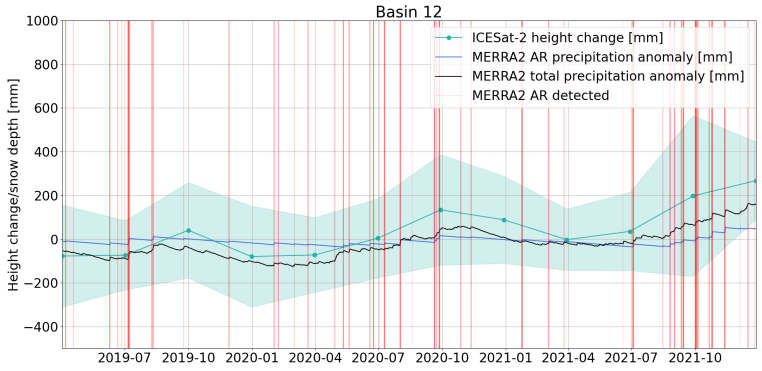

(b) Basin 12, MERRA-2

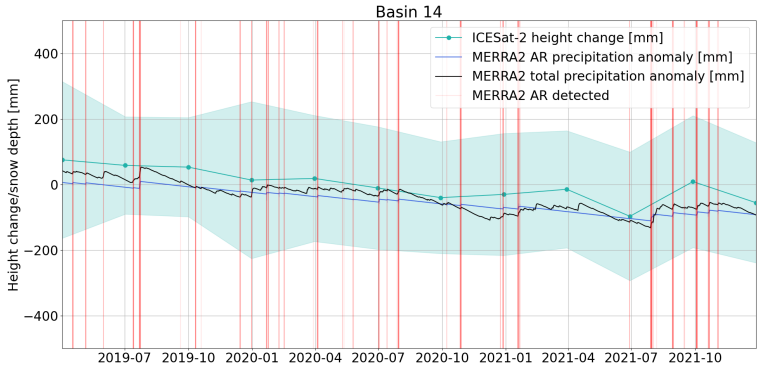

(c) Basin 14, MERRA-2

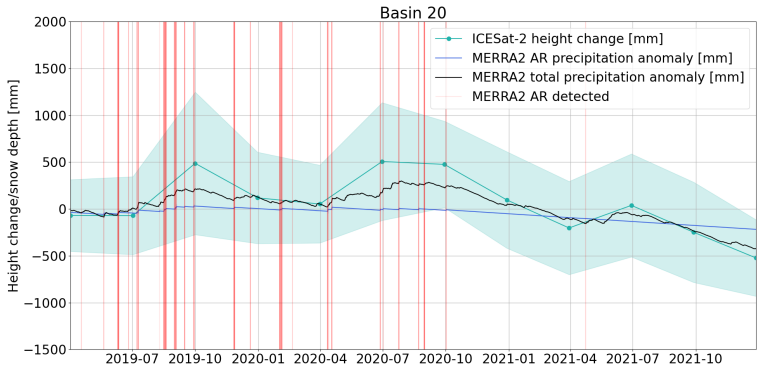

(d) Basin 20, MERRA-2

Figure 4.16: Mean time series between the 1st of January 2019 and 31st of December 2021 for select basins, showing ICESat-2 observed height change (green, with 2σ around it), the AR precipitation anomaly from MERRA-2 reanalysis data (blue), and the total precipitation anomaly from MERRA-2 reanalysis data (black). The red vertical lines indicate when an AR was detected in the basin, brighter lines indicate that ARs were detected in subsequent time steps. The ICESat-2 data has a temporal resolution of 91 days, the precipitation anomalies and AR detections have a temporal resolution of 3 hours.

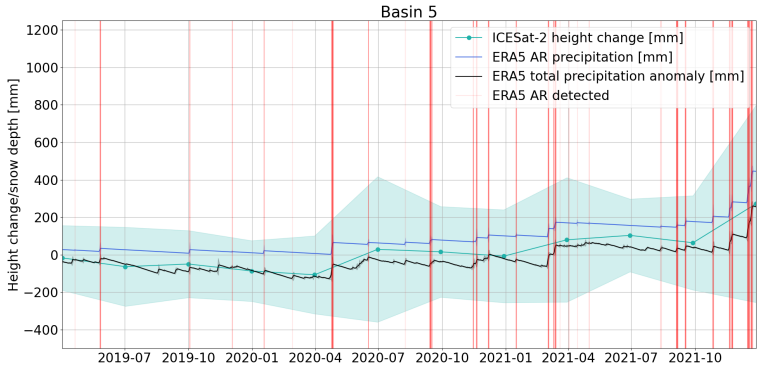

(a) Basin 5, ERA5

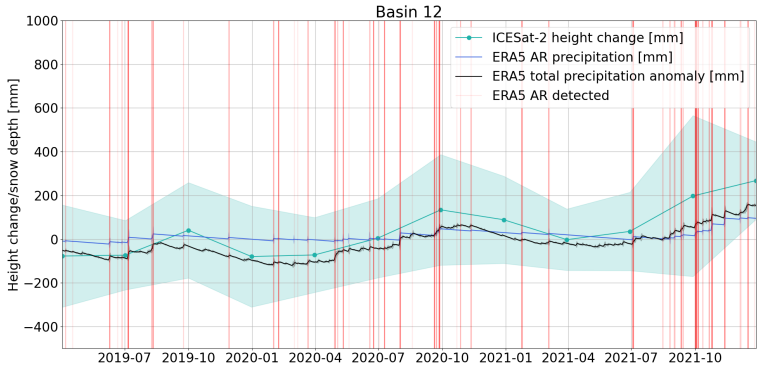

(b) Basin 12, ERA5

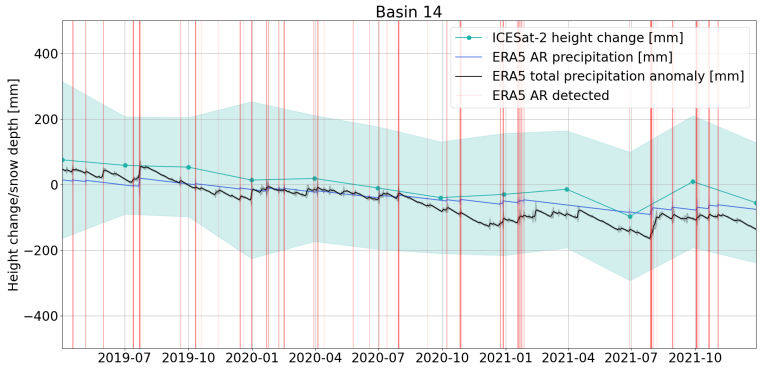

(c) Basin 14, ERA5

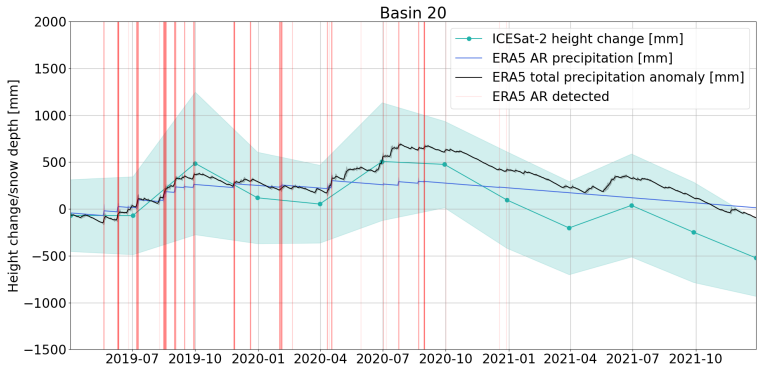

(d) Basin 20, ERA5

Figure 4.17: Mean time series between the 1st of January 2019 and 31st of December 2021 for select basins, showing ICESat-2 observed height change (green, with 2σ around it), the AR precipitation anomaly from ERA5 reanalysis data (blue), and the total precipitation anomaly from ERA5 reanalysis data (black). The red vertical lines indicate when an AR was detected in the basin, brighter lines indicate that ARs were detected in subsequent time steps. The ICESat-2 data has a temporal resolution of 91 days, the precipitation anomalies and AR detections have a temporal resolution of 3 hours.

5 Discussion

This chapter discusses the methods and results. Section 5.1 examines the choice of ICESat-2 data product and how it may affect the results. This section also discusses the challenges related to ICESat-2 data. Section 5.2 delves into the differences between the two reanalysis data-sets analysed in this thesis. Section 5.3 discusses the regridding process used to prepare the data-sets for analysis. The AR detection algorithm employed and the potential effects of using a different detection algorithm on results are discussed in section 5.4. In section 5.5 the significance of pixels where the variance reduction is negative is explored, as well as potential causes. Section 5.6 discusses how non-precipitation AR effects influence the results. Finally, section 5.7 quantifies the results by comparing results on a basin-scale to the continental mean and section 5.8 compares the results to pre-existing literature.

5.1. ICESat2 data product

5.1.1. Choice of ICESat-2 data product

It is important to understand how using different ICESat-2 data products might affect the results of this thesis. In this thesis only the ICESat-2 ATL15 data product was used. ATL15 is a gridded product of Antarctic and Arctic land ice height change. ATL15 was released in December 2021, and as such it is a relatively recent data product. The product is on version 2, and was derived from ATL11, Version 5.

A clear advantage of using ATL15 data is that the data is available in grids, and it is therefore easy to compare the data with the reanalysis data, which are also gridded products. Additionally, downloading the data is fast and the file size is small (3.8 GB for 1km resolution, and 36 MB for 10km resolution). All the data is available in a single .nc file, as opposed to all tracks being in separate files, which is the case for the lower level data products.

ATL15 was specifically designed to provide surface elevation change due to surface mass balance and geodetic processes. It was designed to allow for visualisation of height-change patterns. This is closely related to the topic of interest of this study, namely the height-change pattern related to AR precipitation.

A potential disadvantage of using ATL15 data is that it has undergone more processing steps compared to lower-level data products. As such, it is important to understand the limitations and assumptions, and to consider that the processing steps have introduced potential errors or biases in the data. For example, a number of masks have been applied to create the gridded product, such as a land-ice mask and masking out points identified as having an ice thickness less than 10m. Additionally, grounding lines and ice fronts may not be resolved well by ATL15. Ice fronts are expected to advance and retreat over the course of the ICESat-2 mission. If this is not taken into account, it could lead to large apparent height changes in the product. Large height changes close to ice fronts should thus be treated with caution. This is likely not a big problem in the analyses in this thesis due to the ice speed mask masking out these areas.

Another data products that could be used is ATL06. The ATL06 product provides higher resolution elevation measurements compared to ATL15, meaning it can capture height changes in more detail. The downside is that the ATL06 data is also more complex and computationally intensive to process compared to the ATL15 data.

For the objective of this thesis, which is to determine whether an AR precipitation signal can be recognised in ICESat-2 data, this added spatial resolution is not worth this downside. The resolution of the reanalysis data-set is relatively coarse, and the resolution of the ATL15 gridded product is high enough.

However, it might be interesting to use ATL15 data to identify regions and periods where the AR signal is likely to be strong, and then use ATL06 data to investigate the AR signal more closely. The resolution of ATL06 is much finer than the resolution of either reanalysis data-set. Due to the condition that ARs have to extend at least 20° in the longitudinal direction, they are usually quite large (although it is possible that only a small part of the AR actually makes landfall). Within the larger AR footprint, there may be more detailed precipitation patterns that are interesting to investigate. Using the AR detections from reanalysis data-set, and the contribution of AR precipitation to total precipitation in these moments (so over shorter time periods rather than over years), it might also be possible to determine if AR precipitation is indeed contained to roughly the AR footprint or whether it is much more widespread.

Finally, ATL11 could also be used. ATL11 is primarily meant as an input for higher-level gridded products, but it can also be used on its own. Considering the fact that ATL15 data is derived from ATL11 data, it could definitely be used for this thesis. ATL11 contains spatially organised time series of land-ice surface heights derived from ATL06. Similarly to ATL06, the main advantage of using ATL11 data over ATL15 data is that ATL11 data provides more detailed information of surface height changes. ATL11 provides point-to-point height measurements along the ICESat-2 ground tracks and as such contains more precise height measurements than ATL15, which is a gridded product. This increased precision might result in more accurate detection of the AR precipitation signal. Also, ATL11 would provide more freedom in choosing which masks to apply to the data. Additionally, the data is not limited to specific grid points like it is in ATL15, which means that the higher resolution can provide more insight into the spatial variability of the precipitation signal. Disadvantages of using ATL11 data are mostly the same as for ATL06. Additional pre-processing would be needed compared to ATL15, and it would be more computationally expensive to work with ATL11 data. Also, as ATL11 data is not gridded, additional processing steps would be required to create gridded products for comparison with the reanalysis data.

5.1.2. Limitations in ICESat-2 data

One of the biggest challenges is the coarse temporal resolution of ICESat-2. The ICESat-2 data has a temporal resolution of approximately 91 days, so it provides the height change over a 3 month period. This is a long time compared to the duration of individual AR events. AR conditions in a fixed place typically last between a few hours up to a few days at most, which means that the signal of interest of this study is occurring over a much shorter time period than the ICESat-2 data interval.

This limitation can make it difficult to observe the AR precipitation signal, especially during periods in which AR frequency is low, or non-AR precipitation is high. ARs typically cause extreme snowfall over short periods of time. Over longer time periods, non-AR precipitation can make it difficult to observe the AR precipitation signal in ICESat-2 data, by smoothing out the extreme snowfall that is typically related to ARs.

Additionally, the data record of ICESat-2 is relatively short, which should also be taken into account when interpreting the results of this study. Only 3 years of ICESat-2 data were used in this study, which combined with the 3-monthly resolution leads to 12 height change observations per pixel. This may not be sufficient to capture the full variability of AR events and their impacts on snowfall in a given region. As the ICESat-2 data record increases this problem may become less relevant, although the nominal mission life of ICESat-2 was only 3 years, and ICESat-2 has been out of science mode as of 22 September 2022. Alternatively, ICESat-2 data could be combined with other satellite data such as ICESat, or a potential future mission.

Despite these limitations, there are places where a clear correlation between the predicted AR precipitation signal and the observed height change in ICESat-2 data was found. These are mainly regions with high AR frequency and contribution, and not a lot of negative ICESat-2 height change. This suggests that despite the coarse temporal resolution of ICESat-2, there are some regions where ICESat-2 data can be useful for more detailed study into AR precipitation. Still, it is important to consider the limitations of temporal resolution when interpreting ICESat-2 data.

5.2. Difference in reanalysis data-sets

Overall, both reanalysis data-sets perform very similarly.

AR contribution is very similar, both over a longer time period (1980-2021) as well as over the period of interest (2019-2021).

The pattern of AR detection frequencies between 2019 and 2021 for MERRA-2 and ERA5 is also similar. Both data-sets show high AR frequency in the same locations, but nonetheless there are some small differences in the magnitude of AR frequency. Generally, MERRA-2 detects ARs slightly more often than ERA5 over most of Antarctica, with the exception of Dronning Maud Land. AR contribution is not significantly higher in MERRA-2. This may mean that the extra ARs that were detected in MERRA-2 did not carry a lot of precipitation, for example because the ARs were weak and only just reached the vIVT threshold. It is also possible that in the regions where extra ARs were detected MERRA-2 underestimated the total precipitation compared to ERA5. It has to be noted that in this study only one AR detection algorithm was used. There may be a bigger difference between AR detections when using a different detection algorithm.

Both data-sets appear to capture the AR precipitation pattern to some extent based on the correlation and variance reduction analyses. Correlation and variance reduction for total precipitation are high everywhere, whereas correlation and variance reduction for AR precipitation are clearly higher in the regions where AR contribution is higher, and low in the regions where AR precipitation is low. ERA5 shows slightly higher values in most basins, but not in all basins.

It is important to note that while for both data-sets the AR precipitation pattern appears to be captured to a certain extent, the interpretation of correlation and variance reduction needs to be taken with caution. Correlation and variance reduction do not necessarily indicate causality, and other factors such as data quality, spatio-temporal resolution, and interpolation methods can affect the results. Also, the analysis is based on the assumption that ICESat-2 total height change is primarily due to total precipitation, while in reality there are other factors also contributing to height change, such as ice dynamics or firn compaction.

MERRA-2 has a larger percentage of pixels with a high SNR, which indicates that the AR precipitation pattern present in MERRA-2 is relatively stronger than the noise from the non-AR signal in ICESat-2 height change. This could suggest that MERRA-2 better captures the AR precipitation signal compared to ERA5. However, caution should still be taken when interpreting the SNR results. The method used to calculate the SNR assumes that the non-AR precipitation anomaly in the reanalysis data is a perfect representation of the true non-AR precipitation anomaly. In reality, this is not the case. It is also possible that MERRA-2 simply overestimates the AR precipitation anomaly, which would increase the signal strength relative to the noise, and thus a higher SNR. Similarly, it is possible that ERA5 underestimates the AR precipitation anomaly.

Chapter 3 mentioned that the modest resolution of MERRA-2 data could lead to an underestimation of the highest precipitation rates, and thus an underestimation of AR precipitation. When looking at the detailed time series, the total precipitation anomaly in ERA5 is indeed generally larger than in MERRA-2, so this could very well be the case. However, the difference is not large enough to lead to different conclusions.

Then based on the analyses of this thesis, there is no clear better choice as to which reanalysis data produces the best results. If having the highest spatial resolution is a priority, then ERA5 would be the better option due to its finer resolution. However, if computational speed and data storage are of a larger concern, then MERRA-2 would be the better choice. Thanks to the coarser resolution, data file sizes are significantly smaller.

Another advantage of using MERRA-2 is that vIVT is already provided. For ERA5 it has to be computed separately, which means that a lot of additional data has to be downloaded and stored, and an additional computation step is necessary, increasing running time even further.

5.3. Regridding of data

All of the data products have different resolutions. For some of the analyses it is important that the input grids have the same resolution. This is the case for correlation and variance reduction, and SNR. This presents a challenge, because it means that at least one of the data sets has to be regridded to transform the data to another grid.

In this study, the data with a finer spatial resolution was regridded to match the coarser spatial resolution of the other data. This inevitably leads to a loss of detail that was present in the finer resolution data. Optionally, the coarser grids can also be regridded to the finer resolution grids, which may lead to slightly different conclusions due to the added resolution.

It is important to note that regridding can introduce errors and biases into the data, and the choice of regridding method (ie nearest neighbour, bi-linear, bi-quadratic, bi-cubic etc) can impact the results. In all cases, the regridding method was carefully selected by comparing the regridded product with the original product and with the other grid. For example, if ICESat-2 data was regridded to match MERRA-2 data, the regridded ICESat-2 data was compared with the original ICESat-2 data, and also with the MERRA-2 data, to check if the regridding did not introduce large errors.

Overall, regridding cannot be avoided when working with data-sets with different spatial resolutions.

5.4. AR detection algorithm

A single AR detection algorithm was used to detect ARs. The same algorithm was used for both MERRA-2 as well as ERA5.

The algorithm was developed by (J. D. Wille et al., 2019) and is participating in ARTMIP. The algorithm is regionally specific to polar regions rather than a global algorithm. As such, it detects ARs at a lower frequency compared to other global algorithms. However, as it is designed to capture only high impact events, it might miss weaker AR events that would be captured in global AR detection algorithms with lower thresholds.

Using a different AR detection algorithm might lead to different results. However, using a global AR detection algorithm would most likely lead to less accurate results. Global algorithms based on a percentile generally use a lower threshold that is not really suited for polar regions, and would then detect more ARs, possibly overestimating AR precipitation. On the other hand, global algorithms using an absolute threshold rather than a relative threshold would probably fail to detect some ARs, due to the vIVT values being lower in the polar regions.

It could also be interesting to use the same algorithm but tweaking the threshold values (98th percentile vIVT, extending >20° in the meridional direction) and see if that leads to significantly different results. For example, by setting the threshold value for vIVT lower, currently detected ARs will be larger around the edges and thus cover larger areas, and additional smaller ARs might be detected. In contrast, by setting the threshold value for vIVT higher, currently detected ARs will be smaller, and some ARs might not reach the spatial threshold anymore and thus not be detected at all. When setting the spatial threshold lower, additional smaller ARs might be detected, while setting the threshold higher would likely result in some of the smaller currently detected ARs do not reach the threshold anymore and are thus not classified as ARs.

Additionally, it is also important to note that the method of attributing precipitation to ARs can have a big influence on the results. A too short time-window after a AR is detected might miss precipitation caused by the AR while a too long window may include precipitation that is not related to the AR and thus overestimate precipitation. The area used to assign precipitation to an AR can also have a significant influence on the results, as the precipitation related to an AR may not be limited to the area covered by the AR itself. By choosing to use only the precipitation within an AR footprint, the AR precipitation signal from reanalysis data covers a smaller area than it likely does in reality.

This study is then more likely to underestimate AR precipitation in reanalysis data, both in magnitude per pixel and in covered area, making it more difficult to recognise the AR precipitation signal in ICESat-2 data.

5.5. Negative variance reduction

As already mentioned in chapter 3, the variance reduction maps show a number of areas with negative variance reduction when the signal of interest is total precipitation. These pixels were masked out for subsequent analysis, but it is still unknown why these negative variance reduction values are present. Here, a few possible explanations are further discussed.

Looking back at equation 3.11, this happens when the variability of $\Delta h - \Delta h_{signal\ of\ interest}$ is larger than the variability of Δh. The variance of ICESat-2 does not show the same pattern (see figure A.9 in A). What does stand out, is that in Victoria Land and along the Transantarctic Mountains there are pixels where there is no ICESat-2 ATL15 data. The variance in these pixels is thus 0 in ICESat-2 data,

and the variance in the reanalysis data will therefore never be smaller in the reanalysis data. As for the pixels where there is ICESat-2 data, there are various possible explanations for this.

This can happen for example when the total precipitation anomaly is high, but for some reason the snow does not stay. Then based on the total precipitation anomaly it would be expected to observe a height change of roughly the same magnitude, but instead this height change is not observed.
A possible explanation for this is blue ice, as snow does not stick on blue ice. Instead it is blown away, and therefore snowfall does not lead to a height change observable via ICESat-2. To test this hypothesis, the analysis is re-run while using a mask of known blue ice areas (see figure 4.8c) detected using Landsat ETM+ and MODIS satellite data (Hui et al., 2014). Although this does mask out some of the pixels with negative variance reduction (see figure A.8 in appendix A), it cannot fully explain the negative variance reduction values.

Another possible explanation is that in these areas the height changes are very small, thus the variability of ICESat-2 is very small too. Then even if the precipitation anomaly values are not very large, the variance reduction values could fall below zero. In this case masking out the negative variance reduction values should not greatly influence the further results, because both the height change as well as the precipitation anomaly are small.

To test if this is the case, the mean 3-monthly height changes per pixel and per basin are computed over 2019-2021. The height change in the pixels with negative variance reduction are indeed small compared to the mean height change in the entire basin (See figures A.10 and A.11 in appendix A).

Table 5.1 shows the mean 3-monthly height changes when taking only positive (mean) or negative (mean) height change into account. Positive and negative values were computed separately to give a clearer image. In all cases, the mean value for only pixels where variance reduction < 0 is closest to 0, although the difference is small. Therefore, it is assumed that the pixels with negative variance reduction will not greatly affect the results, and it is thus okay to mask them out. Still, correlation and AR precipitation anomaly variance reduction analyses were also run without masking out pixels with negative total precipitation anomaly variance reduction. This did not lead to different conclusions.

Table 5.1: Mean height changes when taking either mean of all pixels, mean for pixels where variance reduction with $\Delta h_{total\ precipitation}$ < 0, and mean for pixels where variance reduction with $\Delta h_{total\ precipitation}$ > 0. Positive (negative) height change, mean over time means that the mean height change in a pixel over the entire period from 2019-2021 is positive (negative). Positive (negative) height change, anytime means that all the pixels with a positive (negative) height change value are used, regardless of which time step they were recorded.

	All pixels	Only pixels where variance reduction <0	Only pixels where variance reduction >0
Positive height change, mean over time [m]	0.0152	0.0116	0.0119
Negative height change, mean over time [m]	-0.0267	-0.0134	-0.0178
Positive height change, anytime [m]	0.0863	0.0528	0.0657
Negative height change, anytime [m]	-0.0783	-0.0485	-0.0557

The same is done but then with total precipitation anomaly values (already accounted for snow density), for both ERA5 as well as MERRA-2 (see figures A.10 and A.11 in appendix A). If the total precipitation anomaly is very large in the pixels with negative variance reduction, it could be that the reanalysis data-set predicts the precipitation in the wrong place, or that the precipitation did fall, but was blown away, thus not showing up in ICESat-2 observations.

When only looking at the pixels where variance reduction is negative, their values are neither exceptionally large nor exceptionally small. Looking at the mean total precipitation anomaly per basin, for all pixels and for only the pixels where variance reduction is negative, it becomes clear that total precipitation anomalies are very similar.

However, height change values in ICESat-2 were smaller in the pixels with negative variance reduction compared to all pixels. A possible explanation as to why the positive precipitation anomalies do not translate to positive height change in ICESat-2 is that the snow is blown away, which is known as drifting snow. If the reanalysis data predicts a certain amount of precipitation in a location, but it is blown away, then ICESat-2 observes a smaller height change (or more negative) than would be expected based on the reanalysis data. If this happens systematically in the same locations, this could

then explain why the total precipitation anomaly variance reduction is negative in these locations. However, if snow is blown away from the place where reanalysis data expected it to be, it also has to settle down eventually in another place, where reanalysis data does not expect it to be. Then in this place, drifting snow could also cause a too high variance reduction value.

Why this is also the case with negative precipitation anomalies is less straightforward. This could be due to ice dynamics or other atmospheric factors for example, but to be sure more research is required.

5.6. Other effects related to ARs

This thesis only investigated precipitation related to ARs. As chapter 2 mentioned, ARs can have a range of different effects, including but not limited to precipitation. Most importantly, ARs can also cause melting conditions. In some cases, a single AR event can both cause extreme precipitation as well as melting events. This study found that AR frequency between 2019 and 2021 was largest in Antarctic spring and summer, which means it is even more likely that some of the ARs caused melting events.

If an AR causes melting conditions, this can result in a significant decrease in the surface elevation, and thus to a negative height change observed in ICESat-2. This can then mask the precipitation signal in the ICESat-2 observations.

5.7. Comparing basins with values over the entire continent

In this subsection the correlation and variance reduction values found per basin are compared with the mean over the entire continent, to see in which basins there is a higher mean correlation and/or variance reduction value than the continent mean (ice shelves not included). The correlation is the correlation between the AR precipitation from reanalysis data and the ICESat-2 observations, and the variance reduction is the variance reduction with AR precipitation from reanalysis data as the signal of interest. This is based on the contribution weighted values. As mentioned in chapter 4, the mean contribution weighted correlation over the entire continent is 0.272 for MERRA-2 and 0.248 for ERA5. The mean variance reduction with AR precipitation as the signal of interest is 0.0680 for MERRA-2 and 0.0669 for ERA5.

Table 5.2 shows the basins where the mean correlation/variance reduction is larger than the mean over the entire continent, ice shelves not included. The table shows the results for both reanalysis data sets, so the correlation and variance reduction using MERRA-2 data as well as using ERA5 data. Figure 5.1 visually shows for each basin the number of times that the basin mean was larger than the continent mean.

In 20 out of 27 basins both the basin mean correlation and variance reduction values for both reanalysis data sets are all either higher or lower than the continent mean.

If the values are all higher than the continent mean, this can be used as a first indication that in these basins using ICESat-2 data in addition to reanalysis data can be useful and lead to new insights, especially when using ICESat-2 data products with a fine spatial resolution.

If the values are all lower than the continent mean, atmospheric river precipitation expected based on the reanalysis data is not observable in ICESat-2 data. This could be due to a number of reasons, the most likely being that either there is very little AR precipitation in these basins to start with, or because the atmospheric river precipitation signal is small compared to other signals causing height change. Either way, using ICESat-2 data in these basins in addition to reanalysis data is unlikely to improve results.

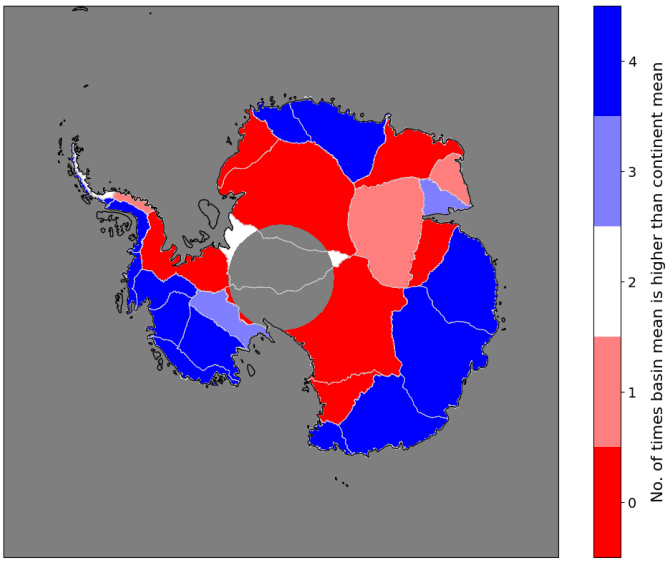

Figure 5.1: Number of times that the contribution-weighted basin mean correlation or variance reduction is higher than the contribution-weighted mean correlation or variance reduction over the entire continent. The maximum is 4, ie the contribution-weighted basin mean correlation for both MERRA-2 and ERA5 is higher than the contribution-weighted mean correlation or variance reduction over the entire continent as well as the contribution-weighted basin mean variance reduction for both MERRA-2 and ERA5. Grey indicates no data, which is in this case over the ocean, and over the interior of Antarctica where the latitude >85°.

Table 5.2: Basins where the mean correlation between the AR precipitation from reanalysis data and the ICESat-2 observations/variance reduction with AR precipitation from reanalysis data as the signal of interest is larger than the mean over the entire continent, ice shelves not included.

		Basins	No. of basins
MERRA-2	Correlation >0.272	5, 6, 9, 10, 12, 13, 14, 15, 18, 19, 20, 21, 22, 23, 24, 25	16 (59%)
	Variance reduction >0.0680	5, 6, 12, 13, 14, 15, 18, 19, 20, 21, 22, 23, 24, 25	14 (52%)
ERA5	Correlation >0.248	2, 5, 6, 8, 9, 12, 13, 14, 15, 18, 19, 20, 21, 22, 23, 24, 25, 26, 27	19 (70%)
	Variance reduction >0.0669	2, 5, 6, 9, 12, 13, 14, 15, 19, 20, 21, 22, 23, 24, 25, 26	16 (59%)

Figures 5.2 and 5.3 show the mean ratio per basin of the contribution-weighted AR precipitation and ICESat-2 height change correlation and the contribution-weighted continent mean correlation, and the mean ratio per basin of the contribution-weighted AR precipitation variance reduction and the mean contribution-weighted AR precipitation variance reduction over the entire continent respectively. This shows in which basins the correlation and variance reduction values are high compared to the continent mean.

Figure 5.2 shows that the ratio for the correlation is highest in basin 5, and also high in basin 12 and 14, for both MERRA-2 and ERA5. The ratio is also high for basin 20 in ERA5, but not in MERRA-2. Figure 5.3 shows that the ratio for the variance reduction is highest in basin 5, and also high in basin 12 for both reanalysis data-sets. Basin 14 has a high ratio in MERRA-2 but less so in ERA5, and basin 20 has a high ratio in ERA5, but not in MERRA-2.

This matches the previous results in which basin 5 and basin 12 showed the most promise when comparing the AR precipitation from reanalysis data and ICESat-2 height change, while basins 14 and 20 showed promise based on the correlation and variance reduction analyses but ultimately did not show a clear link over the study period.

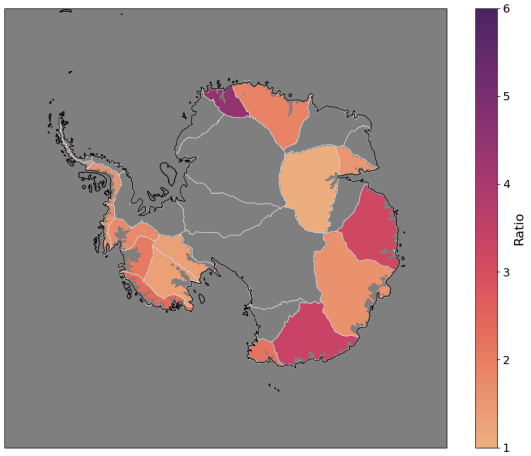

(a) MERRA-2

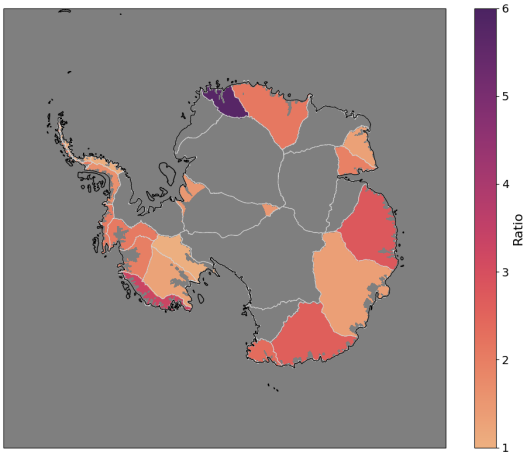

(b) ERA5

Figure 5.2: Mean ratio per basin of the contribution-weighted AR precipitation and ICESat-2 height change correlation and contribution weighted continent mean correlation. See appendix A for the same figure but the ratio per pixel rather than the mean per basin. Basins where the ratio is smaller than 1 (and the continent mean value is thus larger than the basin mean value) have been masked out.

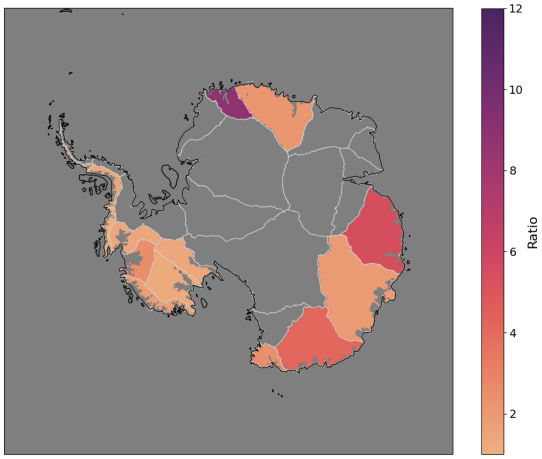

(a) MERRA-2

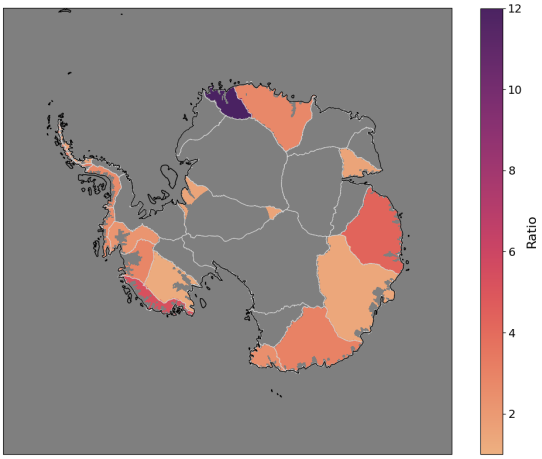

(b) ERA5

Figure 5.3: Mean ratio per basin of the contribution-weighted AR precipitation variance reduction and contribution weighted continent mean AR precipitation variance reduction. See appendix A for the same figure but the ratio per pixel rather than the mean per basin. Basins where the ratio is smaller than 1 (and the continent mean value is thus larger than the basin mean value) have been masked out.

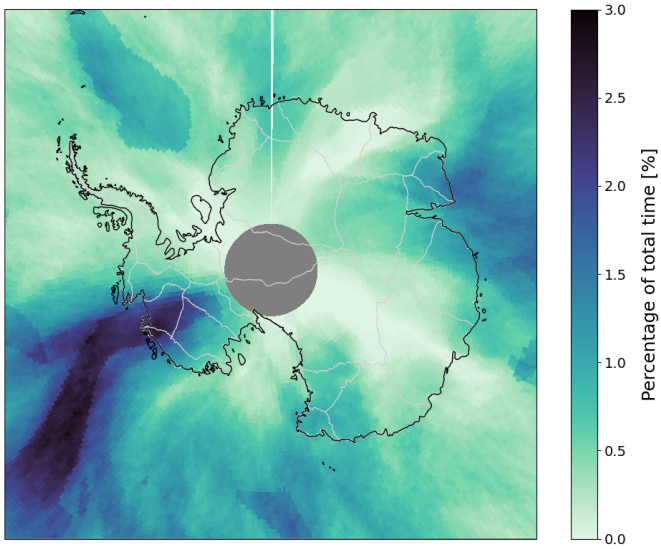

Figure 5.4: Percentage of time that an AR was detected in 2019 in every pixel for MERRA-2. Darker blue shaded areas indicate a higher AR detection frequency, while light green indicates a low AR detection frequency. The grey circle in the middle are pixels where the latitude >85°, meaning they fall outside the study area. The drainage basin divides are shown in light grey contour lines.

5.8. Comparison with literature

There have been a number of studies on AR precipitation in Antarctica. This section aims to compare the findings of this thesis with a number of these previous studies.

Maclennan et al., 2022 studied the contribution of AR precipitation to total precipitation in Antarctica using MERRA-2 reanalysis data, and served as an important source for the precipitation attribution in this thesis. The results of the MERRA-2 precipitation attribution in this thesis closely match the results of this study. One of the recommendations given in Maclennan et al., 2022 is to use higher-resolution data products such as ERA5. This was done in this thesis, and led to a similar but higher-resolution result, at a cost of a longer computational time.

While most studies on ARs in the polar regions have relied on only reanalysis data, Adusumilli et al., 2021 used a combination of MERRA-2 reanalysis data and ICESat-2 height change observations to investigate whether ARs caused rapid surface height increases of the West Antarctic Ice Sheet in 2019. Using data captured between April 2019 and June 2020, the study found that extreme precipitation events were responsible for 41% of the total increases in surface height over the WAIS during the 2019 austral winter. Half of these events occured during or shortly after AR landfalls.

Figure 4.6 shows that there was a clear height increase over most of the WAIS during July-September 2019, but also in large parts from April-June 2019. The time series for the West Antarctic basins (basins 1, 18-23) from April-September 2019 show that nearly all of the large and steep total precipitation anomalies (thus likely to be extreme precipitation events) coincided with ARs. The total precipitation anomalies (figure A.6) show a pattern similar to the ICESat-2 height changes, suggesting a correlation between the total precipitation anomaly and height change.

Adusumilli et al., 2021 detected AR conditions over WAIS during 3.9% of 2019. Figure 5.4 shows the percentage of time that an AR was detected in 2019 in every pixel for MERRA-2. This figure shows that AR conditions were indeed frequent in large parts of the WAIS during 2019, but the detection frequency is lower, namely up to 2.6%. This is likely because Adusumilli et al., 2021 used IWV rather than IVT to detect ARs. Nonetheless, both Adusumilli et al., 2021 as well as this study detected an increase in AR conditions over the WAIS, and found that detected AR conditions matched an increase in surface height of the WAIS during the austral winter in 2019.

6

Conclusion and recommendations

In this final chapter, the conclusions of this thesis research are presented. The research questions stated in chapter 1 are answered. Finally, based on the findings of this studies, a number of recommendations are given.

6.1. Conclusion

The aim of this research is to estimate the amount of precipitation attributed to atmospheric rivers in Antarctica based on reanalysis data, and to determine how well AR precipitation is captured in reanalysis data based on ICESat-2 height change observations. This was done by answering the research questions stated in chapter 1:

Q. 1: *In what way do the reanalysis data-sets detect ARs in different locations?*

MERRA-2 and ERA5 reanalysis data perform very similarly in AR detection. Between 1 January 2019 and 31 December 2021, the pattern where ARs are detected is very similar for ERA5 and MERRA-2. AR conditions are most frequently detected in Dronning Maud Land, and are also often detected near the East Antarctic coast. ARs are least frequently detected near the Antarctic interior, so at the highest latitudes. This is expected, as ARs form in the subtropics, and move towards the poles. When looking at the spatial differences of AR detections between MERRA-2 and ERA5, a few things stand out. Neither of the reanalysis data-sets clearly detects more ARs over the Southern Ocean. In some regions MERRA-2 detects more ARs, and in some regions ERA5. Over land however, MERRA-2 clearly detects more ARs, with the exception of parts of Queen Elizabeth Land and Dronning Maud Land. In Queen Elizabeth Land AR detection frequency was low to start with, but in Dronning Maud Laud the highest AR detection frequencies are found in both data-sets.

Q. 2: *To what extent, spatially and temporally, is the precipitation following an AR detection related to the AR event?*

It is hard to say exactly how much precipitation is related to ARs, both spatially and temporally. Previous studies used the AR footprint as a spatial constraint, and attribute precipitation in the 24 hours after AR detection to the AR. Both are very conservative assumptions. Firstly, it is highly unlikely that AR precipitation is constrained to just the AR footprint. Grid cells surrounding the AR generally also have an IVT-v value that is far greater than average, and therefore it is likely that a greater than average amount of precipitation falls in these surrounding grid cells, as precipitation and IVTv are closely related. However, as they do not meet the 98th percentile threshold this precipitation is not considered to be AR precipitation, thus leading to an underestimation of AR precipitation. Secondly, the temporal constraint is also conservative. A past study by Maclennan et al., 2022 found that precipitation rates decrease by half in the first 10 hours after AR passage, and decrease very slowly from then on. Due to this slow decrease in precipitation rate, it is hard to tell when the precipitation is no longer related to the AR. 24 hours proved to be a suitable choice

because on average, more than 80% of cumulative precipitation has fallen since AR passage, and it is also a convenient choice because it fits nicely in the 3-hourly temporal resolution.

A previous study estimated how much precipitation is related to ARs in Antarctica (Maclennan et al., 2022). This study used MERRA-2 reanalysis data from 1980-2020 and Wille's polar AR detection algorithm, and the same spatial and temporal constraints. This study's results were replicated using the methods used in this thesis. In addition to this the analysis was also performed using ERA5 reanalysis data, to see if the finer spatial resolution improves the quality of the estimate. The long-term AR precipitation and contribution to total precipitation are very similar to MERRA-2, both quantitatively and spatially. On a shorter time scale (yearly) there are small differences. These differences are partly related to AR detection, and partly to differences in total precipitation in the datasets.

When looking at the time series, most AR detections coincide with a (sharp) increase in total precipitation anomaly. This backs the assumption that ARs often cause an in increase in precipitation. However, there are also large precipitation anomalies that do not coincide with AR detections, so not all extreme precipitation events are linked to ARs. Also, in some cases ARs are detected but there is no noticeable positive total precipitation anomaly, or even a negative total precipitation anomaly. This suggests that not all ARs cause extreme precipitation events. However, this could also be because the AR only just makes landfall and therefore covers a very small amount of the basin. Then, AR conditions are only present in a small amount of pixels, and these pixels are also likely to have a smaller IVTv value than pixels that are in the center of an AR event.

Q. 3: *Which processes are responsible for height change observed in ICESat-2 altimetry data?*

There are a lot of processes leading to height change in Antarctica, in different magnitudes.

The main process of interest in this thesis is precipitation, the precipitation anomaly to be more specific. If it is assumed that the Antarctic mass balance is in long-term equilibrium, then that means that the input of snowfall and the output of mass loss should be roughly balanced over a long time period. Anomalies in precipitation should then be the main cause of observed height with a positive anomaly leading to an increase in observed height and a negative anomaly to a decrease in observed height. This was confirmed by performing a variance reduction analysis using ICESat-2 height change observations and the total precipitation as the signal of interest.

Besides precipitation anomalies, ice dynamics is also responsible for height change. The magnitude of ice velocities differ, and are generally largest near the coast and decrease land inwards. Pixels with a speed larger than 100 meters per year were masked out, as in these locations ice dynamics makes it hard to analyse the height change due to precipitation anomalies.

In addition to this, there are multiple other processes that can also cause height change in Antarctica, but were not further studies/incorporated in this thesis. Erosion and sublimation at the surface for example, but also wind patterns and ocean currents can contribute to height change, as well as isostatic rebound.

Melting conditions, which have also been linked to ARs can also lead to a negative height change.

Q. 4: *To what extent can a precipitation pattern be recognised in ICESat-2 altimetry data?*

To investigate whether a precipitation pattern can be recognised in ICESat-2 altimetry data, the total precipitation anomalies from reanalysis data were compared with ICESat-2 height change observations. This comparison showed that overall, the two data-sets match quite well, and the spatial patterns visible in the ICESat-2 data are also visible in the reanalysis total precipitation anomaly maps. However, the magnitude of ICESat-2 height change is slightly higher than the magnitude of total precipitation anomalies. This could be due to other non-precipitation sources of height change in ICESat-2 data. Still, the close match between the spatial patterns suggests that the spatial patterns visible in ICESat-2 height change are related to total precipitation.

Q. 5: *What is the correlation between reanalysis data and ICESat-2 satellite altimetry data?*

To investigate whether there is noticeable correlation between the reanalysis data and the satellite altimetry data, a correlation analysis was carried out.

Correlation between ICESat-2 data and total precipitation anomalies shows that there is overall a high correlation, especially near the coast and in West Antarctica. This indicates that ICESat-2 height change is related to total precipitation patterns, despite the magnitude of the height change being slightly higher than the magnitude of the total precipitation anomalies from reanalysis data.

Correlation between ICESat-2 data and AR precipitation anomalies shows that there is also some correlation. Areas where AR contribution is higher also show a higher correlation between AR precipitation from reanalysis data and ICESat-2 height change.

Additionally, a variance reduction analysis was also carried out. The variance reduction analysis showed that the AR precipitation present in reanalysis data can explain part of the variance in the ICESat-2 data, suggesting that the AR precipitation signal is present in the ICESat-2 data.

Overall, the correlation analysis and variance reduction analysis suggest that the AR precipitation signal is present in the ICESat-2 data, but it varies regionally as to how strong the signal is.

In conclusion, this thesis sheds light on the role of ARs in precipitation in Antarctica. Despite ARs being rare occurrences, this study found that they contribute a significant amount of precipitation to the total precipitation, which is in line with previous research. This highlights the importance of understanding the role of ARs within the overall precipitation regime of the polar regions.

In comparing the expected AR precipitation from reanalysis data with ICESat-2 height observations, we have gained valuable new insights regarding AR precipitation in Antarctica.

Overall, the results suggest that while there is some evidence of a relationship between AR precipitation and ICESat-2 height change, the signal is generally weak and highly variable across the entire continent.

However, a strong correlation between AR precipitation anomalies from reanalysis data and the observed height changes from ICESat-2 is present in select drainage basins. Furthermore, a variance reduction analysis reveals that AR precipitation can explain a significant amount of the variance in ICESat-2 observations in these basins. This suggests that AR precipitation can significantly contribute to the observed height change in certain basins, and thus to the SMB. After a more detailed analysis, specific areas in East Antarctica show the most promise. For these select areas, using ICESat-2 data with a higher spatial resolution in addition to reanalysis data may lead to more insights into precipitation related to ARs on a smaller scale.

Overall, this thesis highlights the importance of studying and understanding AR precipitation in the cryosphere, and demonstrates the value of incorporating ICESat-2 data for a better understanding of the local effects of ARs on the SMB of Antarctica.

6.2. Recommendations

Based on the results, there are a number of recommendations for further research that could contribute to a better understanding of the impact of ARs on Antarctica's SMB.

Currently, the time period over which ICESat-2 data is available is short, as the satellite was launched in 2018 and the first reliable data was collected from April 2019 and onwards. While ICESat-2 was designed for a 3-year life, until September 2021, with a 5-year goal. As of now, ICESat-2 is still active and collecting data, and the projected end of mission is now 2027.

Therefore, future research should aim to include a longer ICESat-2 data record. Additionally, combining ICESat-2 observations with other observational data, such as ICESat or CryoSat-2, could also provide valuable insights.

Secondly, this thesis only investigated the impact of ARs on precipitation, and therefore assumes that ARs contribute positively to Antarctica's Surface Mass Balance. However, ARs are known to also cause melting under certain circumstances, particularly during summer. This melting effect might also be observable in ICESat-2 as a negative height change. Therefore, future research could focus on the effects of ARs on melting conditions to obtain a more comprehensive understanding of their influence on SMB.

As the data record increases, it might also be interesting to look at the data per season to investigate how seasonality affects the results. This is especially interesting considering the fact that ARs can also cause melting conditions rather than (or in addition to) snowfall conditions under certain circumstances, but it is currently unclear how to determine if an AR will cause melting or extreme precipitation.

Furthermore, this study used only one AR detection algorithm. Future research should aim to include more AR detection algorithms, applied to the same data, to estimate how much uncertainty is related to the AR detection algorithm.

Additionally, it could be interesting to categorise detected ARs by strength, based on for example their size and vIVT threshold. This way, it might be possible to determine whether specific AR characteristics lead to high precipitation. This would narrow down in which moments and which locations it would be expected to observe significant height increases related to ARs.

Also, the reason for the negative values when performing variance reduction with total precipitation as the signal of interest should be explored further. A possible explanation could be drifting snow. If this is indeed the case, ICESat-2 data might also be a useful tool in identifying drifting snow.

Finally, ARs are expected to change in frequency and intensity in the future. Future research should take this into account.

References

Abrahamsen, E. (2012). *Oceanographic conditions beneath fimbul ice shelf, antarctica* (Doctoral dissertation).

Adusumilli, S., A. Fish, M., Fricker, H. A., & Medley, B. (2021). Atmospheric river precipitation contributed to rapid increases in surface height of the west antarctic ice sheet in 2019. *Geophysical Research Letters*, *48*(5). https://doi.org/10.1029/2020GL091076

Agosta, C., Amory, C., Kittel, C., Orsi, A., Favier, V., Gallée, H., Broeke, M. R. V. D., Lenaerts, J. T., Wessem, J. M. V., Berg, W. J. V. D., & Fettweis, X. (2019). Estimation of the antarctic surface mass balance using the regional climate model mar (1979-2015) and identification of dominant processes. *Cryosphere*, *13*. https://doi.org/10.5194/tc-13-281-2019

Bao, J. W., Michelson, S. A., Neiman, P. J., Ralph, F. M., & Wilczak, J. M. (2006). Interpretation of enhanced integrated water vapor bands associated with extratropical cyclones: Their formation and connection to tropical moisture. *Monthly Weather Review*, *134*. https://doi.org/10.1175/MWR3123.1

Bozkurt, D., Rondanelli, R., Marín, J. C., & Garreaud, R. (2018). Foehn event triggered by an atmospheric river underlies record-setting temperature along continental antarctica. *Journal of Geophysical Research: Atmospheres*, *123*. https://doi.org/10.1002/2017JD027796

Dacre, H. F., Clark, P. A., Martinez-Alvarado, O., Stringer, M. A., & Lavers, D. A. (2015). How do atmospheric rivers form? *Bulletin of the American Meteorological Society*, *96*. https://doi.org/10.1175/BAMS-D-14-00031.1

Dettinger, M. D., Lavers, D. A., Compo, G. P., Gorodetskaya, I. V., Neff, W., Neiman, P. J., Ramos, A. M., Rutz, J. J., Viale, M., Wade, A. J., & White, A. B. (2020). Effects of atmospheric rivers. In *Atmospheric rivers* (pp. 141–173). Springer.

Espinoza, V., Waliser, D. E., Guan, B., Lavers, D. A., & Ralph, F. M. (2018). Global analysis of climate change projection effects on atmospheric rivers. *Geophysical Research Letters*, *45*. https://doi.org/10.1029/2017GL076968

Gorodetskaya, I. V., Van Lipzig, N. P. M., Van den Broeke, M. R., Mangold, A., Boot, W., & Reijmer, C. H. (2013). Meteorological regimes and accumulation patterns at utsteinen, dronning maud land, east antarctica: Analysis of two contrasting years. *Journal of Geophysical Research: Atmospheres*, *118*(4), 1700–1715. https://doi.org/https://doi.org/10.1002/jgrd.50177

Gorodetskaya, I. V., Tsukernik, M., Claes, K., Ralph, M. F., Neff, W. D., & Van Lipzig, N. P. M. (2014). The role of atmospheric rivers in anomalous snow accumulation in east antarctica. *Geophysical Research Letters*, *41*(17), 6199–6206. https://doi.org/10.1002/2014GL060881

Guan, B., & Waliser, D. E. (2015). Detection of atmospheric rivers: Evaluation and application of an algorithm for global studies. *Journal of Geophysical Research*, *120*. https://doi.org/10.1002/2015JD024257

Hassler, B., & Lauer, A. (2021). Comparison of reanalysis and observational precipitation datasets including era5 and wfde5. *Atmosphere*, *12*, 1462. https://doi.org/10.3390/atmos12111462

Hui, F., T.Y. Ci, X. C., Scambos, T., Y. Liu, Y. Z., Chi, Z., Huang, H., Wang, X., Wang, F., Zhao, C., & Jin, Z. (2014). Mapping blue ice areas in antarctica using etm+ and modis data. *Annals of Glaciology*, *66*, 129–137.

King, M. A., Bingham, R. J., Moore, P., Whitehouse, M. J., Pippa L.and Bentley, & Milne, G. A. (2012). Lower satellite-gravimetry estimates of antarctic sea-level contribution. *Nature*, *491*, 586–589. https://doi.org/https://doi.org/10.1038/nature11621

Lenaerts, J. T., Medley, B., van den Broeke, M. R., & Wouters, B. (2019). Observing and modeling ice sheet surface mass balance. *Reviews of Geophysics*, *57*. https://doi.org/10.1029/2018RG000622

Ma, W., Chen, G., & Guan, B. (2020). Poleward shift of atmospheric rivers in the southern hemisphere in recent decades. *Geophysical Research Letters*, *47*. https://doi.org/10.1029/2020GL089934

Maclennan, M. L., Lenaerts, J. T. M., Shields, C., & Wille, J. D. (2022). Contribution of atmospheric rivers to antarctic precipitation. *Geophysical Research Letters*, *49*. https://doi.org/10.1029/2022GL100585

Markus, T., Neumann, T., Martino, A., Abdalati, W., Brunt, K., Csatho, B., Farrell, S., Fricker, H., Gardner, A., Harding, D., Jasinski, M., Kwok, R., Magruder, L., Lubin, D., Luthcke, S., Morison, J., Nelson, R., Neuenschwander, A., Palm, S., … Zwally, J. (2017). The ice, cloud, and land elevation satellite-2 (icesat-2): Science requirements, concept, and implementation. *Remote Sensing of Environment*, *190*. https://doi.org/10.1016/j.rse.2016.12.029

Mattingly, K. S., Mote, T. L., & Fettweis, X. (2018). Atmospheric river impacts on greenland ice sheet surface mass balance. *Journal of Geophysical Research: Atmospheres*, *123*(16), 8538–8560. https://doi.org/10.1029/2018JD028714

Mattingly, K. S., Mote, T. L., Fettweis, X., van As, D., Tricht, K. V., Lhermitte, S., Pettersen, C., & Fausto, R. S. (2020). Strong summer atmospheric rivers trigger greenland ice sheet melt through spatially varying surface energy balance and cloud regimes. *Journal of Climate*, *33*(16), 6809–6832. https://doi.org/10.1175/JCLI-D-19-0835.1

Morlighem, M. (2020). Measures bedmachine antarctica, version 2. [[mask]. Boulder, Colorado USA. NASA National Snow and Ice Data Center Distributed Active Archive Center. [Accessed: 2022-11-16]]. https://doi.org/10.5067/E1QL9HFQ7A8M

Mottram, R., Hansen, N., Kittel, C., Wessem, J. M. V., Agosta, C., Amory, C., Boberg, F., Berg, W. J. V. D., Fettweis, X., Gossart, A., Lipzig, N. P. V., Meijgaard, E. V., Orr, A., Phillips, T., Webster, S., Simonsen, S. B., & Souverijns, N. (2021). What is the surface mass balance of antarctica? an intercomparison of regional climate model estimates. *Cryosphere*, *15*. https://doi.org/10.5194/tc-15-3751-2021

Muszynski, G., Kashinath, K., Kurlin, V., Wehner, M., & Prabhat. (2019). Topological data analysis and machine learning for recognizing atmospheric river patterns in large climate datasets. *Geoscientific Model Development*, *12*. https://doi.org/10.5194/gmd-12-613-2019

NASA. (2018). Icesat-2 measuring the height of earth's ice from space.

Nash, D., Waliser, D., Guan, B., Ye, H., & Ralph, F. M. (2018). The role of atmospheric rivers in extratropical and polar hydroclimate. *Journal of Geophysical Research: Atmospheres*, *123*. https://doi.org/10.1029/2017JD028130

Neumann, T. A., Brenner, A., Hancock, D., Robbins, J., Saba, J., Harbeck, K., Gibbons, A., Lee, J., Luthcke, S. B., & Rebold, T. (2021). Atlas/icesat-2 l2a global geolocated photon data, version 5 user guide [Boulder, Colorado USA. NASA National Snow and Ice Data Center Distributed Active Archive Center. [Accessed: 2022-01-09]]. https://doi.org/10.5067/ATLAS/ATL03.005

Neumann, T. A., Martino, A. J., Markus, T., Bae, S., Bock, M. R., Brenner, A. C., Brunt, K. M., Cavanaugh, J., Fernandes, S. T., Hancock, D. W., Harbeck, K., Lee, J., Kurtz, N. T., Luers, P. J., Luthcke, S. B., Magruder, L., Pennington, T. A., Ramos-Izquierdo, L., Rebold, T., … Thomas, T. C. (2019). The ice, cloud, and land elevation satellite – 2 mission: A global geolocated photon product derived from the aadvanced ttopographic llaser aaltimeter ssystem. *Remote Sensing of Environment*, *233*. https://doi.org/10.1016/j.rse.2019.111325

Newell, R. E., Newell, N. E., Zhu, Y., & Scott, C. (1992). Tropospheric rivers? – a pilot study. *Geophysical Research Letters*, *19*. https://doi.org/10.1029/92GL02916

Parker, W. S. (2016). Reanalyses and observations: What's the difference? *Bulletin of the American Meteorological Society*, *97*. https://doi.org/10.1175/BAMS-D-14-00226.1

Payne, A. E., Demory, M. E., Leung, L. R., Ramos, A. M., Shields, C. A., Rutz, J. J., Siler, N., Villarini, G., Hall, A., & Ralph, F. M. (2020). Responses and impacts of atmospheric rivers to climate change. *Nature Reviews Earth and Environment*, *1*. https://doi.org/10.1038/s43017-020-0030-5

Pohl, B., Favier, V., Wille, J., Udy, D. G., Vance, T. R., Pergaud, J., Dutrievoz, N., Blanchet, J., Kittel, C., Amory, C., Krinner, G., & Codron, F. (2021). Relationship between weather regimes and atmospheric rivers in east antarctica. *Journal of Geophysical Research: Atmospheres*, *126*. https://doi.org/10.1029/2021JD035294

Ralph, F. M., Dettinger, M. C. L., Cairns, M. M., Galarneau, T. J., & Eylander, J. (2018). Defining "atmospheric river" : How the glossary of meteorology helped resolve a debate. *Bulletin of the American Meteorological Society*, *99*. https://doi.org/10.1175/BAMS-D-17-0157.1

Ralph, F. M., Dettinger, M. D., Schick, L. J., & Anderson, M. L. (2020). The extension of factor analysis to three-dimensional matrices. In *Atmospheric rivers* (pp. 1–13). Springer.

Ralph, F. M., Neiman, P. J., Kiladis, G. N., Weickmann, K., & Reynolds, D. W. (2011). A multiscale observational case study of a pacific atmospheric river exhibiting tropical-extratropical connections and a mesoscale frontal wave. *Monthly Weather Review*, *139*. https://doi.org/10.1175/2010MWR3596.1

Ralph, F. M., Neiman, P. J., & Wick, G. A. (2004). Satellite and caljet aircraft observations of atmospheric rivers over the eastern north pacific ocean during the winter of 1997/98. *Monthly Weather Review*, *132*. https://doi.org/10.1175/1520-0493(2004)132<1721:SACAOO>2.0.CO;2

Ralph, F. M., White, A. B., Wick, G. A., Anderson, M. L., & Rutz, J. J. (2020). Observing and detecting atmospheric rivers. In *Atmospheric rivers* (pp. 45–87). Springer.

Rutz, J. J., Guan, B., Bozkurt, D., Gorodetskaya, I. V., Gershunov, A., Lavers, D. A., Mahoney, K. M., Moore, B. J., Neff, W., Neiman, P. J., Ralph, F. M., Ramos, A. M., Steen-Larsen, H. C., Tsukernik, M., Valenzuela, R., Viale, M., & Wernli, H. (2020). Global and regional perspectives. In *Atmospheric rivers* (pp. 89–140). Springer.

Rutz, J. J., Shields, C. A., Lora, J. M., Payne, A. E., Guan, B., Ullrich, P., O'Brien, T., Leung, L. R., Ralph, F. M., Wehner, M., Brands, S., Collow, A., Goldenson, N., Gorodetskaya, I., Griffith, H., Kashinath, K., Kawzenuk, B., Krishnan, H., Kurlin, V., … Viale, M. (2019). The atmospheric river tracking method intercomparison project (artmip): Quantifying uncertainties in atmospheric river climatology. *Journal of Geophysical Research: Atmospheres*, *124*. https://doi.org/10.1029/2019JD030936

Shields, C. A., Rutz, J. J., Leung, L. Y., Ralph, F. M., Wehner, M., Kawzenuk, B., Lora, J. M., McClenny, E., Osborne, T., Payne, A. E., Ullrich, P., Gershunov, A., Goldenson, N., Guan, B., Qian, Y., Ramos, A. M., Sarangi, C., Sellars, S., Gorodetskaya, I., … Nguyen, P. (2018). Atmospheric river tracking method intercomparison project (artmip): Project goals and experimental design. *Geoscientific Model Development*, *11*. https://doi.org/10.5194/gmd-11-2455-2018

Shields, C. A., Wille, J. D., Collow, A. B. M., Maclennan, M., & Gorodetskaya, I. V. (2022). Evaluating uncertainty and modes of variability for antarctic atmospheric rivers. *Geophysical Research Letters*, *49*. https://doi.org/10.1029/2022GL099577

Skinner, C. B., Lora, J. M., Tabor, C., & Zhu, J. (2023). Atmospheric river contributions to ice sheet hydroclimate at the last glacial maximum. *Geophysical Research Letters*, *50*. https://doi.org/10.1029/2022GL101750

Smith, B. (2022). Icesat-2 algorithm theoretical basis document for land ice dem and land ice height change release 002 [[Accessed: 2022-01-09]].

Smith, B., Sutterley, T., Dickinson, S., Jelley, B. P., Felikson, D., Neumann, T. A., Fricker, H., Gardner, A., Padman, L., Markus, T., Kurtz, N., Bhardwaj, S., III, D. W. H., & Lee, J. (2022). Atlas/icesat-2 l3b gridded antarctic and arctic land ice height change, version 2 user guide [Boulder, Colorado USA. NASA National Snow and Ice Data Center Distributed Active Archive Center. [Accessed: 2022-01-09]]. https://doi.org/10.5067/ATLAS/ATL15.002

Smith, B., Fricker, H. A., Holschuh, N., Gardner, A. S., Adusumilli, S., Brunt, K. M., Csatho, B., Harbeck, K., Huth, A., Neumann, T., Nilsson, J., & Siegfried, M. R. (2019). Land ice height-retrieval algorithm for nasa's icesat-2 photon-counting laser altimeter. *Remote Sensing of Environment*, *233*. https://doi.org/10.1016/j.rse.2019.111352

Smith, S., Dickinson, S., Jelley, B., Neumann, T., Hancock, D., Lee, J., & Harbeck, K. (2022). Atlas/icesat-2 l3b slope-corrected land ice height time series, version 5 user guide [Boulder, Colorado USA. NASA National Snow and Ice Data Center Distributed Active Archive Center. [Accessed: 2022-01-09]]. https://doi.org/10.5067/ATLAS/ATL11.005

Sodemann, H., Wernli, H., Knippertz, P., Cordeira, J. M., Dominguez, F., Guan, B., Hu, H., Ralph, F. M., & Stohl, A. (2020). Structure, process, and mechanism. In *Atmospheric rivers* (pp. 15–43). Springer.

Turner, J., Phillips, T., Thamban, M., Rahaman, W., Marshall, G. J., Wille, J. D., Favier, V., Winton, V. H. L., Thomas, E., Wang, Z., van den Broeke, M., Hosking, J. S., & Lachlan-Cope, T. (2019). The dominant role of extreme precipitation events in antarctic snowfall variability. *Geophysical Research Letters*, *46*. https://doi.org/10.1029/2018GL081517

Waliser, D., & Guan, B. (2017). Extreme winds and precipitation during landfall of atmospheric rivers. *Nature Geoscience*, *10*. https://doi.org/10.1038/ngeo2894

Wick, G. A., Neiman, P. J., Ralph, F. M., & Hamill, T. M. (2013). Evaluation of forecasts of the water vapor signature of atmospheric rivers in operational numerical weather prediction models. *Weather and Forecasting*, *28*. https://doi.org/10.1175/WAF-D-13-00025.1

Wille, J. (2021). *Antarctic atmospheric river climatology and impacts* (Doctoral dissertation). Université Grenoble Alpes.

Wille, J. D., Favier, V., Dufour, A., Gorodetskaya, I. V., Agosta, J. T. C., & Codron, F. (2019). West antarctic surface melt triggered by atmospheric rivers. *Nature Geoscience*, *12*, 911–916. https://doi.org/10.1038/s41561-019-0460-1

Wille, J. D., Favier, V., Gorodetskaya, I. V., Agosta, C., Kittel, C., Beeman, J. C., Jourdain, N. C., Lenaerts, J. T. M., & Codron, F. (2021). Antarctic atmospheric river climatology and precipitation impacts. *Journal of Geophysical Research: Atmospheres*, *126*(8). https://doi.org/10.1029/2020JD033788

Wille, J. D., Favier, V., Jourdain, N. C., Kittel, C., Turton, J. V., Agosta, C., Gorodetskaya, I. V., Picard, G., Codron, F., Santos, C. L.-D., Amory, C., Fettweis, X., Blanchet, J., Jomelli, V., & Berchet, A. (2022). Intense atmospheric rivers can weaken ice shelf stability at the antarctic peninsula. *Communications Earth and Environment*, *3*(90). https://doi.org/10.1038/s43247-022-00422-9

Zhu, Y., & Newell, R. E. (1998). A proposed algorithm for moisture fluxes from atmospheric rivers. *Monthly Weather Review*, *126*. https://doi.org/10.1175/1520-0493(1998)126<0725:APAFMF>2.0.CO;2

A

Appendix A

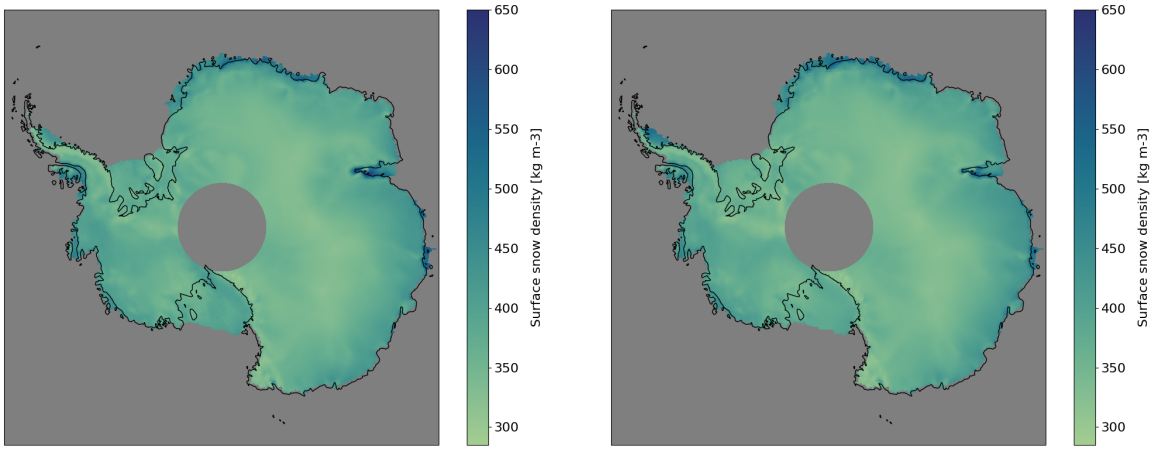

(a) 2019 **(b)** 2020

Figure A.1: Mean surface snow density in 2019 and 2020 in $[kg\ m^{-3}]$, as provided by IMAU. Grey indicates no data, which is in this case over the ocean, and over the interior of Antarctica where the latitude >85° (as the study area in this thesis is also up to a latitude of 85°).

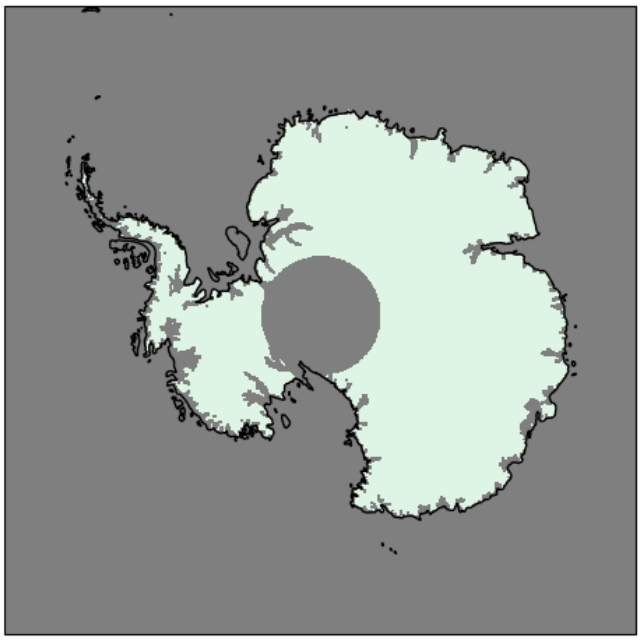

Figure A.2: Mask of Antarctica where regions with ice speed >100 m/year have been removed. Mask is based on MEaSUREs InSAR-Based Antarctica Ice Velocity Map, Version 2. The grey circle in the middle are pixels where the latitude >85°, meaning they fall outside the study area.

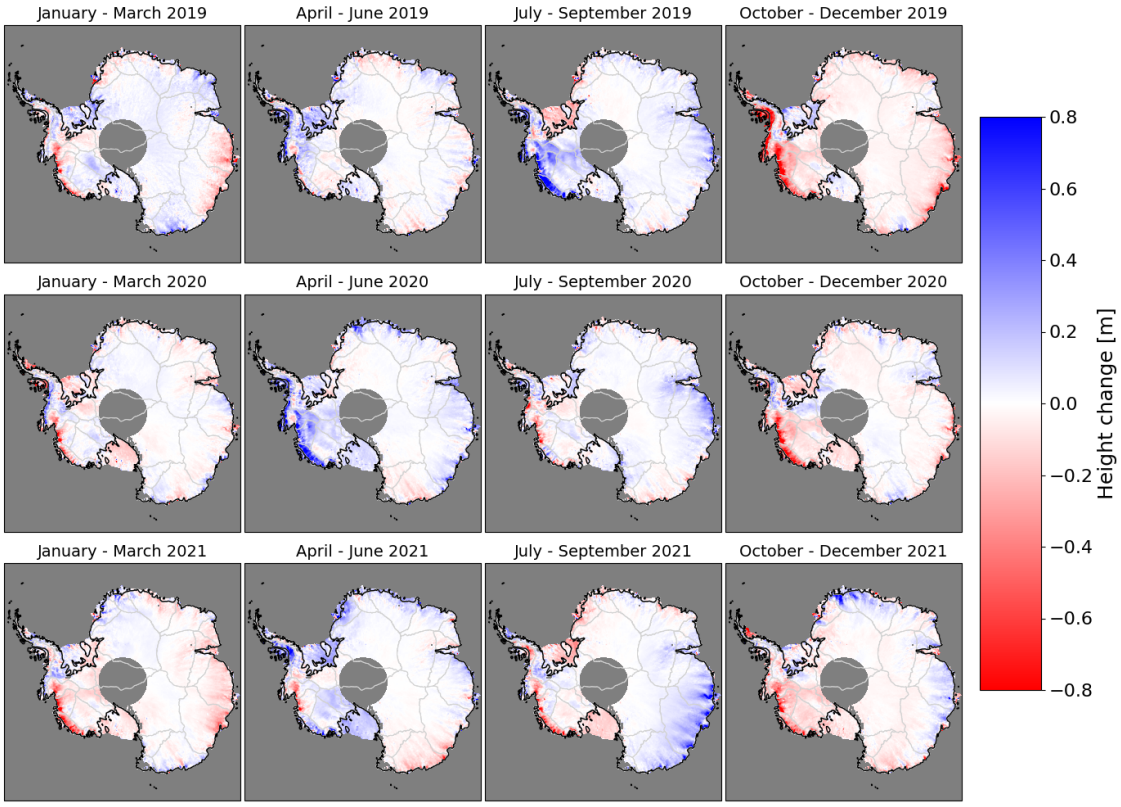

Figure A.3: ICESat2 satellite altimetry derived height changes, without ice speed mask applied. This figure shows the recorded height at the end of the period minus the recorded height at the beginning of the period, so the height change recorded over said period. Each period lasts 91 days, and starts at the beginning of the first month and lasts until the end of the last month indicated above each subfigure. The ice shelves are excluded. The grey circle in the middle are pixels where the latitude >85°, meaning they fall outside the study area. Positive height changes are shown in blue and negative height changes in red. The drainage basin divides are shown in light grey contour lines.

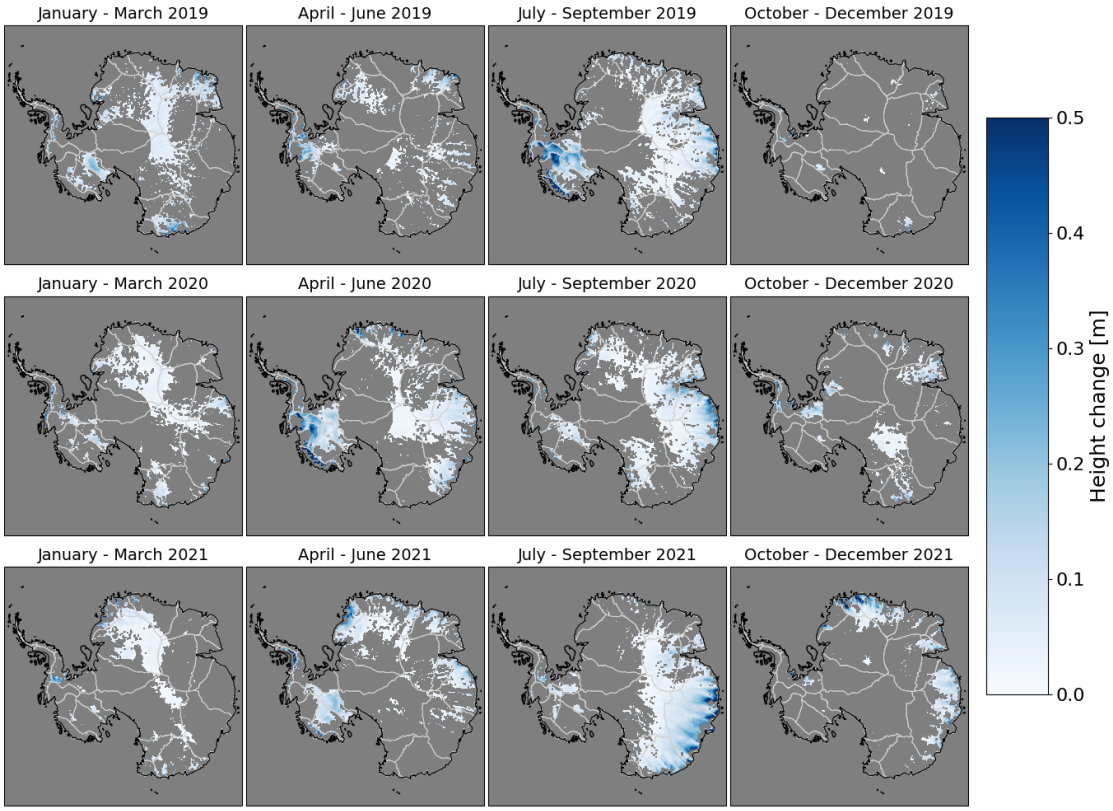

Figure A.4: ICESat2 satellite altimetry derived height changes, ice speed mask applied, only showing positive height change. This figure shows only the positive recorded height changes over the period indicated above the subfigure. Each period lasts 91 days, and starts at the beginning of the first month and lasts until the end of the last month indicated above each subfigure. The ice shelves are excluded, as well as pixels where the ice speed exceeds 100 m per year. The grey circle in the middle are pixels where the latitude >85°, meaning they fall outside the study area. The drainage basin divides are shown in light grey contour lines.

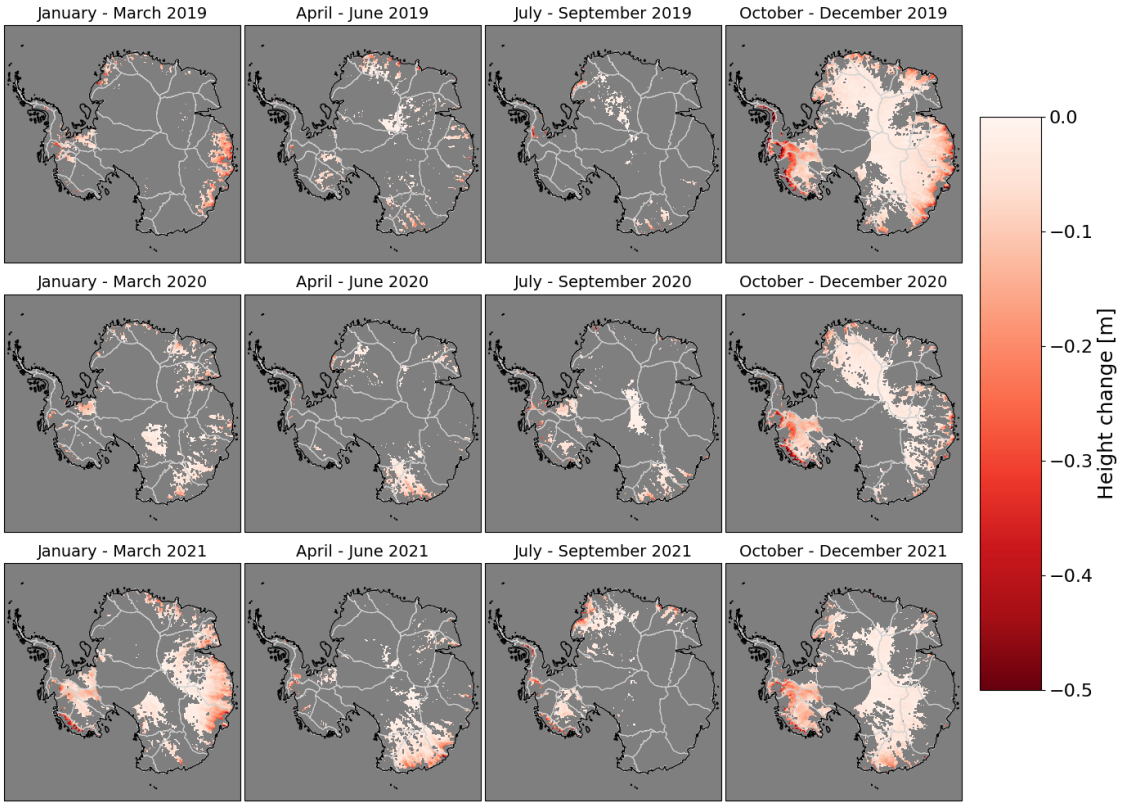

Figure A.5: ICESat2 satellite altimetry derived height changes, ice speed mask applied, only showing negative height change. This figure shows only the negative recorded height changes over the period indicated above the subfigure. Each period lasts 91 days, and starts at the beginning of the first month and lasts until the end of the last month indicated above each subfigure. The ice shelves are excluded, as well as pixels where the ice speed exceeds 100 m per year. The grey circle in the middle are pixels where the latitude >85°, meaning they fall outside the study area. The drainage basin divides are shown in light grey contour lines.

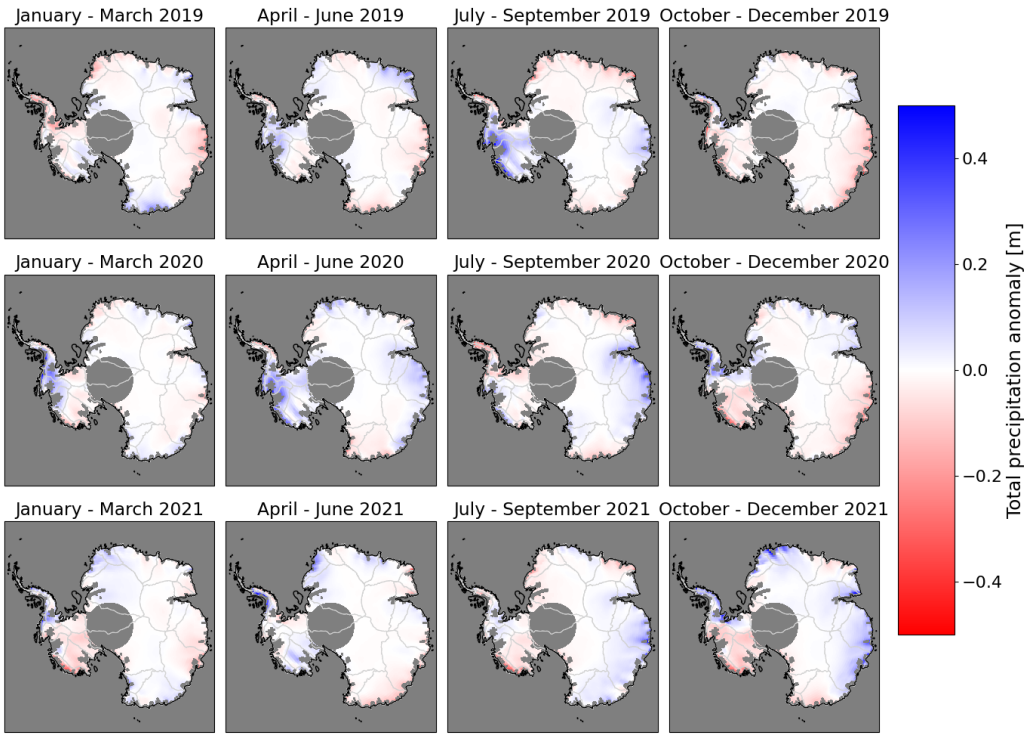

Figure A.6: Total precipitation anomaly MERRA-2, ice speed mask applied. This figure shows the total precipitation anomaly over the period indicated above the subfigure. Each period lasts 91 days, and starts at the beginning of the first month and lasts until the end of the last month indicated above each subfigure. The ice shelves are excluded, as well as pixels where the ice speed exceeds 100 m per year. The grey circle in the middle are pixels where the latitude >85°, meaning they fall outside the study area. Positive anomalies are shown in blue and negative anomalies in red. The drainage basin divides are shown in light grey contour lines.

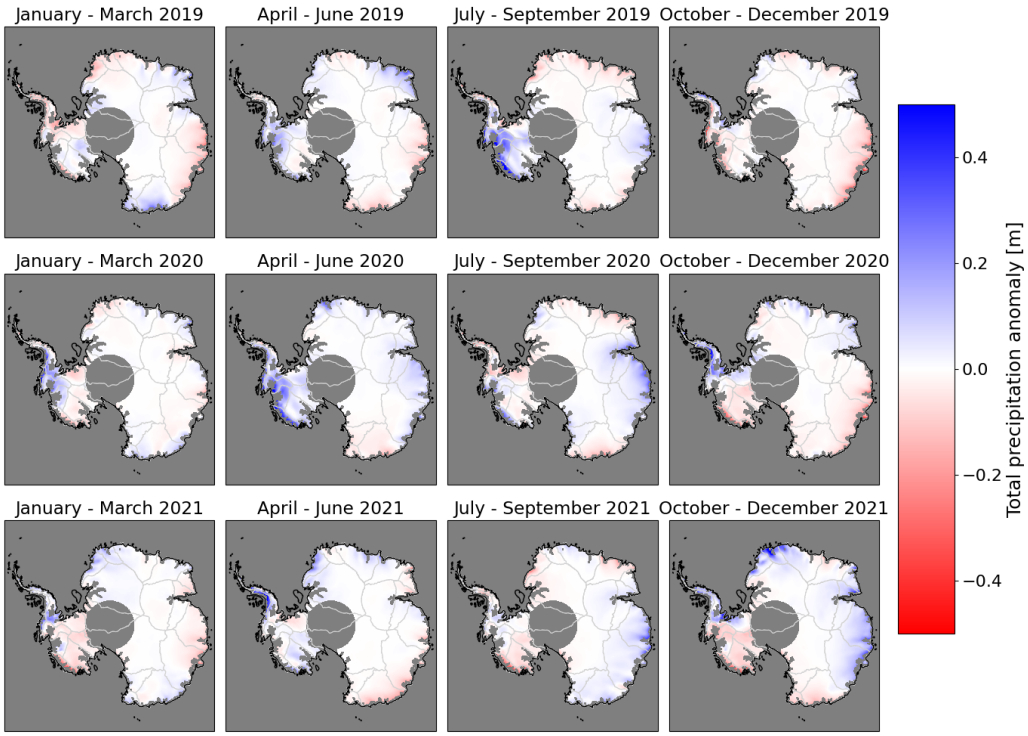

Figure A.7: Total precipitation anomaly ERA5, ice speed mask applied. This figure shows the total precipitation anomaly over the period indicated above the subfigure. Each period lasts 91 days, and starts at the beginning of the first month and lasts until the end of the last month indicated above each subfigure. The ice shelves are excluded, as well as pixels where the ice speed exceeds 100 m per year. The grey circle in the middle are pixels where the latitude >85°, meaning they fall outside the study area. Positive anomalies are shown in blue and negative anomalies in red. The drainage basin divides are shown in light grey contour lines.

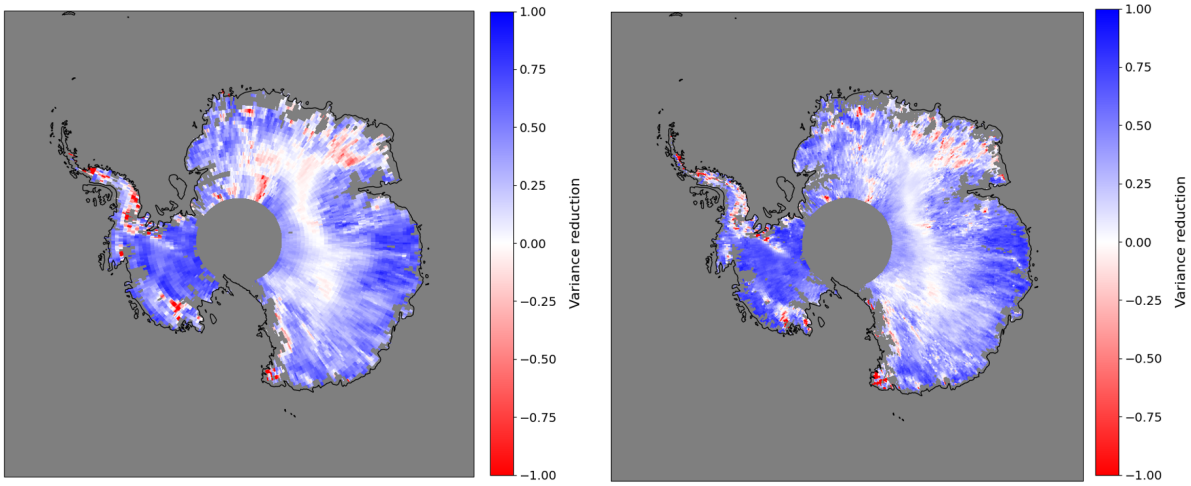

(a) MERRA-2 **(b)** ERA5

Figure A.8: Map showing the variance reduction with total precipitation as the signal of interest, with blue ice areas masked out using a mask of known blue ice areas detected using Landsat ETM+ and MODIS satellite data (Hui et al., 2014). The grey circle in the middle are pixels where the latitude >85°, meaning they fall outside the study area.

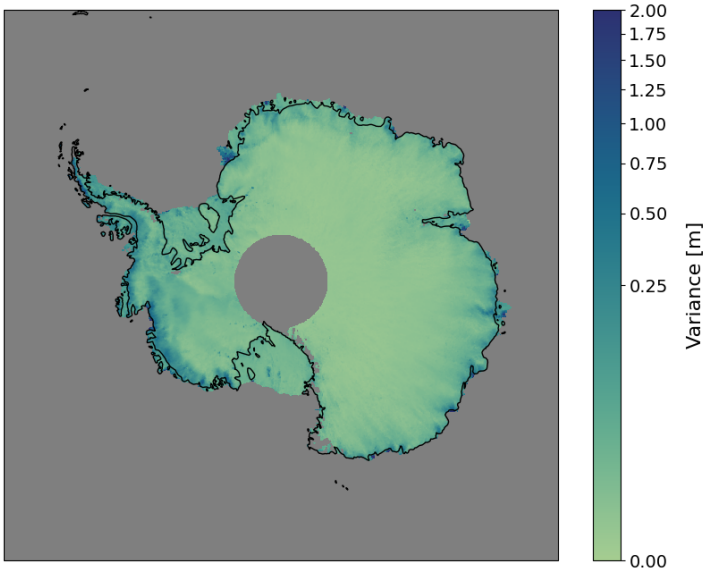

Figure A.9: Variance of ICESat-2 observations between 1 January 2019 and 31 December 2021. The grey circle in the middle are pixels where the latitude >85°, meaning they fall outside the study area.

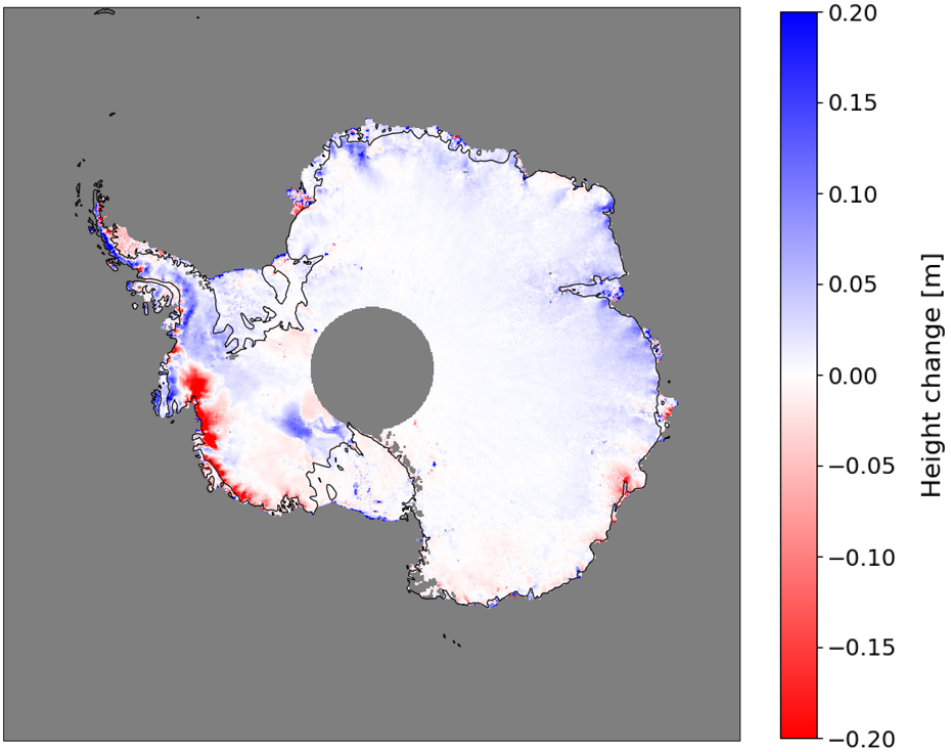

(a) All pixels

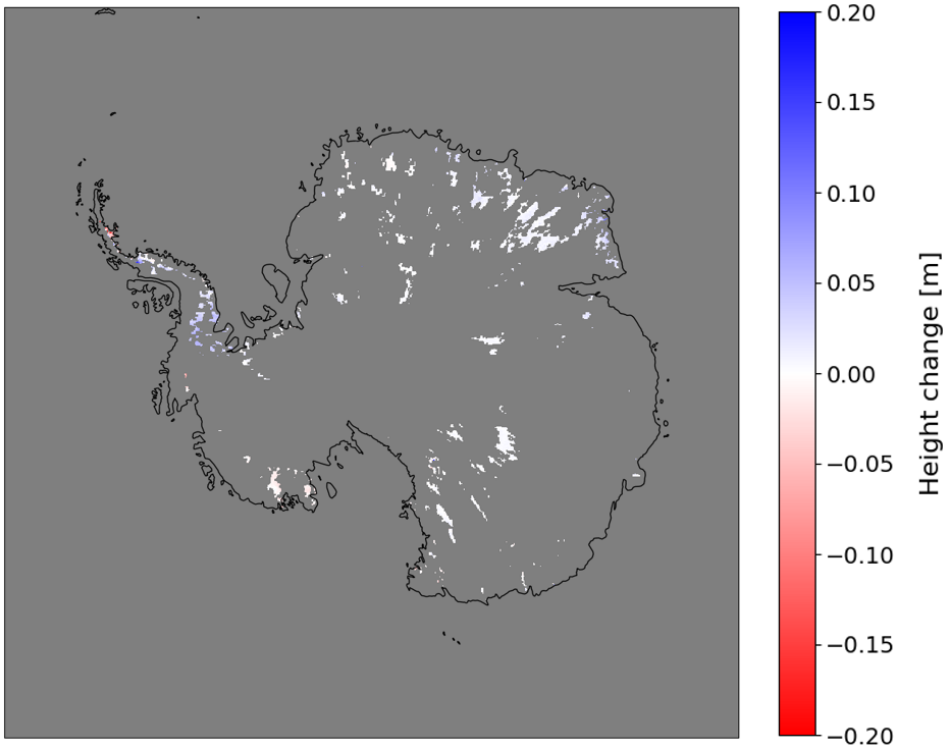

(b) Only pixels where variance reduction with $\Delta h_{signal\ of\ interest}$ = total precipitation is negative

Figure A.10: Maps showing the ICESat-2 mean height change per pixel between 1 January 2019 and 31 December 2021. a) All pixels shown, b) only pixels where the total precipitation variance reduction was negative shown.

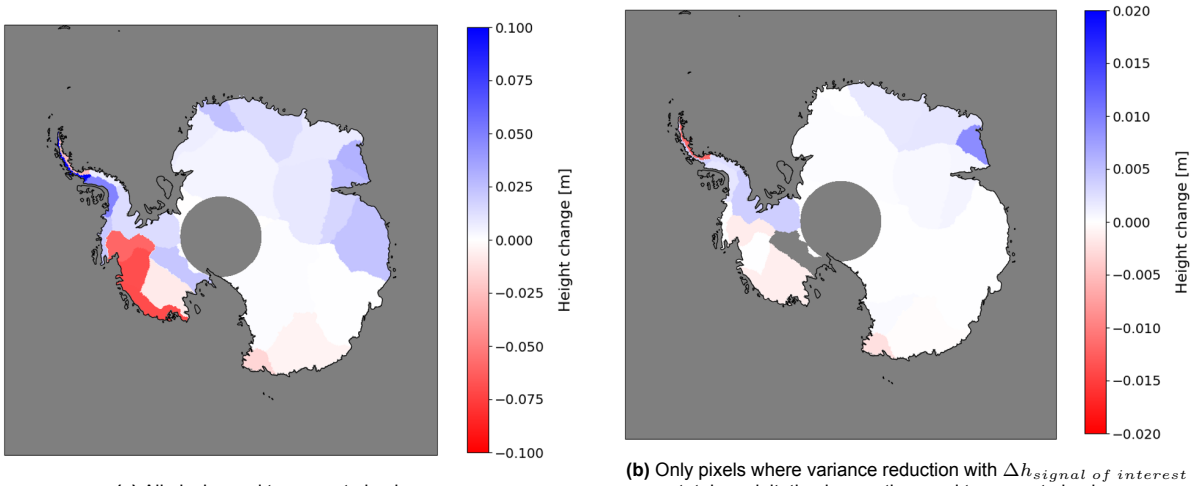

(a) All pixels used to compute basin mean

(b) Only pixels where variance reduction with $\Delta h_{signal\ of\ interest}$ = total precipitation is negative used to compute basin mean

Figure A.11: Maps showing the ICESat-2 mean height change per basin between 1 January 2019 and 31 December 2021. Note the different scale bars. a) All pixels used to compute the mean height change per basin, b) only pixels where the total precipitation variance reduction was negative used to compute the mean height change per basin.

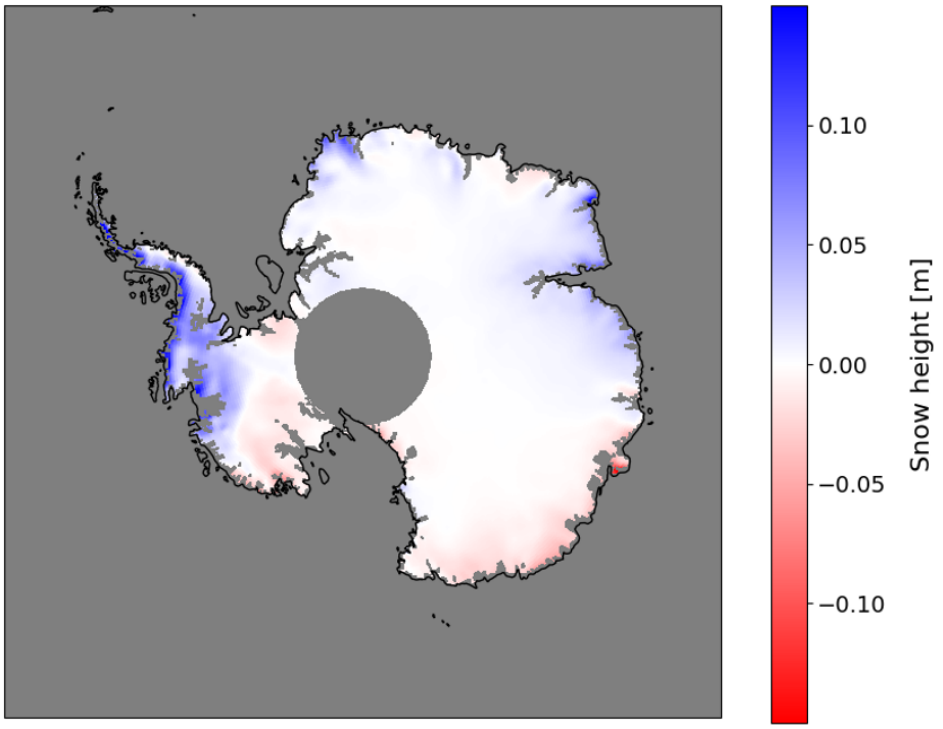

(a) All pixels

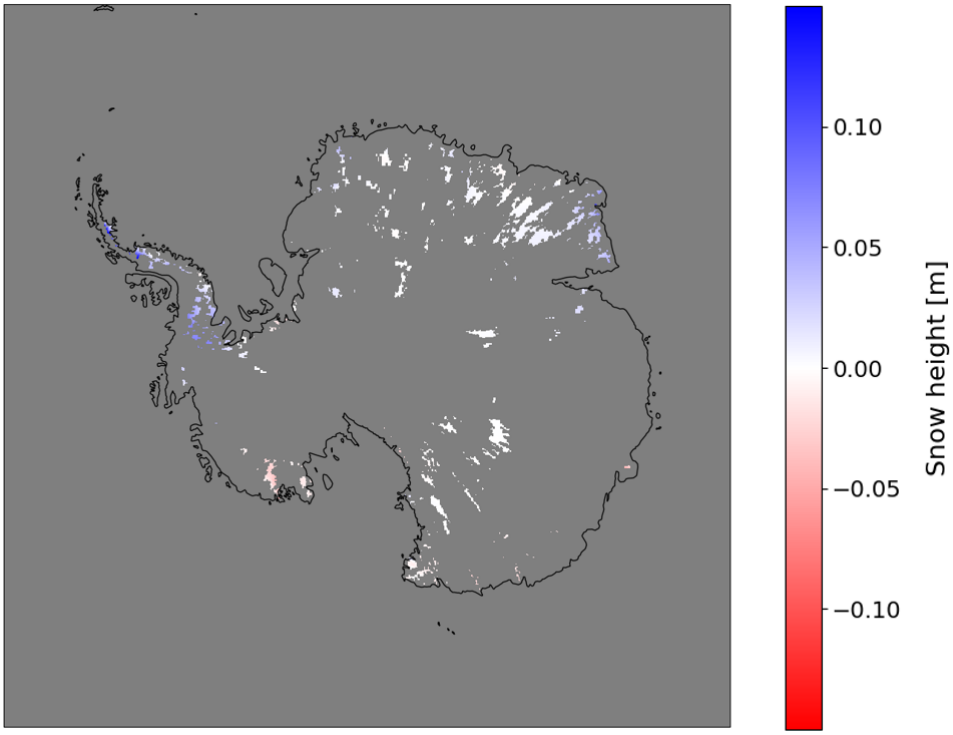

(b) Only pixels where variance reduction with $\Delta h_{signal\ of\ interest}$ = total precipitation is negative

Figure A.12: Maps showing the ERA5 mean total precipitation anomaly per pixel between 1 January 2019 and 31 December 2021. a) All pixels shown, b) only pixels where the total precipitation variance reduction was negative shown.

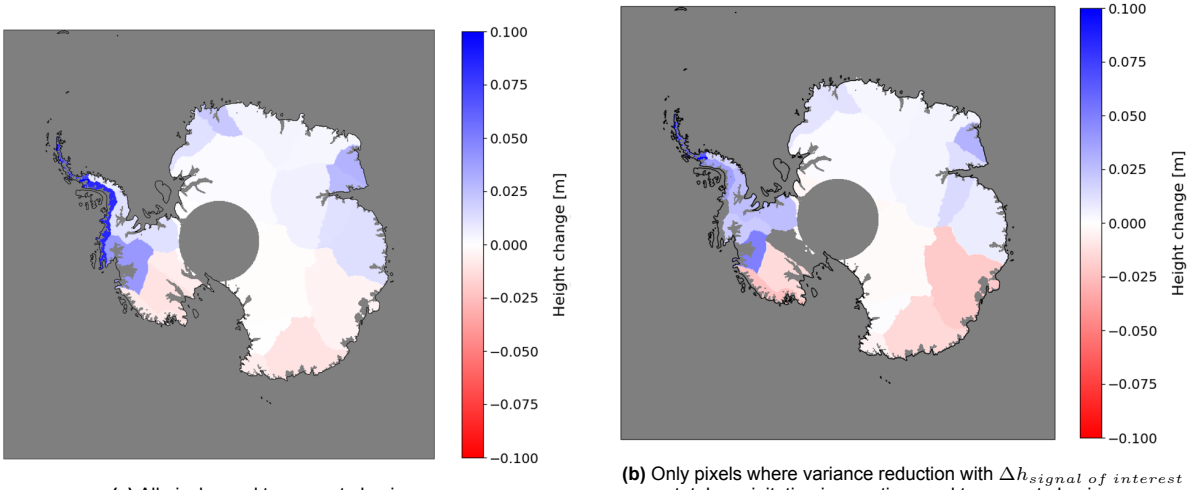

(a) All pixels used to compute basin mean

(b) Only pixels where variance reduction with $\Delta h_{signal\ of\ interest}$ = total precipitation is negative used to compute basin mean

Figure A.13: Maps showing the ERA5 mean total precipitation anomaly per basin between 1 January 2019 and 31 December 2021. Note the different scale bars. a) All pixels used to compute the mean total precipitation anomaly per basin, b) only pixels where the total precipitation variance reduction was negative used to compute the mean total precipitation anomaly per basin.

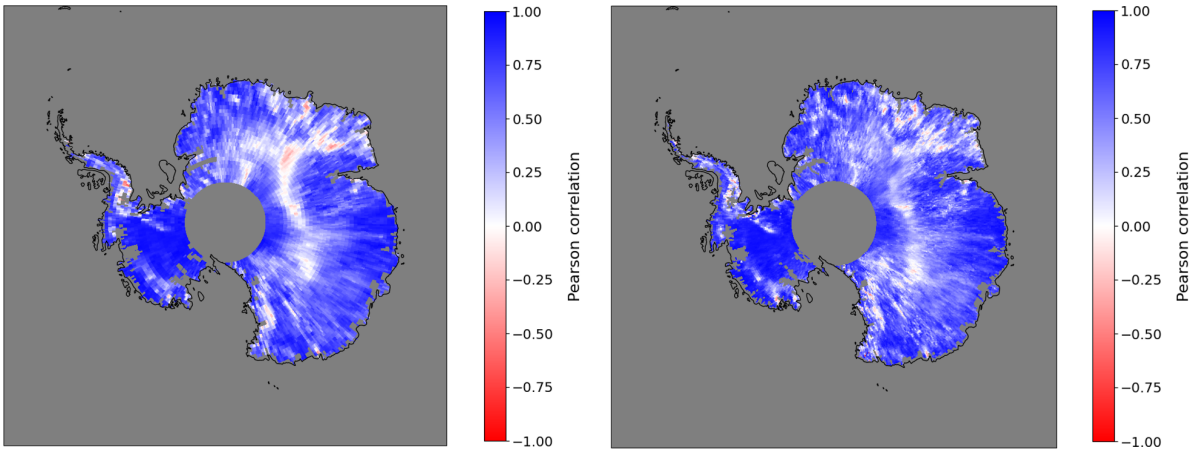

(a) MERRA-2

(b) ERA5

Figure A.14: Correlation between height differences observed by ICESat-2 and total precipitation anomaly derived from a) MERRA-2 and b) ERA5. Positive correlation shown in blue, negative correlation shown in red.

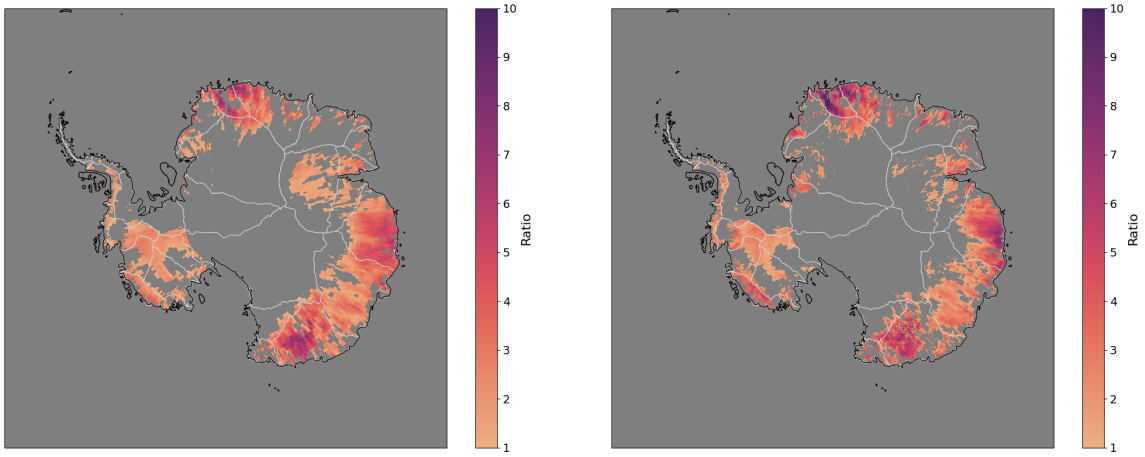

(a) MERRA-2 **(b)** ERA5

Figure A.15: Ratio of the contribution-weighted AR precipitation and ICESat-2 height change correlation value per pixel and the contribution weighted continent mean. Pixels where the ratio is smaller than 1 (and the continent mean value is thus larger) have been masked out.

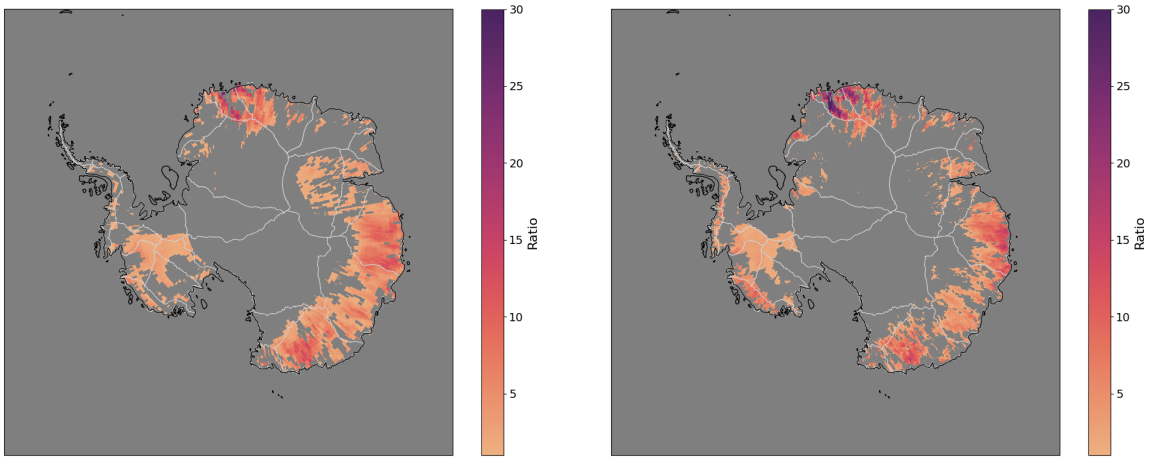

(a) MERRA-2 **(b)** ERA5

Figure A.16: Ratio of the contribution-weighted AR precipitation variance reduction value per pixel and contribution weighted continent mean AR precipitation variance reduction. Pixels where the ratio is smaller than 1 (and the continent mean value is thus larger) have been masked out.

B

Appendix B - time series

This appendix shows the time series per basin for basins not included in chapter 4,

For every basin, the mean time series between the 1st of January 2019 and 31st of December 2021 is included, showing ICESat-2 observed height change (green, with 2σ around it), the AR precipitation anomaly from reanalysis data (blue), and the total precipitation anomaly from reanalysis data (black). The red vertical lines indicate when an AR was detected in the basin, brighter lines indicate that ARs were detected in subsequent time steps. The temporal resolution of ICESat-2 data is 91 days, and the temporal resolution of the precipitation anomalies and AR detections is 3 hours.

B.1. East Antarctica

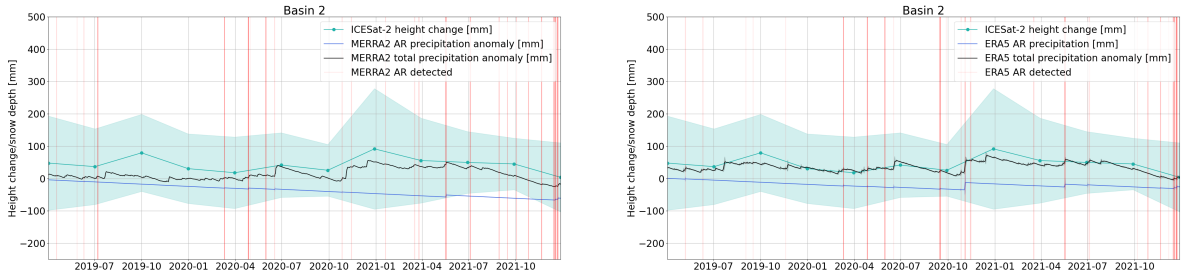

(a) MERRA-2 **(b)** ERA5

Figure B.1: Time series for basin 2. a) MERRA-2 and b) ERA5

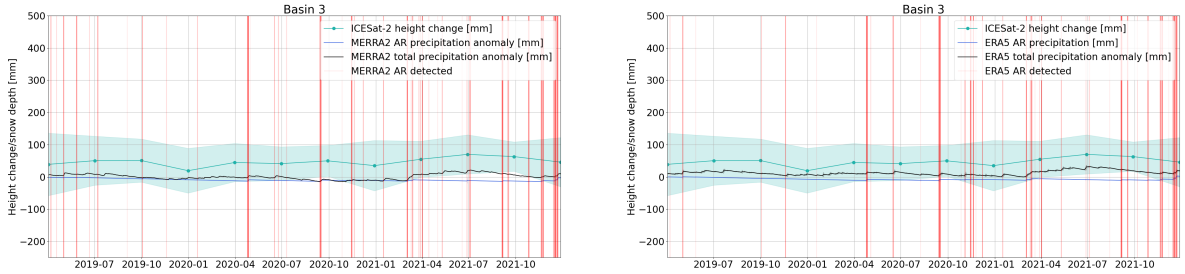

(a) MERRA-2 **(b)** ERA5

Figure B.2: Time series for basin 3. a) MERRA-2 and b) ERA5

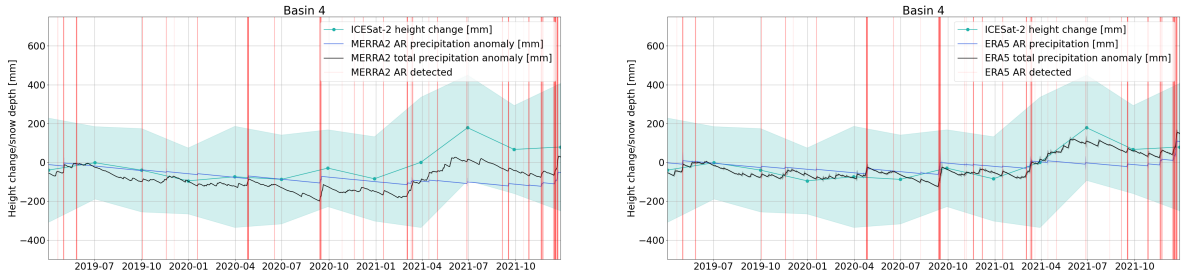

(a) MERRA-2 **(b)** ERA5

Figure B.3: Time series for basin 4. a) MERRA-2 and b) ERA5

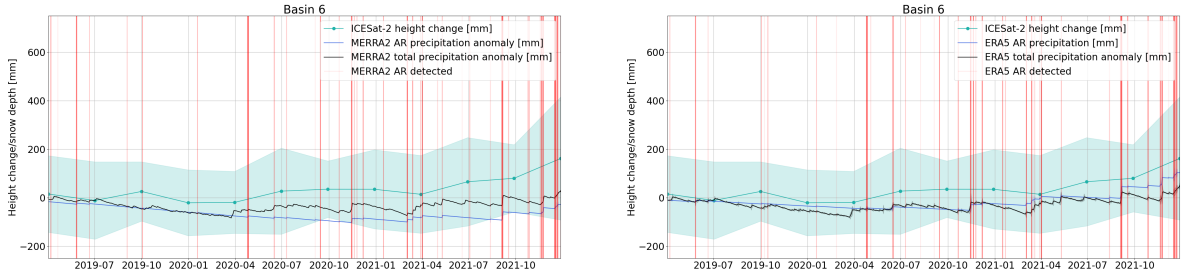

(a) MERRA-2 **(b)** ERA5

Figure B.4: Time series for basin 6. a) MERRA-2 and b) ERA5

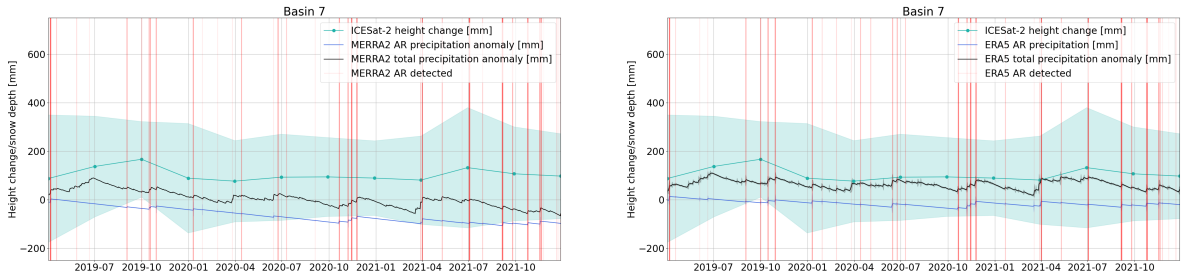

(a) MERRA-2 **(b)** ERA5

Figure B.5: Time series for basin 7. a) MERRA-2 and b) ERA5

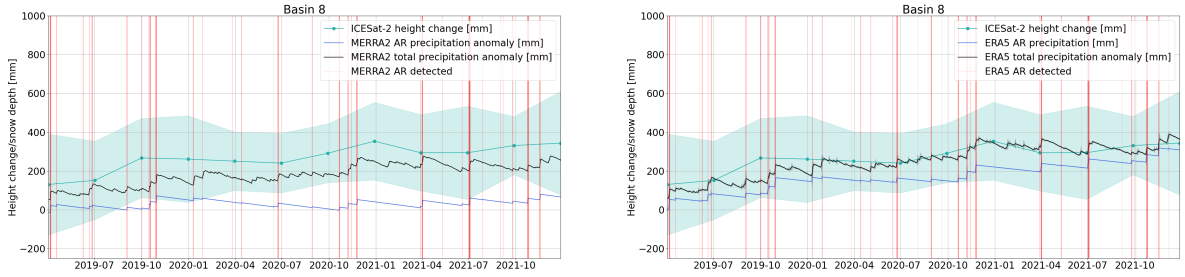

(a) MERRA-2 **(b)** ERA5

Figure B.6: Time series for basin 8. a) MERRA-2 and b) ERA5

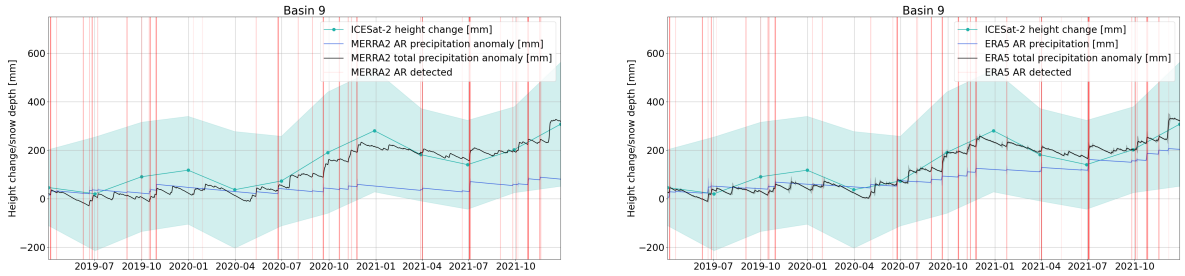

(a) MERRA-2 **(b)** ERA5

Figure B.7: Time series for basin 9. a) MERRA-2 and b) ERA5

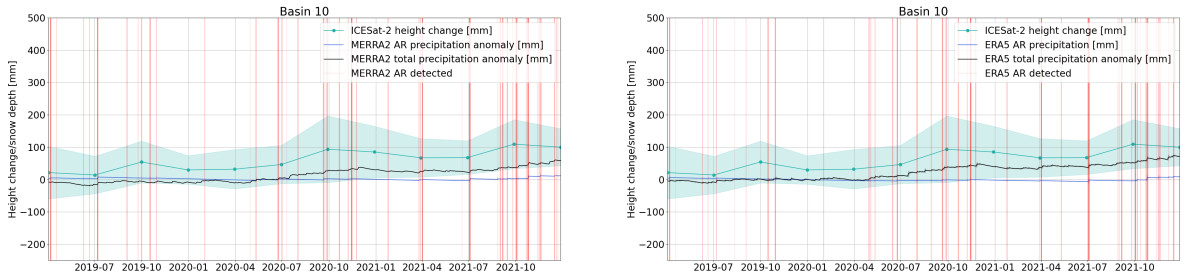

(a) MERRA-2 **(b)** ERA5

Figure B.8: Time series for basin 2. a) MERRA-2 and b) ERA5

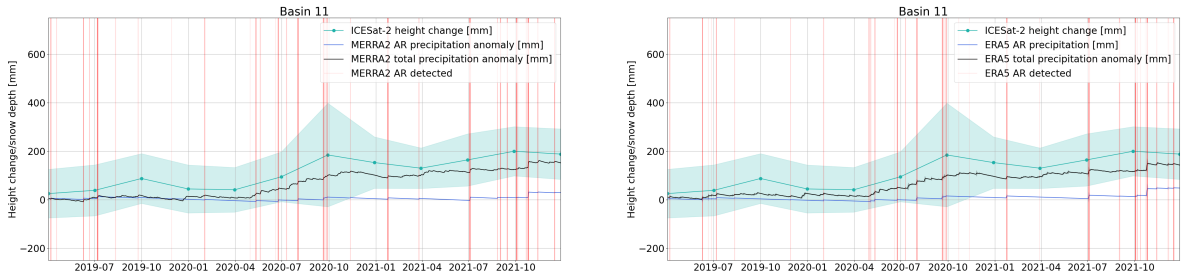

(a) MERRA-2 **(b)** ERA5

Figure B.9: Time series for basin 11. a) MERRA-2 and b) ERA5

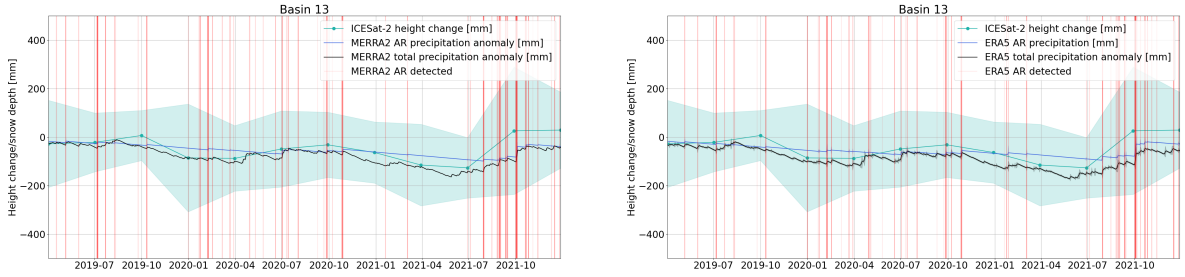

(a) MERRA-2 **(b)** ERA5

Figure B.10: Time series for basin 13. a) MERRA-2 and b) ERA5

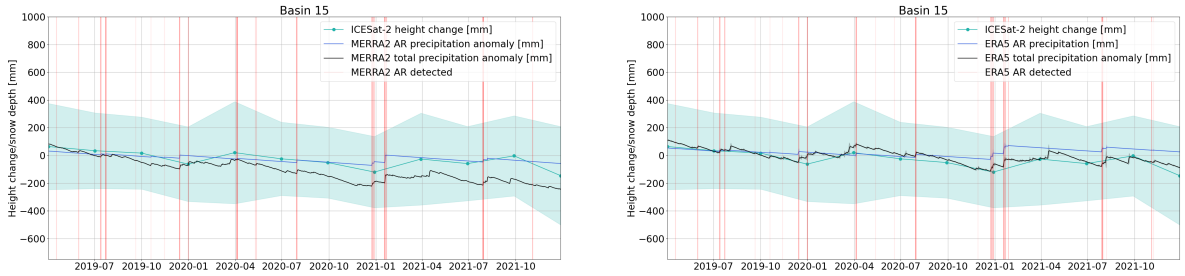

(a) MERRA-2 **(b)** ERA5

Figure B.11: Time series for basin 2. a) MERRA-2 and b) ERA5

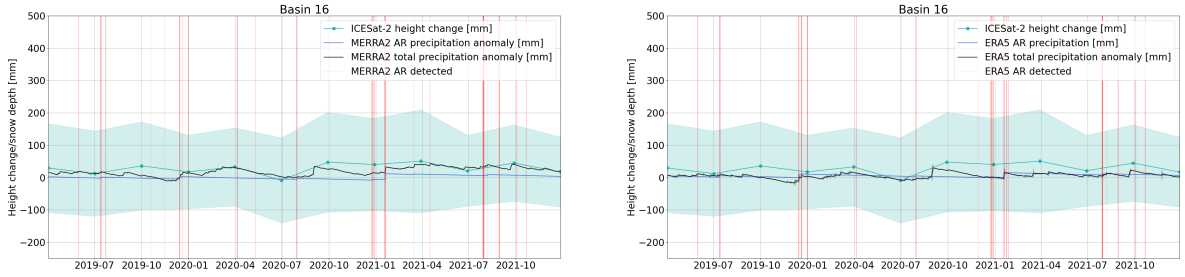

(a) MERRA-2 **(b)** ERA5

Figure B.12: Time series for basin 16. a) MERRA-2 and b) ERA5

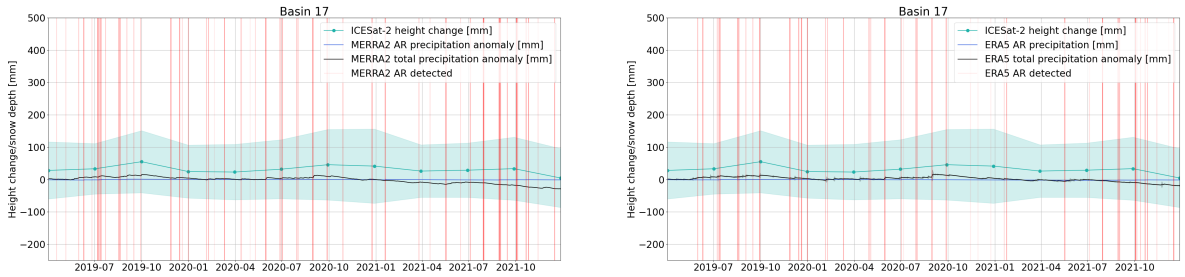

(a) MERRA-2 **(b)** ERA5

Figure B.13: Time series for basin 2. a) MERRA-2 and b) ERA5

B.2. West Antarctica

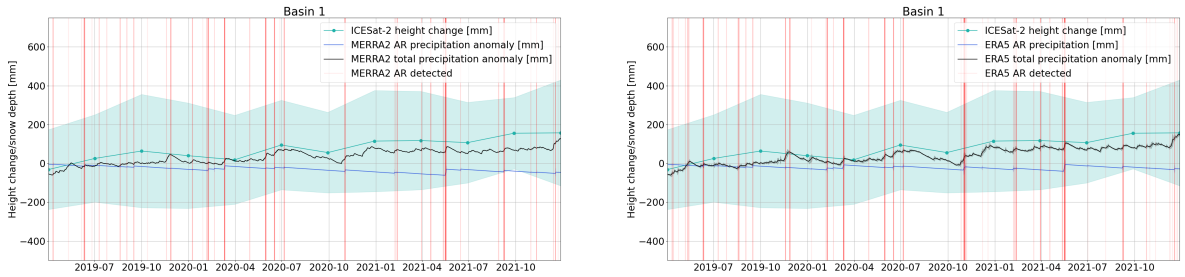

(a) MERRA-2 **(b)** ERA5

Figure B.14: Time series for basin 1. a) MERRA-2 and b) ERA5

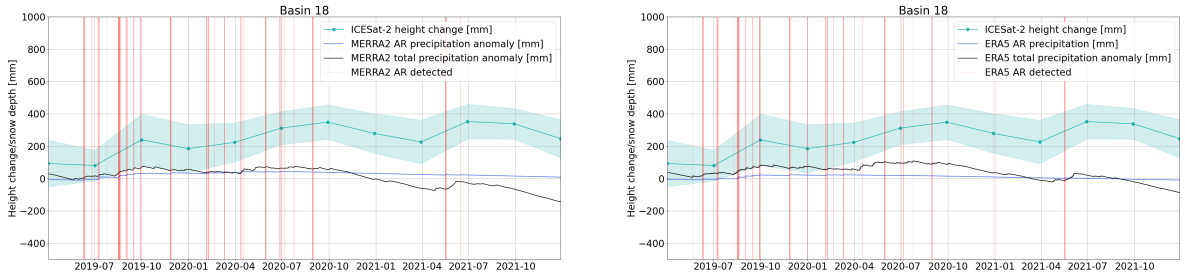

(a) MERRA-2 **(b)** ERA5

Figure B.15: Time series for basin 18. a) MERRA-2 and b) ERA5

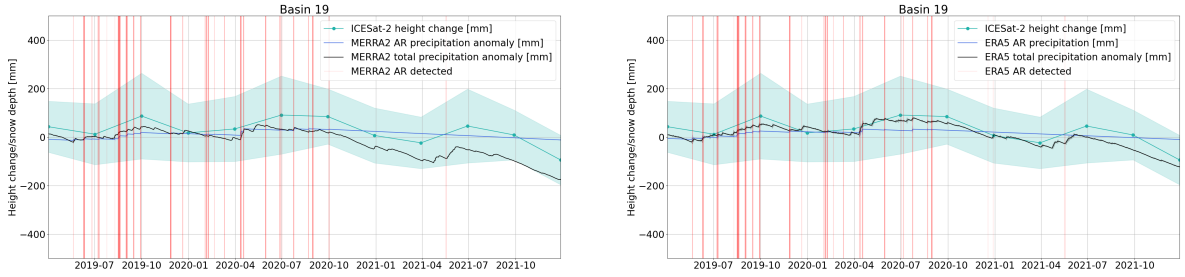

(a) MERRA-2 **(b)** ERA5

Figure B.16: Time series for basin 19. a) MERRA-2 and b) ERA5

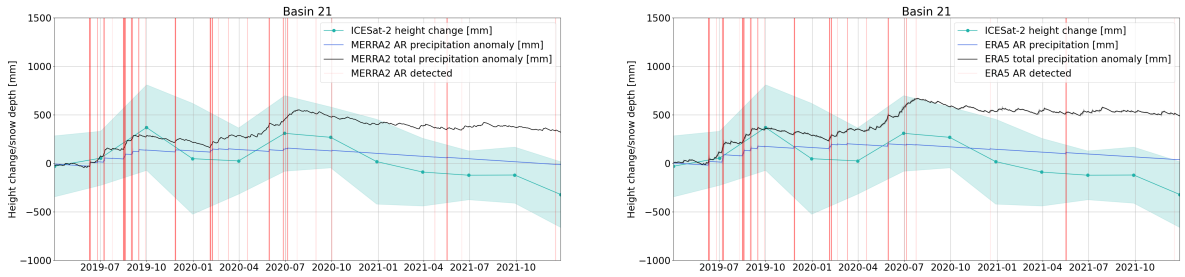

(a) MERRA-2 **(b)** ERA5

Figure B.17: Time series for basin 21. a) MERRA-2 and b) ERA5

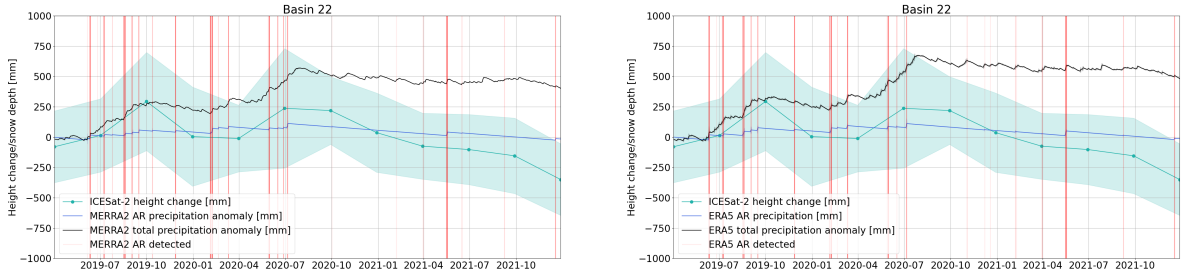

(a) MERRA-2 **(b)** ERA5

Figure B.18: Time series for basin 22. a) MERRA-2 and b) ERA5

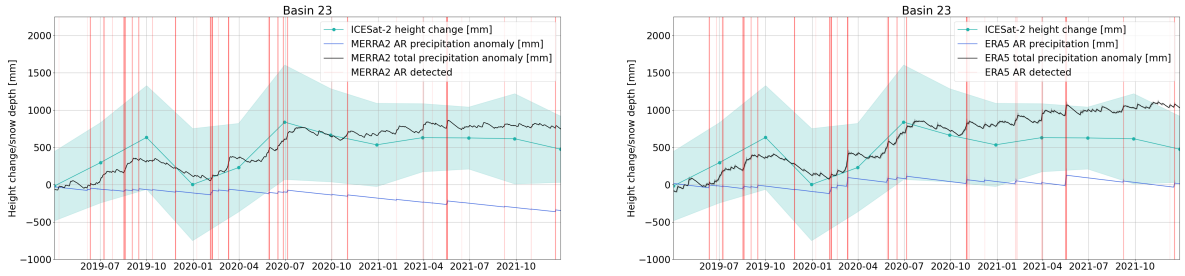

(a) MERRA-2 **(b)** ERA5

Figure B.19: Time series for basin 23. a) MERRA-2 and b) ERA5

B.3. Antarctic Peninsula

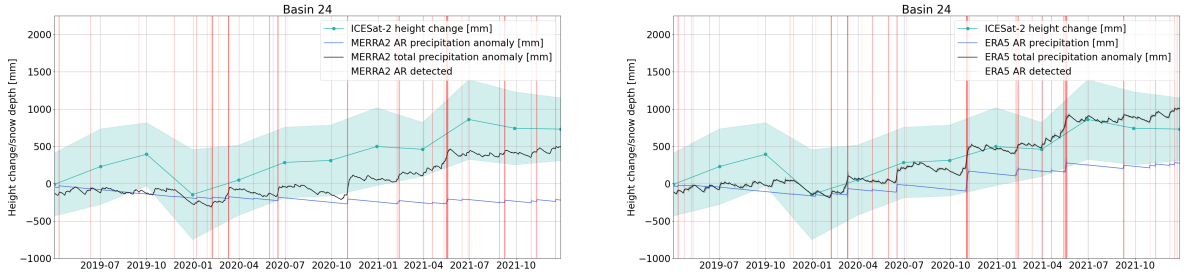

(a) MERRA-2 **(b)** ERA5

Figure B.20: Time series for basin 24. a) MERRA-2 and b) ERA5

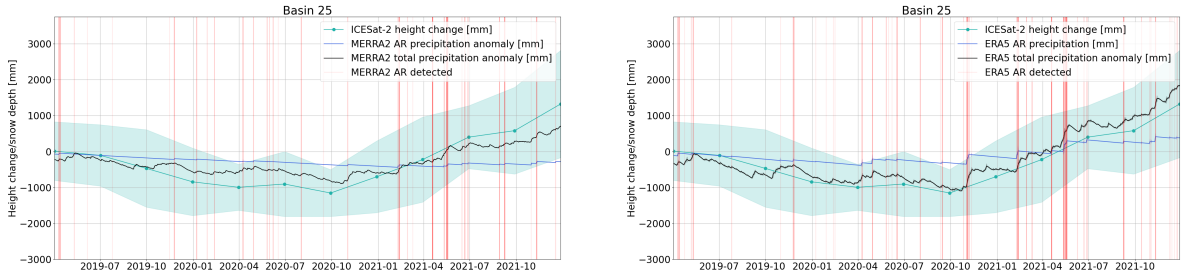

(a) MERRA-2 **(b)** ERA5

Figure B.21: Time series for basin 25. a) MERRA-2 and b) ERA5

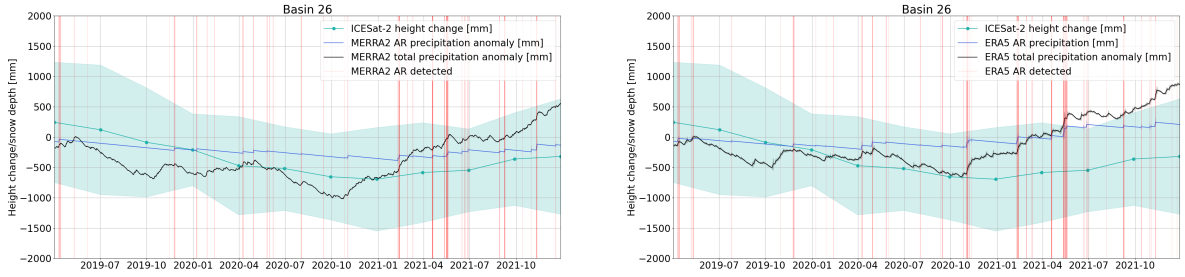

(a) MERRA-2 **(b)** ERA5

Figure B.22: Time series for basin 26. a) MERRA-2 and b) ERA5

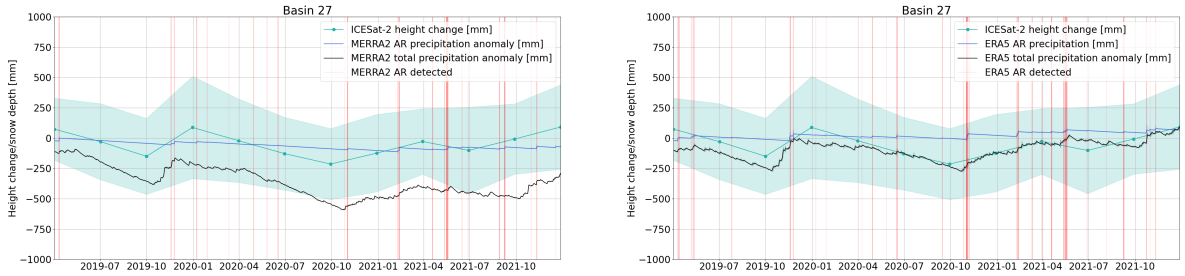

(a) MERRA-2 **(b)** ERA5

Figure B.23: Time series for basin 27. a) MERRA-2 and b) ERA5